ACOUSTIC SOUNDING OF SNOW WATER EQUIVALENT

A Thesis Submitted to the College of

Graduate Studies and Research

In Partial Fulfillment of the Requirements

For the Degree of Master of Science

In the Department of Geography

(Centre for Hydrology)

University of Saskatchewan

Saskatoon

By

NICHOLAS JOHN STANISLAUS KINAR

Keywords: snow, sound, snow water equivalent, acoustics, snow measurement, Saskatchewan, British Columbia, prairie snowpack, mountain snowpack

Permission to Use

In presenting this thesis in partial fulfilment of the requirements for a Postgraduate degree from the University of Saskatchewan, I agree that the Libraries of this University may make it freely available for inspection. I further agree that permission for copying of this thesis in any manner, in whole or in part, for scholarly purposes may be granted by the professor or professors who supervised my thesis work or, in their absence, by the Head of the Department or the Dean of the College in which my thesis work was done. It is understood that any copying or publication or use of this thesis or parts thereof for financial gain shall not be allowed without my written permission. It is also understood that due recognition shall be given to me and to the University of Saskatchewan in any scholarly use which may be made of any material in my thesis.

Requests for permission to copy or to make other use of material in this thesis in whole or part should be addressed to:

Head of the Department of Geography

Department of Geography

University of Saskatchewan

9 Campus Drive

Saskatoon, Saskatchewan S7N 5A5

ABSTRACT

An acoustic frequency-swept wave was investigated as a means for determining Snow Water Equivalent (SWE) in cold wind-swept prairie and sub-alpine environments. Building on previous research conducted by investigators who have examined the propagation of sound in snow, digital signal processing was used to determine acoustic pressure wave reflection coefficients at the interfaces between 'layers' indicative of changes in acoustic impedance. Using an iterative approach involving boundary conditions at the interfaces, the depth-integrated SWE was determined using the Berryman equation from porous media physics. Apparatuses used to send and receive sound waves were designed and deployed during the winter season at field sites situated near the city of Saskatoon, Saskatchewan, and in Yoho National Park, British Columbia. Data collected by gravimetric sampling was used as comparison for the SWE values determined by acoustic sounding. The results are encouraging and suggest that this procedure is similar in accuracy to SWE data collected using gravimetric sampling. Further research is required to determine the applicability of this technique for snow situated at other geographic locations.

ACKNOWLEDGEMENTS

I would like to thank my thesis supervisor, Dr. John Pomeroy, for supporting this research, and I am grateful for receiving some of his wisdom and experiencing his unique perspectives on such an endeavour. I would also like to thank my thesis committee, comprised of Dr. Xulin Guo and Dr. Cherie Westbrook, for providing moral and logistical support, as well as helpful suggestions. The external examiner of this thesis, Dr. Doug Degenstein, brought the unique perspective of a physicist to this project, and I am thankful for his comments which have greatly improved the exposition of the work. I am appreciative of the support received from the University of Saskatchewan and the Department of Geography in the form of scholarships, and I acknowledge the PGS-M scholarship received from the National Sciences and Research Council of Canada (NSERC).

TABLE OF CONTENTS Page

LIST OF TABLES

LIST OF FIGURES

LIST OF SYMBOLS

S_E	Snow Water Equivalent (kg m^{-2} or mm)
$\{L_1,\ldots,L_N\}$	Snowpack layer identifiers (i.e. Figure 1a)
L_0	Air layer above the surface of the snowpack
$\{\Omega_1,\ldots,\Omega_N\}$	Interfaces between the layers of the snowpack (i.e. Figure 1a)
$\overline{c}_k$	The average phase velocity of the slow wave in layer L_k (m s^{-1})
ξ_k	The acoustic impedance of a layer L_k (kg m^{-2} s^{-1})
ω	Angular frequency of air pressure wave at source (rad s^{-1})
f	Frequency of air pressure wave at source (Hz or s^{-1})
y_0	Distance from the source to the surface of the snowpack (m)
$\{y_0,\ldots,y_N\}$	Vertical dimension of layer L_k (m)
Y_N	Total depth of snow in the snowpack (m)
p_0^+	Pressure of the air wave approaching the snowpack surface (Pa)
p_0^-	Pressure of the reflected wave from the snowpack surface (Pa)
p_1^t	Pressure of the wave transmitted into the snowpack (Pa)
c_0^+	Phase velocity of the air wave approaching the snowpack surface (m s^{-1})
c_0^-	Phase velocity of the reflected wave from snow surface (ms^{-1})
Γ_k	Pressure reflection coefficient at snowpack interface Ω_k
$\alpha(\omega)$	Frequency-dependent dynamic tortuosity (dimensionless)
γ	Shape factor dependent on the snow
ϕ_k	Average porosity of a layer L_k of the snowpack
$s(t)$	Pressure amplitude of the plane wave at the source (Pa)
f_0	Starting frequency of the linear frequency sweep (Hz)
f_1	Ending frequency of the linear frequency sweep (Hz)
$B = f_1 - f_0$	Bandwidth of the linear sweep (Hz)
t_0^*	Starting time of the linear frequency sweep (s)
t_1^*	Ending time of the linear frequency sweep (s)
Δt^*	Total time (s) of the frequency sweep
$\partial f / \partial t$	Rate of change of linear sweep (Hz s^{-1})
c_k	Instantaneous phase velocity of sound pressure wave (m s^{-1})
f_i	Instantaneous frequency of the sound pressure wave (Hz)

f_c	Critical frequency of the sound pressure wave (Hz)
f_t	Threshold frequency (Hz)
$\overline{c}_k$	Average phase velocity of the sound pressure wave in layer (m s^{-1})
t_k	The one-way time (s) required for a pressure wave to traverse a given layer L_k
$T_k = 2t_k$	Total round-trip time (s) taken to traverse a given layer L_k of the snowpack
$s'(t)$	Overall reflection from the snowpack (as a continuous function)
$s'[t]$	Overall reflection from the snowpack (as a discrete function)
$r(t)$	Reflection response of the snowpack (as a continuous function)
$r[t]$	Reflection response of the snowpack (as a discrete function)
$a(t)$	Attenuation function of snow as a porous (dispersive) medium
$a[t]$	Attenuation function of snow (discrete function)
τ	Time shift caused by the convolution process (s)
λ_0	Wavelength of sound pressure wave in air (m)
f_s	Sampling frequency of the Analog-to-Digital Converter (Hz)
$s[t]$	Original digitally-generated frequency sweep
$s_r[t]$	Frequency response of the loudspeaker in the time domain
$m_r[t]$	Frequency response of the microphone in the time domain
$n_s[t]$	Noise introduced by the recording system
$n_{m\nearrow}[t]$	Sound wave of the original sweep from the loudspeaker that travels directly through the air to the microphone
$n_e[t]$	Noise introduced due to wind and blowing snow
n_p	Number of samples of each of the signals collected
$card(\cdots)$	The cardinality, which is the number of elements in the set $(\cdots)$
$s''[t]$	Convolution of the reflection response of the snowpack with its attenuation
k_0	Angular wavenumber in the air medium (m^{-1})
$FFT[\cdots]$	Denotes application of the discrete FFT to $[\cdots]$
ρ_{ice}	Approximate density of ice (917 kg m^{-3})
$\overline{\rho}_k$	Average bulk density of a layer L_k (kg m^{-3})
$s_d[f]$	Homodyned signal as a result of the signal processing flow
N	Total number of layers in the snowpack
t_0	Time taken for the sound to travel to the snow surface (s)
T^*	Ambient environmental temperature (Kelvin)

$\Delta f_{b,k}$	Frequency shift caused by reflection from interface Ω_k (Hz)
$\Delta F_{b,k}$	Total frequency shift caused by reflection from interface Ω_k (Hz)
$\varphi = 1\ \mathrm{m}^2 \cdot \mathrm{kg}^{-2} \cdot \mathrm{mm}$	Continuity constant for calculation of SWE
$R = 287\ \mathrm{N} \cdot\ \mathrm{m} \cdot\ \mathrm{kg}^{-1} \cdot\ \mathrm{K}^{-1}$	Thermodynamic gas constant for air
ρ_0	Equilibrium air density (kg m^{-3})
$J_0[\cdots]$	Bessel function of the first kind
θ_g	Grazing angle of incidence (radian)
$j = \sqrt{-1}$	Complex number
r_f	Radius of area of snowpack insonified by loudspeaker (m)
x_0	Horizontal distance between loudspeaker and microphone (meters)
$x_{\max}$	Maximum separation distance between speaker and microphone (meters)
$\theta_{x,\max}$	Maximum angle of displacement between transducers (radians)
δy	Accuracy of depth measurement (meters)
L_c	Characteristic length of transducer (meters)
y_f	Distance to the far field of transducer (meters)
θ_w	Angular beam width of source (radians)
x_f	Fetch distance, unobstructed distance of travel of blowing snow (meters)
dS / dt	Rate of snow accumulation (kg m^{-2} s^{-1})
P	Snowfall rate (kg m^{-2} s^{-1})
F	Transport rate of snow (kg m^{-2} s^{-1})
E_B	Sublimation due to blowing snow (kg m^{-2} s^{-1})
E	Rate of snow sublimation at snowpack surface (kg m^{-2} s^{-1})
M	Snowmelt rate (kg m^{-2} s^{-1})

1. INTRODUCTION

1.1. Objective

Snow Water Equivalent (SWE) is conceptually defined as the depth of water that results from the melting of the seasonal snowpack. Point measurements of SWE are typically determined by the use of invasive devices (Goodison et al., 1981). These current methods of determining SWE are either time consuming or prone to human error (Davis, 1973; Pomeroy and Gray, 1995). The objective of this research is to find a procedure to obtain SWE using simple, non-destructive means.

1.2. Problem

Snow distribution is highly variable over prairie (Pomeroy et al., 1991), arctic (Pomeroy et al., 1997), forested (Pomeroy and Dion, 1996; Woo and Giesbricht, 2000), sub-alpine (Gustafsson et al., 2004), and alpine (Elder et al., 1991; Marks et al., 2002) landscapes. This makes representative measurements of SWE difficult to obtain due to the spatial heterogeneity of snow (Derksen et al., 2002). Fassnacht et al. (2002) note that in January 1999, southern Ontario received more than 1 m mean depth of snowfall, but regional flooding did not occur due to low snow densities resulting in relatively small amounts of SWE at the time of ablation. It is therefore beneficial to be able to efficiently measure SWE as an indicator of the depth of water that will result from melting of the seasonal snowpack, rather than simply taking snow depth as an indicator of the equivalent water content.

1.3. Issue

Snow is a major source of runoff in western Canada (Male and Gray, 1975) and has strong climatic feedback (Marshall et al., 2003; Gorodetskaya et al., 2006). The western Canadian prairies receive approximately 39% of annual precipitation in the form of snow (Pomeroy and Gray, 1995). In addition, snow comprises approximately one-third of all precipitation that falls in Canada each year. More than 80% of water in the streams of the Canadian Prairies is derived from runoff that originates as snowmelt (Pomeroy and Goodison, 1997). Approximately the same percentage of water contributes to streamflow and soil moisture in the western United States (Marks et al., 2001). Due to its large contribution to the hydrologic cycle, the amount of snow present on the land surface is important to observe under current scenarios of climate change (Groisman and Davies, 2001).

During the winter months, the presence of snow cover protects the underlying soil from desiccation (Pomeroy and Brun, 2001). When snow melts, the equivalent water content of the snowpack can infiltrate into the ground, thereby providing additional soil moisture for summer plant transpiration. This effect has led Steppuhn (1981) to strongly suggest that farmers should trap snow on fields during the winter months to ensure that crops are provided with water during subsequent periods of drought. Knowledge of SWE is therefore important to estimate the amount of water that is available from snow to mitigate the effects of water shortages and to reduce the cost of artificial irrigation. Models such as the Cold Regions Hydrological Model can be used in water resources management to predict the spatial distribution and movement of SWE (Hedstrom et al., 2001).

Conversely, knowledge of SWE can contribute to flood prediction measures. In areas of Canada such as the Red River Valley of Manitoba, knowledge of the spatial distribution of SWE

is important to predict the timing of runoff and the occurrence of the nival freshet. Flooding in this area of Canada has increased due to climate change. As Ashmore and Church (2001) note, between 1892 and 1945, the discharge in the Red River exceeded 2000 m s^{-1} only twice. From 1945 to 1999, however, this level has been exceeded 11 times. One example of the devastation caused by snowmelt is the 1997 Red River Flood. During this event, the Canadian Armed Forces evacuated more than 25 000 people from the Red River area. The entire operation involved over 7000 personnel and more than $800 million in damages was accrued by the Government of Canada (Ashmore and Church, 2001). Such an event is an example of the need to accurately determine SWE, especially because this quantity is one of the most poorly-estimated of all hydrological variables.

1.4. The Spatial Distribution of SWE

The upscaled mass balance of snow over a landscape element can be considered in terms of the following equation (Pomeroy and Li, 2000):

$$\frac{dS}{dt}\left(x_f\right) = P - \nabla F\left(x\right) + \frac{\int E_B\left(x\right)dx}{x_f} - E - M \qquad (1.1)$$

, where the rate of accumulation of snow on the land surface as a function of fetch distance x_f (m) is given by dS/dt (kg m^{-2} s^{-1}); the rate of snowfall is P (kg m^{-2} s^{-1}); the transport rate of snow is F (kg m^{-2} s^{-1}); the sublimation due to blowing snow is E_B (kg m^{-2} s^{-1}); E is the sublimation rate of snow at the surface of the snowpack (kg m^{-2} s^{-1}); and M is the rate of snow melt (kg m^{-2} s^{-1}). Fetch distance x is the unobstructed distance of travel of blowing snow (given in meters). The variables on the right-hand side of Eq. 1.1 can be considered as causal factors of the accumulation and redistribution of snow. Other methods of classification which deal with

the spatial distribution of snow have been devised by researchers such as Gray (1970), McKay (1970), McKay and Gray (1981), and Sturm et al. (1995), but such schemes have been conceived for a particular purpose or for a certain geographic area (Pomeroy and Brun, 2001).

1.4.1. The Rate of Snowfall *P*

The rate at which snow accumulates on the land surface is largely influenced by macroscale (10-1000 km) processes of atmospheric phenomena (McKay and Gray, 1981). One of the global influences on snow accumulation in North America is the El Niño Southern Oscillation (ENSO), which causes a reduction in the amount of snowfall in Canada due to increased zonal winds which shift frontal masses to lower latitudes during the winter period (Karl et al, 1993). As Lee et al. (2004) observed in the Upper Rio Grande basin of New Mexico and Colorado, this causes an increase in the amount of SWE during winters when ENSO is most active. Jin et al. (2006) realized that these effects were spatially variable across the western United States. In particular, ENSO years amounted to increased snowfall in the southwest, whereas during years when ENSO was not active, the rate of snowfall was greater in the northwest. The results of Jin (2006) generally agree with those of Canyan (1996), who also demonstrated that variability in SWE across the western United States may be affected by regional climatic variations including the Pacific North American (PNA) circulation. The findings of Woodhouse (2003) from dendrochronology of tree ring samples taken from the Gunnison River basin in western Colorado confirm that these large-scale atmospheric trends and some regional variations were apparent in SWE since the year 1569.

Synoptic-scale air masses passing over the Pacific Ocean contribute to regional variability of snowfall in Canada. Due to close proximity of the Rocky Mountains to the Pacific

Ocean, the air masses are subjected to orographic lifting, and after these air masses move over the mountains, precipitation occurs on the leeward slopes. At high elevations in the mountains, precipitation falls in the form of snow due to low temperatures, although some locations on the stoss side of the Rocky Mountains also receive snow due to a cold winter climate in some areas situated near the Pacific Ocean (Schemenauer et al., 1981). Unlike the Scottish Highlands (mean elevation ~1 km)—which can lose all snow cover for at least a month—temperatures are cold enough at some elevations in the Rocky Mountains for snowfall events to occur over the entire year (Collier, 1998). Cold temperatures at high elevations ensure low ablation rates, and due to the greater frequency of precipitation events at higher elevations, SWE tends to increase with elevation, given that other complicating factors such as vegetation, topography, and surface roughnes are constant within a given elevation range (Pomeroy and Gray, 1995). Ryerson and Bates (1990) found that this was also the case for the Appalachian, northern Cascade, and Sierra Nevada mountain chains of the United States. Despite the effects of adiabatic heating as air masses descend from the Rocky Mountains, baroclinic wave disturbances can cause cyclogenesis on the lee side of the mountains, and this is responsible for depositing heavy snowfall in Alberta (Chung et al., 1976).

Orographic effects associated with snowfall are also prevalent in the Arctic, where areas situated within the Mackenzie and St. Elias Mountain ranges receive more snowfall than the continental interior of Yukon, Nunavut, and the North-western Territories due to orographic effects. Mean snow depth in these mountain chains can be greater than 1 m per annum, whereas the majority of precipitation in the arctic falls as rain during the snow-free season. The rate of snowfall in the continental interior is relatively low due to the influence of marine polar air masses which form over the Arctic Ocean. Due to the presence of ice cover, the Arctic Ocean

contributes very little moisture to these air masses, and consequently, this reduces the rate of snowfall on the Arctic Interior Plain (Prowse, 1990). Rates of snowfall in the Arctic are often uncertain due to inadequate spatial coverage of measuring networks and the lack of representative data, but the annual SWE at locations ranging from Resolute to Eureka and Mould Bay is normally less than 15 cm yr^{-1} (Woo, 1982). However, based on intensive measurements conducted in four research basins on Cornwallis Island, Woo and Marsh (1977) determined that the rate of snowfall for the 1975/1976 snow year was ~80 cm yr^{-1} in this regional location of the eastern arctic. Alternately, for the entire Canadian arctic region, Groisman and Davies (2001) observe from snowfall data that for latitudes in the elevation band of 55-70°N, there has been a general increase in annual SWE of nearly 7 mm yr^{-1} between the years 1950 to 1990.

Derksen et al. (2000) investigated mesoscale atmospheric circulation effects on SWE in a study area centered over Saskatchewan and the prairie grasslands of the central United States, finding that the effects of an atmospheric prairie trough caused greater accumulation of snow in the northern extents of the study area, whereas an atmospheric ridge or meridional flow was responsible for more accumulation of snow in the south. Huges and Robinson (1993) found that between 1910 and 1988 there had been an increase in the rate of snowfall by 2.8 mm yr^{-1} on the Great Plains of the northern United States. Alternately, Akinremi et al. (1999) have noted that between 1961 and 1995, there had been a significant decrease of nearly 1 mm yr^{-1} of the rate of snowfall on the Canadian prairies.

In areas such as the Great Lakes of Ontario, cold air masses are destabilized by sensible heat and moisture fluxes from the water surfaces which characterize this region, thereby causing an increase in snow on land situated to the south-east of these large bodies of water (Schemenauer et al., 1981). Often the cause of the most extreme snow events in this region is a

southward-moving low pressure trough (Paine and Kaplan, 1971), which can be capped by a temperature inversion at distances of 1500 m to 2000 m above the land surface (Weickmann, 1970). Alternately, northern Ontario receives approximately 200 mm yr^{-1} of snow, which is usually deposited by air masses from the south-west that convey moisture from the Great Lakes (Carr, 1983). These effects tend to increase the rate of snowfall in southern Michigan (Isard and Schaetzl, 1993) and on the windward slopes of the southern Appalachian Mountains (Perry and Konrad, 2005). Niziol et al. (1990) note that snow deposition events of 70 cm depth over a period of two days can be caused by lake effect snow in the lee of Lake Ontario. However, as Leathers and Ellis (1993) reported, much of this snow deposition is created by cyclonic action, and is not statistically dependent on daily ice cover or the surface temperatures of these bodies of water. This is due to water temperatures (~2°C) that are higher than the mean temperature (-15°C to -35°C) of the cold air masses (Byrd et al., 1988), as well as patchy amounts of ice cover on these large bodies of water that still permit vertical fluxes of moisture and temperature to travel though the boundary layer overlying the lakes (Environment Canada, 1992). Alternately, Jiusto and Kaplan (1971) point out that a more moderate rate of annual snowfall may occur in the lee of the Great Lakes due to lessened difference between mean air mass temperature and lake surface temperature over the period of the snow accumulation season. Aside from the thermal effects of large water bodies, local undulations of topography in the area immediately south of the Great Lakes may have the potential to intensify snowfall by orographic lifting (Lansing, 1964).

In eastern North America, snowfall is greatly influenced by air masses which originate in the arctic and travel down the Atlantic coast of Canada and the United States, thereby depositing large amounts of snow (Hartley and Keables, 1998). Hartley (1997) postulated that a depression

in the sea surface temperature of the Atlantic Ocean off the coast of New England might cause an increase in the rate of snowfall on the nearby land surface due to a change in preferential storm paths taken by Atlantic storms. However, Trivett and Waterman (1980) point out that in the Saint John River Basin of Maine, New Brunswick, and Quebec, areas of the basin situated closer to the Bay of Fundy receive less snow due to the moderating effects of a large body of water on land surface temperatures, whereas the northern part of the basin has a greater snowfall rate. Further north, Adams and Rogerson (1968) acknowledge that the mean annual rate of snowfall at a site in Labrador is 33 cm yr^{-1}, and the frequency of snowfall is strongly associated with freezing of the nearby Hudson Bay since lessened rates of snowfall are observed during January, which is the month of maximum ice extent on this large body of water.

At a more local scale, the presence of a forest canopy has a moderating influence on the rate of snowfall within and outside of a forested area. Church (1912) suggested that a forest should be harvested in a "honeycombed" fashion to increase runoff during the time of ablation due to the additional snow trapped by this harvesting pattern. Golding and Swanson (1978) set up an experiment that resulted in a series of 10 circular forest clearings situated in an area of flat topography 40 km from Rocky Mountain House, Alberta. For this experiment, the clearing patterns were not systematic and did not resemble the pattern that had been proposed by Church (1912). The results of the Golding and Swanson (1978) experiment showed that more snow accumulated in the clearings between the trees due to lessened interception of snow caused by the lack of a forest canopy. Thus, SWE was greater in a forest that had been cut in this manner than in an area of uncut forest. Golding and Swanson (1978) also realized that increased turbulence caused by the clearing created discontinuity in the airflow over the forest canopy, thereby causing vertical deposition of snow and increasing the rate of snowfall in the clearings.

The largest amounts of SWE were found in clearings with diameters two times the mean tree heights of the forest, whereas the smallest amounts of SWE were found in clearings with diameters less than these distances. SWE in clearings with diameters greater than the two times height rule was found to have values intermediate between the amounts of SWE in the other two clearing diameters. Building on this prior research, Swanson and Golding (1982) created the forest that Church (1912) had envisioned. During the period of September 1977 to December 1979, Swanson and Golding (1982) systematically cut 2103 circular clearings in the Marmot Creek watershed in the Kananaskis Valley of Alberta. Swanson and Golding (1982) found that this particular application of the "honeycombed" treatment increased the accumulation of snow in the clearings of the watershed by 128%, compared to the control section of the watershed that was not subjected to the cuttings.

From observations in the boreal forest and consideration of a physically-based interception model, Hedstrom and Pomeroy (1998) noted that a decrease in interception efficiency occurs for an increase in the rate of snowfall, temperature, and the initial amount of snow present in the canopy. During rates of higher snowfall, more snow will reach the ground surface in forests where the trees are spaced a greater distance apart as opposed to a dense forest where individual trees are situated very closely together due to the higher probability of a snowflake being able to reach the sub-canopy ground surface by traversing the gaps between trees, given that the snowflake is falling vertically (Hedstrom and Pomeroy, 1998). An increased rate of elastic rebound of snow particles from the branch of the tree will also cause more snow to accumulate on the ground surface. Elastic rebound depends on the geometry of the snowflakes, which governs the ability of a falling snowflake to interlock with other snowflakes on the tree branch (Schmidt and Gluns, 1991). Higher windspeeds also have the potential to shake the

branch, thereby causing snow unloading (Pomeroy and Goodison, 1997). Lower temperatures ensure that the geometric structure of snowflakes are relatively well preserved, and metamorphic processes resulting in changes of the snowflake structure do not occur at high rates. This allows the snowflake to have a complicated geometry, which makes it more likely to interlock with other snowflakes on the tree branch, thereby causing an accumulation of snow in the canopy (Bunnell et al., 1985).

Interception can play a large role in preventing snow from reaching the ground surface. For example, Pomeroy et al. (1998) found that black spruce canopies could intercept 67% of annual snowfall. Interception efficiency also depends on the point of collision of the snowflake with the branch. Kobayashi (1987) found that at temperatures in the range of -3°C to 0°C, ice crystals were more cohesive, and the rate of elastic rebound decreased due to intermolecular forces associated with the formation of ice bonds between snowflakes (Langham, 1981). Higher temperatures also increase the bending efficiency of the tree branches due to the melting of ice crystals in the parenchyma cells of the branch, and this causes increased unloading of snow (Schmidt and Pomeroy, 1990). Snowflakes that fall near the edges of the branch are likely to be rebounded more effectively than snowflakes that fall on the branch at distances closer to the tree (Kobayashi, 1987). When branches become heavy from intercepted snow, the probability of unloading increases due to increased branch bending under the accumulated mass (Miller, 1966). However, interception and accumulation of snow is more efficient for tree species that have greater leaf area during the winter season, and consequently, a forest of coniferous trees tends to have greater interception efficiency of snow than forests comprised of deciduous species, which lose foliage during the snow season (Meiman, 1970). These interception processes occur at different scales within a forest. Pomeroy et al. (2002) found that

at the sub-stand scale, snow accumulation in clearings, the leaf area of a canopy, and the seasonal interception rate were not well correlated with the spatial variation of snow due to snow unloading and other processes such as wind transport. However, over the much larger spatial area of the stand scale, the amount of snow in clearings and the leaf area of the canopy were found by Pomeroy et al. (2002) to generally agree with the results of other researchers that were reported in the studies previously discussed in this section of the thesis.

1.4.2. The transport rate of snow *F*

The Red Book of Hergest (*Llyfr coch Hergest*), a medieval Welsh collection of stories and poetry compiled in the early 15th century (Parry, 1955), is quite possibly the oldest written text in western literature to speak of wind transported snow: "Mountain snow—the wind scatters it" (Skene, 1868: pg. 586; Book IV, Section CXIV). The many different manifestations of snow are still a prevalent part of the human psyche in Canada (Pomeroy and Goodison, 1997). Blowing snow is a major redistribution mechanism on the Canadian prairies. In Saskatchewan and in the High Arctic, 48% to 58% of snow deposited at a given location is redistributed by wind action (Pomeroy and Li, 2000). Approximately 77% of snow is redistributed on a fallow field in the Canadian prairies (Pomeroy and Gray, 1995). Stepphun and Gray (1978) reported that 2.6 tonnes m^{-1} to 21.5 tonnes m^{-1} of snow per annum is redistributed on the Canadian prairies over the distance of a uniform fetch. Pomeroy and Goodison (1997) refined this estimate for a number of geographical locations in Saskatchewan, noting that the annual transport rate ranges between 9 tonnes m^{-1} to 250 tonnes m^{-1}.

The initiation of blowing snow transport is dependent on the shear stress transferred to the surface of the snowpack, the partitioning of the shear stress applied to the snowpack and

vegetation layer, the ambient environmental temperature, and the shear strength of the snowpack surface (Pomeroy and Gray, 1995). Wind moving over the surface of the snowpack will dislodge a greater number of snow particles at higher wind speeds. This is because at high wind speeds, the shear stress of the wind transferred to the surface of the snowpack will be greater than the shear strength of the cohesive forces holding together the particles that comprise the erodable bed. Moreover, at higher temperatures approaching the melting point of ice (~0°C), the snow particles comprising the surface of the snowpack have greater cohesion, and this provides an impediment to the initiation of wind-transported snow. Threshold wind speeds for dry snow in the northern prairies is ~8 m s^{-1}, whereas for wet snow, the threshold wind speed is ~10 m s^{-1} (Li and Pomeroy, 1997a). When snow is dislodged from the snowpack at higher wind speeds, movement of the particles can be classified into three basic forms of transport: creep, saltation, and suspension (Pomeroy and Brun, 2001).

Creep is characterized by the movement of heavier particles that roll along the snow surface. Alternately, snow particles that move by saltation have typically less mass than the particles that move along the surface of the snowpack (Pomeroy and Gray, 1995). Snow occurs in suspension above the layer of saltating particles and the speed of transport is approximately the same as the magnitude of the average horizontal wind speed vector (Pomeroy and Brun, 2001). The rate of suspended snow transport is proportional to the fourth power of the wind speed (Pomeroy and Male, 1992). Approximately 75% of wind-transported snow is conveyed by suspension in the airflow, with the other remaining 25% moving by saltation or suspension (Pomeroy and Gray, 1990). Wind speed during blowing snow events generally has a logarithmic distribution above the land surface (Budd et al., 1966; Schmidt, 1982). The mass concentration of snow tends to decrease with height (Shiotani and Arai, 1953), but mass flux increases with

height due to greater wind speeds at higher distances above the ground surface. As the wind speed progressively increases, snow particles undergo movement by successively passing through the stages of creep, saltation, and suspension, with the final stage (suspension) being indicative of wind speeds capable of sustaining particulate matter in the airflow (Pomeroy and Brun, 2001). The suspension height of snow tends to be higher over rough land surfaces than smooth land surfaces due to increased turbulence and wind speed. The motion of saltating particles near the snow surface also contributes to the apparent surface roughness during blowing snow events (Pomeroy et al., 1993). However, the transport of snow over rough land surfaces is relatively inefficient, and greater rates of transport can be observed for smooth land surfaces such as wind-packed snow (Pomeroy and Brun, 2001).

Burkard et al. (1991) note that an increase in surface roughness is proportional to the amount of snow that will be deposited at a given location on the landscape; rougher surfaces will have a greater snowdepth, and vice versa. This is because the roughness of the surface creates more turbulence which causes the snow to drop out of the airflow due to a reduction in the amount of wind energy available for transport. Golding and Swanson (1978) realized that turbulence and windspeed increased in forest clearings, thereby causing more variable rates of snow redistribution and greater snow depths in the clearings. Alternately, Pomeroy et al. (1997a) found that in the Prince Albert Model Forest of Saskatchewan, it is possible for clearings on the scale of 100 m to have the same amount of snow as clearings spanning distances of kilometers due to low wind speeds, low rates of sublimation, and the presence of vegetation and stumps that help to retain snow cover. Vegetation inhibits the movement of blowing snow by increasing surface roughness and providing an impediment to snow movement by trapping particles in transport. Gray (1979) found that SWE on a brush-covered hillslope is ten times greater than a

hillslope that is not covered by brush. Sturm et al. (2001) showed that when moving from graminoid to shrum tundra, the vegetation will be higher, more snow will be trapped, and 10% to 25% more runoff could occur. The observation that an increased vegetation height leads to increased trapping efficiency agrees with van der Kamp et al. (2003), who showed that brome grass and stubble trapped similar amounts of SWE at the St. Denis National Wildlife Area near the city of Saskatoon, Saskatchewan. However, Essery and Pomeroy (2004) found that in the Trail Valley Creek watershed, an increase in shrub height will increase the trapped depth of snow, but snow depth will decrease in an area of vegetation given a reduction in the amount of snow available for transport. Thus, geographic areas with a lower snowfall rate will have less snow available for wind transport. Moreover, Pomeroy et al. (2005) recognized that snow accumulation is not simply related to shrub height; factors such as shrub species and the snow depth before the initiation of transport also affect the amount of snow that remains trapped by vegetation. Moreover, when snow depth is greater than the height of vegetation, transport is encouraged due to a reduction in surface element roughness caused by the smooth snow surface. This is also the reason why blowing snow transport tends to occur later in the snow accumulation season on a stubble field than on a fallow field. On the fallow field, snow must fill in the gaps between vegetation for more effective transport to occur.

Essery (2001) observed that the probability distribution of windflow is matched with terrain gradients. Thus, the influence of topography can play a large role in increasing the spatial variability of snow distribution in complex terrain. In the Wolf Creek Basin, Yukon Territories, Pomeroy et al. (1999) found that twice the amount of snow is lost from alpine terrain than from shrub tundra. Marks et al. (2002) note that in some wind-exposed areas of the mountains, nearly all of the snow can be lost due to wind transport prior to the time of ablation. Rhea and Grant

(1974) found that in the Rocky Mountains of Colorado, the deposition of snow was spatially associated with a change in slope that occurred 20 km upwind of the study site, thereby indicating that complex topography can have unusual effects on the wind transport and deposition of snow. Turbulence and the resulting reduction of wind speed in the lee of an obstacle such as a sharp mountain ridge can create depositional features such as snow cornices (Föhn and Meister, 1983) or accumulations of snow around an object in the shape of a "horseshoe vortex" (Kind, 1981). In areas such as the gully of a creek near the city of Regina, Saskatchewan (McKay, 1970), or in the valley bottom situated upwind of an arctic tundra plateau (Pomeroy and Gray, 1995) an increased rate of snow accumulation tends to occur due to increased turbulence and a local reduction in windspeed. Kind (1981) has pointed out that when blowing snow passes over an obstruction such as a hill or a ridge, greater snow deposition will occur in the lee of slopes that are more perpendicular, as compared to slopes that are relatively smooth and do not encourage flow separation. In areas where obstructions are few and the topography is relatively flat, an increase in the fetch will cause a resulting increase in the transport rate of snow up to a distance of 300 m for low wind speeds, and up to a distance of 1000 m for locations with high wind speeds. The transport rate of snow remains constant after 300 m distance for the low wind speed regime. Alternately, for the high wind speed regime, snow transport decreases for fetches exceeding 1000 m (Pomeroy et al., 1993).

1.4.3. Sublimation due to blowing snow E_B

The sublimation of snow while in transport is an important but often overlooked aspect of the blowing snow phenomenon (Pomeroy et al., 1998). Water vapour from sublimated snow represents a loss of SWE that occurs over a given fetch distance. Less SWE is lost due to

sublimation over a smaller fetch, as compared to a fetch that spans a greater distance. For example, Bowling et al. (2004) found that more sublimation occurs on the Arctic coastal Plain than in the foothills of the Brooks Range due to larger fetches. Pomeroy and Gray (1995) found that the sublimation of blowing snow in transport could exceed five times the amount of snow removed by saltation and suspension over the distance of a 1 km fetch. Blowing snow fluxes beyond a 1 km fetch tend to decrease with increasing flux distance due to the amount of snow lost to sublimation (Pomeroy and Goodison, 1997). Pomeroy and Essery (1999) showed that sublimation rates ranging between 1.2 mm day^{-1} and 1.8 mm day^{-1} could be observed during blowing snow events on the western Prairies of Canada. Sublimation occurs for 28% of snowfall in the western Canadian Arctic (Pomeroy et al., 1997b). Pomeroy and Marsh (1997) estimated that approximately 31% of annual snowfall in the arctic is lost to the atmosphere due to sublimation during blowing snow events. Déry and Yau (2001) showed that accounting for sublimation during blowing snow improved the output of an atmospheric model applied to the Trail Valley Creek watershed. Although Harazono et al. (2002) observed that sensible and latent heat fluxes of 270 W m^{-2} and 320 W m^{-2} could be present during blowing snow events, fluxes of latent heat during blowing snow events over sea ice were reported to be much smaller (~10-20 W m^{-1}) by Savelyev et al. (2006).

The effects of environmental factors on the sublimation due to blowing snow were examined by Pomeroy and Gray (1994). An increase in relative humidity tends to increase the mass flux of transported snow due to a decrease in sublimation which thereby allows for more snow to be transported as particulate matter by the wind. An increase in wind speed causes an increase in sublimation due to the additional amount of turbulent wind energy available for phase changes. However, temperature does not have a simple relationship with the amount of

sublimation that occurs during blowing snow events. Increased sublimation tends to occur at lower air temperatures because of the higher turbulent kinetic energy caused by the greater number of particles present in the transported wind flow due to reduced cohesion of the erodable bed of particles comprising the surface of the snowpack.

1.4.4. Sublimation at the Surface of the Snowpack *E*

In the lee of the Rocky Mountains, adiabatic heating of air masses results in the production of warm seasonal winds referred to as "Chinooks," which are often responsible for the advection of sensible heat to the surface of the snowpack, thereby causing sublimation to occur (Nkemdirim, 1991a; 1991b). In other cold regions of Canada, the physical processes of sublimation also contribute to changes in the mass balance of snow. For example, Pomeroy et al. (1997b) concluded that in the low Arctic, 28% of seasonal snowfall could be removed from the tundra land surface by the process of sublimation. Uneven heating of the land surface due to differences in albedo causes the horizontal transport of sensible heat between snow-covered and snow-free areas. Advection of sensible heat from snow-free areas can be greater in magnitude than energy provided to the surface of the snowpack by insolation (Neumann and Marsh, 1998). The advected sensible heat energy can be modelled as a power function of the fractal geometry of snowpack area (Granger et al., 2002). Moreover, snowpacks adjacent to a rough field will have energy advected at a much quicker rate due to enhanced growth of a boundary layer upwind of the patch (Granger et al., 2006). Many of these processes associated with the sublimation of snow has been modelled by Essery et al. (2006) using a numerically-stable algorithm.

Vegetation tends to have an effect on the sublimation of snow. Pomeroy et al. (2005) found that an increase in the height of shrubs above the surface of the snowpack will decrease

sublimation fluxes due to a reduction in turbulent transfer under the shrub canopy and the small contributions of sublimation from the branches of the shrubs. The forest canopy can also shelter snow from insolation (Price, 1988). For example, the "honeycombed" forest of Church (1912) was intended to prevent sublimation from occurring during the winter months by allowing the trees to reduce the amount of insolation incident on the surface of the snowpack. However, Golding and Swanson (1978) remark that sensible heat advected to the land surface by the Alberta Chinook can cause a loss of 400 mm of SWE in forest clearings. Alternately, a large amount of snow intercepted by the canopy of a forest tends to be sublimated. Pomeroy et al. (1998) found that seasonal sublimation losses from the canopy in the boreal forest could range from as small as 13% in an aspen-spruce mixed-wood stand to 40% in a spruce stand of high density. The finding of higher sublimation loss due to interception by a spruce stand is in agreement with the study by Lundberg and Koivusalo (2003) which was conducted in Finland. Sublimation of snow from the canopy tends to widely vary with geographic area and climatic region (Pomeroy and Gray, 1995).

1.4.5. The Rate of Snowmelt *M*

The rate of snowmelt influences the spatial distribution of SWE in a temporal fashion over the ablation period. An increase in insolation and rising temperatures is generally coincident with melting of the seasonal snowpack (Marsh and Pomeroy, 1996; Marks et al., 2002). A number of other environmental factors can also influence the rate at which snow undergoes ablation. Iacozza and Barber (2001) found that the snowmelt rate for snow overlying Arctic sea ice was influenced by snow depth, with consistent melt rates exhibited for snow with depths greater than 16 cm. For snowpacks with depths less than 16 cm, the melt rate was more

variable due to differences in surface albedo associated with shallow snow. This finding is in agreement with Marsh and Pomeroy (1996), who found at an arctic forest-tundra site that the contribution of meltwater to runoff is often spatially variable due to the retention of meltwater by the snowpack and consequently, the release of meltwater will occur at a later time on deep drift snowcovers. The presence of vegetation protruding above the surface of the snowpack lowers the albedo of the snow surface, thereby increasing the rate of snowmelt. Uneven heating of the stalks of vegetation protruding above the snowpack can also encourage snowmelt processes. The spatial variability of melt in an area of buried vegetation changes over the snow ablation season due to "spring up" of shrubs as snow is gradually removed during ablation (Pomeroy et al., 2005).

In high latitude environments where shortwave radiation fluxes are small due to low solar elevation and increased atmospheric path length, longwave emission from the sky and surrounding snow-covered landscape can contribute more radiation to snowmelt processes than shortwave radiation from insolation (Sicart et al., 2006). In general, south-facing slopes tend to have less SWE than north-facing slopes due to a greater receipt of solar radiation. Pohl and Marsh (2006) found that north-facing and south-facing slopes can have a difference of 32 mm of SWE. Slopes that face at a perpendicular angle to the rays of the sun have a greater snowmelt rate than slopes with smaller angles. However, due to cloudy conditions and an uneven spatial distribution of radiation and surface energy fluxes, it is possible for snowpack ablation to be similar between the bottom of a valley and a north-facing slope (Pomeroy et al., 2003). Alternately, north-facing slopes can have enhanced snowmelt due to reflection of longwave radiation from south-facing slopes with less snow and higher albedo (Sicart et al., 2006).

Pomeroy and Granger (1997) found that snowmelt increases with the size of clearings in a forest due to increased exposure of the snow to radiation and turbulent heat fluxes. Melloh et al. (2002) reported that although the albedo of the snowpack was higher under the canopy of a forest as compared to an adjacent clearing, the rate of snowmelt was greater in the clearing than under the canopy due to the effects of insolation. Alternately, Pomeroy and Dion (1996) found that the net radiation balance beneath the canopy is not dependent on the albedo of the intercepted snow, but has a greater dependency on light extinction and LAI. These radiation effects are also prevalent in the vicinity of trees within the forest. Woo and Steer (1986) found that snow depth was reduced by 60% within 2 m of a tree trunk. This is caused by a reduction of shortwave radiation from the sun by canopy cover and longwave radiation fluxes from the tree trunk (Woo and Giesbrecht, 2000). Ablation of snow around a tree first occurs near the trunk, and then spreads outward, leaving a greater amount of SWE at larger distances from the tree (Faria et al., 2000). However, when the surface of the snowpack has a lower albedo due to the presence of forest litter, the rate of snowmelt of snow under the canopy can increase due to less radiation being reflected from the snow surface (Hardy et al., 2000). Sicart et al. (2004) found that positive values of net radiation were correlated with an increase in snowmelt. Net radiation does not decrease at some forest sites, even when the forest density is high. This is due to low solar elevations, low atmospheric emissivity, a dry regional climate, and a high snow albedo. Moreover, an increase in canopy density can provide enough longwave radiation to compensate for a decrease in incident shortwave radiation, thereby indicating that radiation fluxes are often more important than insolation in determining the spatial distribution of snowmelt.

1.5. Methods to Determine SWE

1.5.1. Introduction

To be able to characterize the spatial distribution of SWE, researchers use a number of methods to determine SWE at a given geographic area. The methods currently in operational use can be divided into two categories: (1) those that estimate SWE by the determination of snow depth or density; and (2) those that estimate SWE without the determination of snow depth or density. These methods are closely related with devices used for the collection of data.

1.5.2. Devices that Determine SWE by Snow Depth or Density

1.5.2.1. Snow Ruler

The snow ruler is a simple device that consists of a graduated stick used to find the distance from the ground surface to the top of the snowpack (Goodison et al., 1981). The depth of snow is then related to snow density by the use of an empirical relationship (Steppuhn, 1976). When a large number of snow depth samples are required, it is possible to use a device that automatically records the depth of snow. The device developed by Sturm and Holmgren (1999) determines snow depth by the use of a pole inserted into the snowpack. The depth of snow is found by the use of a sliding attachment, the position of which is recorded with an accuracy of ± 0.5 cm by a portable datalogger placed in a backpack. To signal the start of a sample, the observer presses a button mounted on the pole. Such a device is characterized for operation down to temperatures of -30°C, and approximately 200 measurements can be taken within only ten minutes (Sturm, 1999).

Despite the fact that such a device allows for the determination of snow depth within a very short period of time, snow depth and density are required for estimating SWE. Relationships between snow depth and density are complicated due to the influence of thermal

effects and compaction, the processes of which serve to increase the density of the snowpack immediately after snow has been deposited on the ground surface. The correlation between snow depth and SWE increases for snowpacks with a greater depth due to an increase in the density caused by compaction of snow situated closer to the ground surface by the weight of the overlying snow layers (Pomeroy and Gray, 1995). The estimation accuracy of SWE can be improved by determining the density of the snowpack, which is also generally found by the use of invasive devices.

1.5.2.2. Density by Gravimetric Sampling

The density of the snowpack has been found in an invasive manner by the extraction of a snow sample. Concomitant measurements of snow depth can then be taken to determine SWE. One of the more accurate techniques for determining snow density is gravimetric sampling, which involves the weighing of samples taken from the snowpack. However, the creation of a snowpit and the associated extraction of snow samples is a time-consuming and tedious process. Sampling must be performed in a careful manner to ensure that snow is not lost from the scoop when it is extracted from the side of the snowpit. As an alternative, another device capable of determining SWE is the snow tube, invented by Church (1933). The snow tube is used to take a sample of the snowpack in a fashion perpendicular to the deposited layers of snow (Pomeroy and Gray, 1995).

The snow tube is a metal pipe with a serrated cutting end. For shallow snowpacks with a depth smaller than the length of the pipe, the snow tube is simply inserted through the snow surface until the ground is reached. The tube is then twisted by the use of a pair of handling grips mounted on the side of the tube situated closest to the investigator. On some versions of this device, the handle can be removed so that the snow collected inside of the tube is easily

extracted. The twisting causes the serrated cutting end to extract a small plug of soil from the ground, which serves to hold the snow inside of the tube when the sample is removed from the snowpack (Dingman, 2001). Care must be taken to ensure that loss of snow does not occur at the bottom of the tube. The presence of vegetation or depth hoar near the base of the snowpack can also cause the loss of snow from the bottom of the tube (Pomeroy and Gray, 1995).

1.5.2.3. Radar

Radar is a form of remote sensing that is commonly used to determine the distance between two objects by the reflection of an electromagnetic wave. The electromagnetic wave is reflected due to a change in dielectric constant between air and an object. One type of radar is monopulse radar, which involves the production of a finite-duration pulse at a fixed frequency. The pulse is then transmitted by an antenna toward the object. An alternate application of radar technology is Frequency-Modulated Continuous-Wave (FMCW) radar (Luck, 1949; Stove, 1992). Both of these devices are examples of active radar, which is a technology associated with the transmission of a pulse or series of pulses toward a reflective object. Active radar is to be contrasted with passive techniques involving the detection of electromagnetic radiation in the MHz to GHz range. In this sense, passive radar does not require the production of a pulse, and the associated processing circuitry is only used to receive electromagnetic signals in the same frequency spectrum (Skolnik, 1990).

A major challenge exists in the application of single pulse radar to determining the depth and density of layered media. Because a single pulse is sent from the antenna, the pulse must be of duration less than the time taken for the signal to propagate through the layer. If the pulse has a greater duration, reflection will occur in a complex manner due to the overlap of reflections between successive interfaces. The detection of smaller pulses necessitates the sampling of the

received signal at a higher frequency by an Analog-to-Digital Converter (ADC). However, in the context of radar, this requires ADCs that operate at sampling frequencies in the MHz to GHz range. Due to a technological limitation on the sampling rate of ADCs that are currently available, and also due to the high cost and low availability of ADCs that sample at higher frequencies (Marshall et al., 2004), alternate radar devices (such as FMCW radar) have been used to determine snow depth and snowpack stratigraphy (Ellerbruck and Boyne, 1979; Gubler and Hiller, 1984).

FMCW radar is a specialized form of radar which originated in the 1930s (Luck, 1949). This form of radar consists of a system where two horn antennas are situated above the snowpack. A continuous signal is sent from the antenna serving as the transmitter. The signal is swept in a linear fashion between two frequencies, with one frequency situated higher or lower than the other. The accuracy of depth estimates depends on the linearity of the sweep with respect to time. Propagating through the snowpack, the signal is reflected at each of the layers due to changes in electrical permittivity. Consequently, the signal reflected from the layers in the snowpack is returned to the receiving antenna, where it is mixed with the signal being sent out from the transmitter. The mixing can occur by the use of an analog circuit (i.e. Maas, 1986) or by the use of a circulator which enables only one horn to be used for the transmitting and receiving of the pulse (i.e. Arcone, 1997). Once the two signals have been mixed, the resulting signal is low-pass filtered and then taken into the frequency domain by the use of an algorithm such as the Fast Fourier Transform (FFT). Other spectral analysis techniques can also be used (i.e. Orfanidis, 1988). A resulting series of peaks will be observed in the frequency spectrum. Each of the peaks corresponds to a reflection at the interface between the layers in the snowpack. The frequency spectrum is proportional to the depth beneath the surface of the snowpack.

However, to determine depth, either (i) the real part of the snow dielectric constant; (ii) the index of refraction; or (iii) the density of the snow must be known. Thus, FMCW radar has shown utility in determining either the depth of the snowpack or its density, but not both.

Some investigators have attempted to use a compromise so that the structure of the snowpack can be determined by the use of FMCW radar. Ellerbruch and Boyne (1980) related the mean snow density of the snowpack to the dielectric constant of snow so that the depth of snow could be determined. Gubler and Hiller (1984) determined the depth of snow by the use of an ultrasonic snow depth gauge so that SWE could be calculated using density estimates from a stationary FMCW device situated beneath the snowpack. Alternately, for a portable FMCW device on skis, Gubler and Hiller (1984) measured the mean density of the snowpack so that the depth to the layers could be determined. Koh (1993) used the real part of the snowpack's mean dielectric constant so that the frequency spectrum axis could be scaled with respect to depth. Marshall (2004) determined that lower radar frequencies ranging from 4.0-8.0 GHz would be able to penetrate the snowpack to greater depth than higher radar frequencies in the range of 12.5-18.0 GHz. However, Marshall (2004) found that the higher frequencies were able to better resolve finely-structured layers within the snowpack. Yankielun et al. (2004) used a ski gondola to convey an FMCW device up the side of Mammoth Mountain, California. Estimates of snow depth were determined from the radar by measuring the density of the snow beneath the gondola track via gravimetric sampling. The density of the snow was then related to the index of refraction between the layers in the snowpack. Most of these investigators found that in the same manner as Koh et al. (2002), the presence of water attenuated the electromagnetic signal. This caused extreme reductions in the amplitude of the reflected signal, and as a result, the

interfaces between layers in the snowpack situated closer to the ground surface (and further away from the receiving antenna) could not be resolved.

1.5.2.4. Acoustic Depth Gauge

An acoustic depth gauge consists of an ultrasonic transducer positioned at a distance above the snowpack. In an operational context, such a device is attached to the mast of a meteorological station and the transducer is situated perpendicular to the snow surface. In this sense, the acoustic depth gauge is a stationary instrument which is used to determine the depth of snow that has been deposited on the ground surface. Because the height of the transducer above the ground surface is known by the investigator, the distance to the top of the snowpack can be measured by determining the time that a finite acoustic impulse takes to travel to the snow surface. Concomitant measurements of the speed of sound in air by a thermocouple or an electronic thermometer with an embedded microcontroller allows the distance to the snowpack (as measured from the transducer) to be determined by the use of simple kinematics (Gubler, 1981). One major difficulty with this method is that for snowpacks with a light layer of low-density surface snow, the acoustic pulse can propagate through the snow surface, thereby measuring the distance to the next acoustically-hard surface. However, in the same manner as the snow ruler, the SWE can be estimated by the use of an empirical relationship because measurements of density are not available. The first use of such a device was by researchers affiliated with the Department of Physics at the University of Saskatchewan in the 1970s, yet other investigators such as Gubler (1981), Goodison et al. (1984), and Goodison et al. (1988) have replicated this technique.

1.5.2.5. Images in the Visible Light Spectrum

Images in the visible light spectrum are also used to determine the depth of snow so that SWE can be estimated by the use of an empirical relationship. Such techniques have taken two different forms. (1) One form of these techniques uses the reflectance of the snowpack in the visible light spectrum to determine snow depth (Donald et al., 1991). An empirical relationship utilizing snow reflectance is then used to determine the depth of snow on the ground surface. However, this technique works best for shallow snowpacks with a depth of less than 20 cm. In a similar fashion, the Snow Covered Area (SCA) can be determined from visible imagery by the use of an algorithm (i.e. Metsämäkia et al., 2002; Wang et al., 2005). However, the SCA must then be related to the SWE by the use of an empirical equation. Snow depth can also be determined by photogrammetry (Otake, 1980), where two offset images of the study area taken during (i) the snow-free season and (ii) during the snow season are used in conjunction with a triangulation algorithm to determine snow depth. However, in the same manner as other visible light spectrum images, it is not possible to directly estimate the density (and hence the SWE).

1.5.3. Devices that Determine SWE without Estimating Snow Depth or Density

1.5.3.1. Snow Pillow

The snow pillow is a large device used for determining the mass of snow that has been deposited on the ground surface. Installed during the snow-free season, the snow pillow is a fluid-filled pouch which is permanently situated at a field site. This makes the snow pillow efficient for monitoring SWE at locations that are not readily accessible during the winter. The fluid that fills the pillow has a low freezing point to ensure that the device remains operational during cold temperatures. Displacement of the fluid by the overlying snow is determined by the

use of a manometer. Alternately, a pressure transducer can be placed inside of the pillow so that the weight of snow can be detected and recorded by a datalogger. As noted by Granberg and Kingsbury (1984), a variation on the snow pillow was proposed by researchers working at the Cold Regions Research and Engineering Laboratory (CRREL). The CRREL researchers placed load cells at the three apexes of a triangular platform situated a short distance above the ground. This eliminated some of the difficulties associated with the presence of a large pouch filled with fluid, but as Granberg and Kingsbury (1984) note, fluxes of heat and moisture were still exchanged between the elevated snow pillow and the ground surface. However, despite most snow pillows being made out of a durable plastic or synthetic rubber material, the potential for leaks in the plastic material of the snow pillow still exists. Thermal expansion of the antifreeze fluid or the entrapment of air can also cause rupture of the snow pillow or artificial displacement of the liquid. Such devices are also destroyed by animals (Engman, 1966). Moreover, ice layers or the presence of a snow pack undergoing ablation can affect the determination of mass (Pomeroy and Gray, 1995). Johnson and Marks (2004) recognized that when the rate of snowmelt is greater on the surrounding land surface than on the snow pillow, more snow is left on the top of the pillow, thereby causing a measurement error. The detection and correction of these errors has been examined by Johnson and Marks (2004).

1.5.3.2. Passive Microwave Radiation

Because the surface of the earth emits longwave radiation, changes in the emissivity of the land surface due to the complex dielectric scattering coefficient can be readily discerned by the use of an instrument similar to a radiometer. Since the emissivity of snow is less than the emissivity of the earth, snow covered area can be identified. By the use of an empirical algorithm, the SWE can be estimated from the energy detected by the radiometer

(Cork and Loijens, 1980; Carroll, 1987). An example of this technique is the study by Goodison and Walker (1995), which resulted in an algorithm for identifying SWE over prairie landscapes. Four caveats of this approach is (1) new algorithms relating brightness to SWE need to be developed for different geographic areas; (2) the resolution is limited to a large area spanning 100 m if the radiometer is mounted on an aircraft, or alternately, a resolution of 20 km if the observations are taken from a satellite (Pomeroy and Gray, 1995); and (3) SWE cannot be easily determined in forests by the use of passive microwave radiation (i.e. Hall et al, 1993), but some newer methods have shown promise in overcoming this limitation (Goita et al., 2003).

1.5.3.3. Gamma Radiation

In the same manner as detecting gamma radiation by the use of a semi-invasive device, the measurement of SWE by the use of a non-invasive instrument entails observing the attenuation of ionizing radiation by the snow cover. This requires two separate flights to be made on an aircraft over the study area. The first flight is conducted during the late fall, when the ground is free of snow and a count of gamma radiation is naturally obtained. Radioactive decay which provides this background is due to isotopes such as ^{238}U and ^{40}K which occur naturally in the earth. On the second flight, which is conducted during the winter, the attenuated background radiation is recorded. The SWE is then found by an empirical relationship based on the attenuation of the radiation. However, this method is not appropriate for use in a forest or when the snowpack has a very deep depth. Both of these conditions serve to attenuate the small amounts of radiation that are detected. Moreover, the returned signals must be calibrated to remove the attenuation effects of other environmental radioactive sources such as radon (Pomeroy and Gray, 1995).

1.5.4. Conclusions: Current Devices that Determine SWE

The survey presented above gives an overview of the deployment and limitations of devices that are currently used in an operational context to determine SWE. Implicit in this overview are two major caveats associated with such devices. (1) First, most devices used to determine SWE involve the use of destructive sampling. These devices are tedious to use, and are not easy to deploy at remote field locations. (2) Second, devices which use some sort of pulse to determine SWE require (i) other invasive measurements; or (ii) empirical relationships particular to a certain geographical location. Because SWE is generally determined by gravimetric sampling, the use of semi-invasive devices is rarely justified, and it is conceivable that SWE is more efficiently determined by the use of invasive devices, despite the fact that such an approach is tedious. Thus, it would be beneficial if a non-invasive device could determine SWE by giving estimates of snow depth and density. It is the contention of this thesis that an acoustic pulse passing through a layered snowpack can be used to determine estimates of these quantities.

1.6. Prior Work in Snow Acoustics

To place this thesis in the context of past developments, a brief overview is given of research that has examined the propagation of sound through snow. The development of snow acoustics research can be considered in terms of the instrumentation used by investigators. Some of the early work in snow acoustics consisted of qualitative observations of the effect of snow on the propagation of sound in natural environments (Seligman, 1939; Kaye and Evans, 1939; Colliander, 1954; Krasser, 1967). Quantitative research conducted on snow acoustics has involved the use of three different types of instruments or experimental setups: (1) an acoustic impedance tube; (2) a cylinder used to examine the propagation of a pulse through a sample of

snow extracted from the snowpack; and microphones or geophones placed either (3) above or (4) below the surface of the snowpack to capture a sound wave that has been reflected from or transmitted through the surface of the snowpack. It is important to note that nearly all of these investigators have disrupted the natural structure of the deposited snow while taking acoustic measurements.

1.6.1. Acoustic Impedance Tube Measurements

The theory of an acoustic impedance tube is discussed by authors such as Blackstock (2000) and Raichel (2000). The purpose of such an apparatus is to measure the acoustic impedance $\xi = \rho c$ of a material, which is normally defined as the mathematical product of the density ρ (kg m^{-3}) of the material and the speed of sound c (m s^{-1}) in the material. This definition of acoustic impedance is modified in a later section of this thesis for snow as a porous material. The experimental setup consists of a tube, at the end of which is situated a loudspeaker. A sample of a substance is placed at the opposite end of the tube, and a broadband pulse is then sent from the loudspeaker into the tube. This creates a standing wave in the tube. A probe microphone is either pulled along the inside of the tube, or alternately, two microphones are used to measure the pressure standing wave ratio (SWR), which is the ratio of the maximum value of the pressure in the tube to the minimum value of the pressure created by the standing wave. The SWR is then related to the density ρ and the pressure refection coefficient Γ of the material. The pressure reflection coefficient is the ratio of the reflected pressure of the sound wave to the pressure of the sound wave that is incident on the material situated at the end of the tube. From these measurements, the acoustic impedance of the material is determined.

Oura (1952a, 1952b) removed samples of snow from the snowpack and placed the samples into an impedance tube. From these experiments, Oura (1952a, 1952b) was able to conclude that snow removed from the snowpack attenuated most of the incident sound waves. Takada et al. (1954) also arrived at this same conclusion. Aside from conducting experiments with a closed tube of a fixed length, Ishida (1965) also adjusted the length of the tube to use resonance as a means to determine the acoustic impedance of snow. Ishida (1965) determined from his experiments that the impedance of fresh snow is less than the impedance of compressed snow, and that the phase velocity of a sound wave in snow continues to increase with increasing frequency, eventually approaching the speed of sound in air. Impedance tube measurements were also made by Buser (1986), who found that as a porous material, the structural framework of snow could be considered as having a rigid frame.

1.6.2. Measurements Involving a Cylinder

Investigators have also used a cylinder to extract a sample of snow from the snowpack. An acoustic pulse was sent through the cylinder to examine the phase velocity of sound in the sample. Bogorodskii and Dobrotin (1963) measured the time taken for an ultrasonic pulse to propagate through a 30 cm sample of snow. The acoustic pulse was sent from a transducer situated at one end of the cylinder, whereas another transducer situated at the other end of the cylinder received the transmitted pulse. By examining the time of flight of the pulses, it was possible for Bogorodskii and Dobrotin (1963) to measure the speed of sound in snow. Using a similar method, Bogorodskii et al. (1974) were able to determine that sound in the ultrasonic frequency range can pass through snow.

Smith (1965) and Smith (1969) used a similar technique to investigate the acoustic properties of snow on the Greenland Ice Sheet. Smith (1965) extracted snow samples from a snow drift and placed the samples between two piezoelectric transducers. A pulse was sent from one of the transducers, and time-of-flight measurements were used to determine the phase velocity of the sound pulse in the snow sample. An empirical relationship was then used to relate the measured density of the snow sample to the phase velocity of sound in the snowpack. Smith (1969) extracted samples of snow from the walls of a trench and cut the samples in the shape of a cylinder. Two transducers with operating frequencies in the range of 0.4 to 5000 Hz were fastened to the ends of the snow cylinder, and the snow cylinder was vibrated in a vertical fashion using a vibration table. The vibration frequency was adjusted until resonance occurred in the sample. This procedure was used to determine the complex moduli and Poisson's ratio of the snow samples.

1.6.3. Devices Deployed Below the Snow Surface

Measurement devices placed below the surface of the snowpack have been used to find the physical properties of snow. Oura (1952b) buried two microphones beneath the surface of the snowpack, and found that the phase velocity of propagation of sound in snow was less than the phase velocity of sound in the air. Ishida (1965) dug into a deep snowpack and created a reverberant "room" that was used to conduct transmission loss measurements on samples of snow. Moore et al. (1991) buried microphones beneath the surface of the snowpack, disrupting the snowpack stratigraphy. A loudspeaker situated above the surface of the snowpack radiated sound waves toward the snow surface. By the use of a rigid-porous model, Moore and

Attenborough (1991) found that it was possible to determine the porosity of snow with a measurement error of approximately 15%.

1.6.4. Devices Deployed Above the Snow Surface

Only a handful of researchers have explored the possibility of determining the properties of snow by the use of non-invasive acoustic techniques. Lee and Rogers (1985) used a broadband frequency generator to produce a sound pulse above a 2 cm thick snow layer on a metal roof of a building. A microphone was used to capture the reflection of the sound pulse from the snow. Zarek's (1978) model was then applied by Lee and Rogers (1985) to determine the porosity of snow. The technique used to determine this quantity involved a procedure where a computer is used to generate an impulse similar to the recorded reflection. By an iterative approach, the parameters of Zarek's model were modified until the modelled reflection approximately matched the recorded reflection. Albert (1998a, 2001) used broadband acoustic waves produced by firing blanks from a .45 caliber pistol situated approximately 1 m above the snow surface. A linear array of geophones placed on the surface of the snowpack captured the wave that was reflected from the ground surface. By using a simplified version of Attenborough's (1985) model for sound propagation, Albert (1998a, 2001) was able to determine snow depth on a natural land surface to within approximately ±2 cm.

The technique described in this thesis can be placed in the same category of techniques utilized by Lee and Rogers (1985) as well as Albert (1998a, 2001). Albert (1993a) has acknowledged that physical disruption of the snow cover caused by the extraction of a sample may affect the acoustic properties of snow, and for this reason, measurements should be conducted above the snow surface. Takada (1954) found that sound is strongly attenuated by

snow, but the measurements used to arrive at this conclusion were taken using snow that had been removed from the snowpack. To circumvent this possible measuring difficulty, and for the reasons discussed in Section 1.5.4 above, the possibility of taking measurements above the snow surface was considered.

1.6.5. The Biot Theory and Snow

To be able to determine the physical properties of the snowpack using acoustics, a mathematical model can be used in the analysis of the reflected wave. Johnson (1982) was the first to apply the porous media acoustics theory of Biot (1956a, 1956b) to the propagation of sound through snow (Sommerfeld, 1982). It was assumed by Johnson (1982) that snow is a porous medium, comprised of air spaces and an ice structure composed of snow particles. The Biot theory is widely regarded as being one of the more accurate theories capable of describing the propagation of sound in porous media (Berryman, 1980). Johnson (1985) also examined the attenuation of sound in snow, showing that the magnitude of the transmission of an acoustic pressure wave into snow was much greater than the reflection of the pressure wave from the surface of the snowpack, thereby indicating that much of the sound from a source situated above the surface of the snowpack would travel across the air-snow boundary. The effects of this phenomenon, referred to as "acoustic-to-seismic coupling," were studied by Albert and Orcutt (1990), and Albert (1992). Although Albert (1998b) would later model the propagation of seismic waves in firn, these investigators were more concerned with the effect of snow on the propagation of sound above the surface of the snowpack. For example, Albert (1993a) applied the Biot (1956a, 1956b) theory to model the effects of snow on the attenuation of sound from a revolver. Albert (1993a, 1993b) also concluded that the ice matrix of the snowpack could be

taken as being rigid when modelling the propagation of sound through snow because it is the air pressure wave travelling in the pore spaces of the snowpack that has the greatest magnitude. Thus, Albert (1993b) concluded that it is possible to treat snow as a modified fluid if the propagation of energy in the ice matrix of the snowpack is not of interest.

The full Biot (1956a, 1956b) theory as applied by Johnson (1982) assumes that the snowpack is a porous medium consisting of an elastic framework that is saturated with air. Moreover, it is assumed (Johnson, 1982) that three types of sound waves (two longitudinal waves and one shear wave) are present in the snowpack. The two longitudinal waves have a compressional motion. One of the longitudinal waves travels in the ice matrix of the snowpack (which is referred to as the "first" longitudinal wave), whereas the other longitudinal wave (referred to as the "second" longitudinal wave) is a strongly-attenuated air pressure disturbance that propagates in the pore spaces. Both waves are coupled, in that there is transfer of momentum between the air spaces and the ice matrix of the snowpack. The phase velocity of the first longitudinal wave is often higher than the phase velocity of the second longitudinal wave (Albert, 1993a), but it is possible for either the first or the second longitudinal wave to travel faster or slower than the other. Because of this, the first longitudinal wave is referred to as the "fast wave," whereas the second dilatational wave is considered to be the "slow wave." Given the findings of Albert (1993a, 1993b), it is therefore possible to neglect the second longitudinal wave and the shear wave in a model of sound propagation in snow, focussing instead on the physics of the first longitudinal wave which propagates through the pore spaces of the medium.

2. THEORY

2.1. Introduction

In this section of the thesis, a conceptual model of the snowpack system is considered so that the reflection of an acoustic wave from the snowpack can be used to determine SWE. The Biot theory discussed in the previous section is adapted to this purpose in a novel fashion. Such an approach builds upon the established literature associated with the investigation of sound propagation in snow (Oura, 1952a; Oura, 1952b, Smith, 1965; Smith, 1969; Bogorodskii et al., 1974; Johnson, 1982; Sommerfeld, 1982) and the important conclusions made by Johnson (1982), Lee and Rogers (1985), Attenborough and Buser (1988) Moore et al. (1991), and Albert (2001) that sound can be successfully used to determine the physical properties of the snowpack.

2.2. Physical System

The snowpack is assumed to consist of a series of N layers $\{L_1,\ldots,L_N\}$, where $\{\Omega_1,\ldots,\Omega_N\}$ are the interfaces between the layers (Figure 2.1a). The interfaces are introduced as a conceptual construct and are assumed to be massless. Although it is conceivable that a velocity gradient might exist within some of the layers due to gradual changes in physical properties with increasing depth in the same manner as a layered earth (i.e. Kennett, 2001), it is assumed that the kinematics of a sound wave through the snowpack at normal incidence to the first interface Ω_1 is describable by the average phase velocity $\overline{c}_k$ in a specific layer L_k as it travels over the vertical dimension of the layer. Even if the phase velocity of the wave gradually changes over depth, it is impossible in the context of this experiment to obtain physical properties of the layers until there is a reflection of the pressure wave. The interface between two layers of the snowpack is

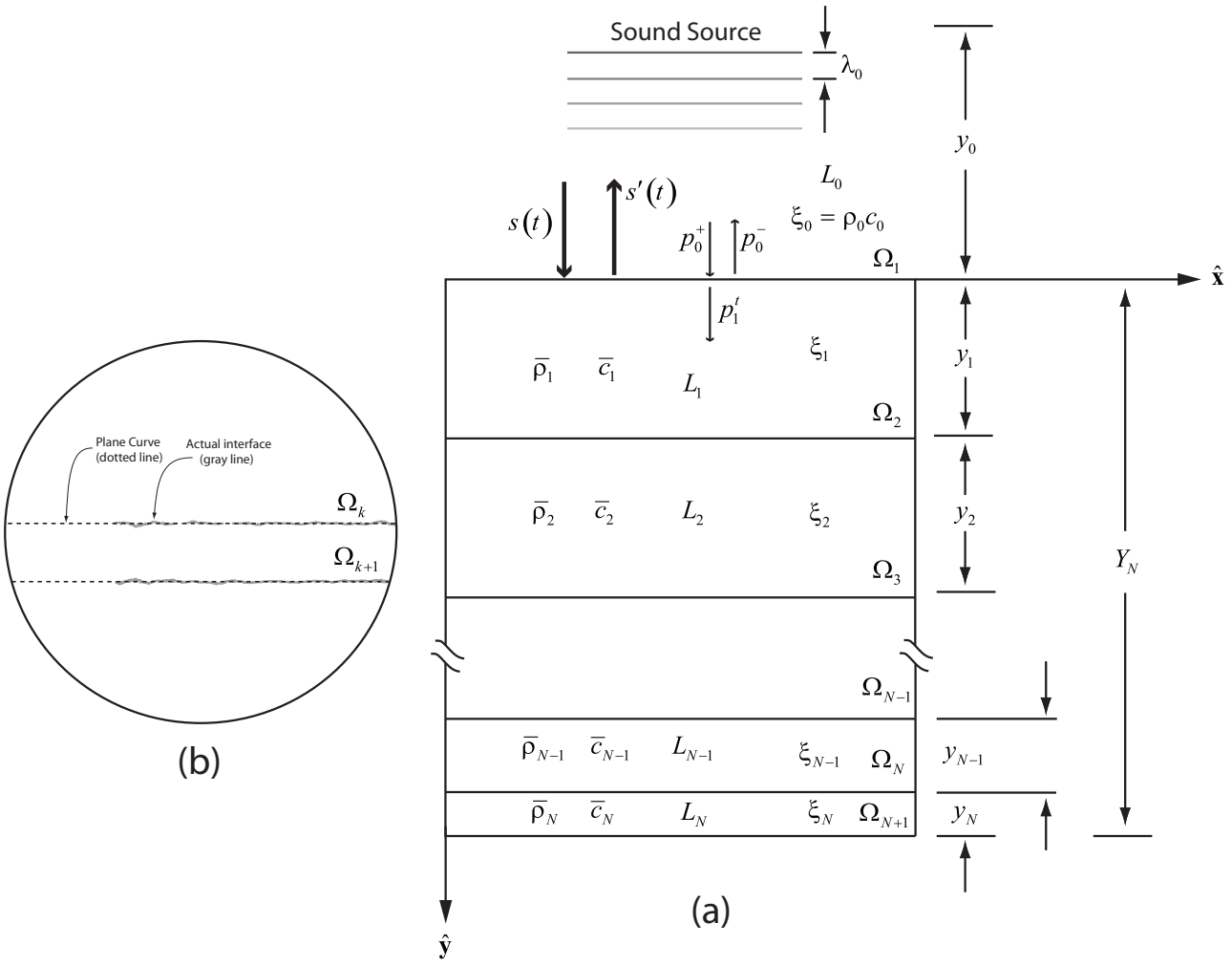

Figure 2.1. Conceptual diagram of the snowpack system. The wavelength of the sound source in the air layer L_0 above the surface of the snowpack is λ_0; the distance from the source to the surface of the snowpack is y_0; the acoustic impedance of the air layer is ξ_0; the acoustic impedance of the layers of the snowpack is $\{\xi_1,\ldots,\xi_N\}$; the equilibrium density of the air layer is ρ_0; the phase velocity of the sound wave in the air layer is c_0; the angular frequency of the plane wave source is ω; the frequency of the source is f; the original sound wave sent from the source is expressible as the continuous function $s(t)$; the overall reflection from the snowpack is $s'(t)$; the pressure of the acoustic wave arriving at the first interface of the snowpack is p_0^+; the pressure of the reflected wave is p_0^-; the pressure of the transmitted wave across the interface Ω_1 at the surface of the snowpack is p_1^t; the bulk density of the layer and speed of an acoustic impulse in a given layer L_k of the snowpack is $\overline{\rho}_k$ and $\overline{c}_k$, respectively; the vertical dimension of each of the layers is $\{y_0,\ldots y_N\}$, and the total cumulative depth of the snowpack is Y_N.

assumed to be a plane curve that represents the best-fit surface of the actual (undulating or rough) interface (Figure 2.1b). Although such a definition is not precise it strongly implies that an acoustic pressure wave traveling through the snowpack will be reflected at the interface between two layers due to a change in acoustic impedance ξ_k.

Consider an acoustic pressure wave with an angular frequency ω that originates in air at a height of y_0 above the surface of the snowpack. The air layer above the snowpack is considered to be layer L_0 in this physical system (Figure 2.1a). Assume that the wave radiates toward the snowpack in a positive direction that is perpendicular to the snow surface and parallel to the $\hat{\mathbf{y}}$-axis of the coordinate system. The distance y_0 is assumed to be sufficiently large such that when the pressure wave reaches the snow surface Ω_1 it can be assumed to be planar. The pressure fluctuations in the air layer above the snowpack transfer momentum to the snow structure and to the air in the pore spaces of the snow by means of acoustic-to-seismic coupling. Due to an impedance mismatch between the air and snow, the wave is reflected at the boundary. The boundary conditions for the pressure wave at the air-snow interface are:

$$p_0^+ + p_0^- = p_1^t \tag{2.1}$$

$$c_0^+ + c_0^- = p_1^t \;\Leftrightarrow\; \left(p_0^+ / \xi_0\right) + \left(p_0^- / \xi_0\right) = \left(p_1^t / \xi_0\right) \tag{2.2}$$

where the pressure of the air wave approaching the snow surface is p_0^+, the pressure of the reflected wave is p_0^-, the pressure of the wave that is transmitted into the snowpack is p_1^t, and the nomenclature is similarly defined for the phase velocity in the air layer. It is assumed that Eq. 2.1 and Eq. 2.2 are approximations when the sound source is situated at small angles to a line that is taken to be normal to the surface of the snowpack. Further research could be conducted to ascertain the effects of small angular deviation on the results of this method.

Dividing Eq. 2.1 by p_0^+ and recalling that the effective pressure reflection coefficient is defined by the ratio $\Gamma_1 = p_0^- / p_0^+$, it follows that:

$$\Gamma_1 = \frac{\xi_1 - \xi_0}{\xi_1 + \xi_0} \tag{2.3}$$

The next step is to find expressions for the acoustic impedances of air and snow.

Estimation of the acoustic impedance of a snow layer requires a measure of the tortuosity, which can be defined as the deviation from a straight line of a path through the connected pore space in a porous medium. Johnson et al. (1987) demonstrated that their theory is an extension of the work of Biot (1956a, 1956b) and therefore the constituent equations of the Biot theory can be taken as a special case. They conclude that their expression for the dynamic tortuosity $\alpha(\omega)$ can be applied in general to a fluid-saturated porous medium. In this context, the dynamic tortuosity is an approximation of the tortuosity that is determined by acoustics (rather than being determined by physical measurement), and as such, is dependent on the angular frequency ω of the incident sound wave. Building on the research of Johnson et al. (1987), Champoux and Allard (1991), and Lafarge et al. (1997), it was recognized by Umnova et al. (2005) that the real-valued acoustic impedance of a porous medium is:

$$\xi_1 = \frac{\rho_0 c_0 \sqrt{\alpha(\omega)}}{\phi} \tag{2.4}$$

Note that Eq. 2.4 is not normalized with respect to the characteristic impedance of air. Returning to Eq. 2.3, it follows that:

$$\Gamma_1 = \frac{\rho_0 c_0 \sqrt{\alpha_1(\omega)} - \phi \rho_0 c_0}{\rho_0 c_0 \sqrt{\alpha_1(\omega)} - \phi \rho_0 c_0} \tag{2.5}$$

and,

$$\phi_1 = \sqrt{\alpha_1(\omega)}\left(\frac{1-\Gamma_1}{1+\Gamma_1}\right) \tag{2.6}$$

Eq. 2.6 is also given by Umnova et al. (2005). An implicit assumption of Eq. 2.6 is that the porosity of the first snow layer can be calculated without knowledge of the characteristic acoustic impedance $\rho_0 c_0$ of the air layer above the snowpack or the acoustic impedance of the air-filled pore spaces of the snowpack.

Although snow is a dispersive (lossy) medium that strongly attenuates sound, it is assumed that the pressure wave travels through snow until a change in impedance is significant enough to cause a reflection at the interface Ω_2 between two layers L_1 and L_2 of the snowpack. Taking boundary conditions once again at this interface, the effective reflection coefficient is given by:

$$\Gamma_1 = \frac{\xi_2 - \xi_1}{\xi_2 + \xi_1} \tag{2.7}$$

$$\Gamma_1 = \frac{\phi_1\rho_0 c_0\sqrt{\alpha_2(\omega)} - \phi_2\rho_0 c_0\sqrt{\alpha_1(\omega)}}{\phi_1\rho_0 c_0\sqrt{\alpha_2(\omega)} + \phi_2\rho_0 c_0\sqrt{\alpha_1(\omega)}} \tag{2.8}$$

$$\phi_2 = \frac{\phi_1\sqrt{\alpha_2(\omega)}}{\sqrt{\alpha_1(\omega)}}\left(\frac{1-\Gamma_2}{1+\Gamma_2}\right) \tag{2.9}$$

Assuming that the wave continues traveling through the snowpack, it will be reflected at each successive boundary Ω_k until the energy in the pressure disturbance of the medium is dispersed. Thus, generalizing Eq. 2.9 for a particular boundary k :

$$\phi_k = \frac{\phi_{k-1}\sqrt{\alpha_k(\omega)}}{\sqrt{\alpha_{k-1}(\omega)}}\left(\frac{1-\Gamma_k}{1+\Gamma_k}\right) \tag{2.10}$$

Eq. 2.9 and 2.10 represent a means of calculating the porosity of a snow surface, given the dynamic tortuosity $\alpha_k(\omega)$ of each layer and the effective reflection coefficient Γ_k at the interface Ω_k between an air layer and a snow layer, or between a snow layer and another snow layer. It is assumed that the average porosity ϕ refers to the air-connected pore spaces in snow, following Moore et al. (1991) and Buser (1986). Based on thin section observations of snow, Buser (1986) notes that most of the spaces in snow are air-connected, and this assumption should be reasonable for snow of lower densities not approaching the density of glacial ice or firn (< 550 kg m^{-3}). Both equations involve two variables expressible as the set $\{\phi_k, \alpha_k(\omega)\}$. A relationship between these two variables, the porosity ϕ_k of a porous medium and the tortuosity α_k, was found by Berryman (1980) as a consequence of the Biot theory. Because the relationship found by Berryman (1980) is derived by manipulations of the constituent mathematics of the Biot theory, the assumptions of the Biot theory also hold for this equation. Johnson (1982) has shown that the Biot theory can be successfully applied to snow, and so this equation, by extension, can be applied in snow acoustics. Berryman (1980) noted that:

$$\alpha_k = 1 - \gamma\left(1 - \frac{1}{\phi}\right) \tag{2.11}$$

where γ is a shape factor dependent on the geometry of the particles comprising the porous medium. Berryman (1980, 1983) has proven that $\gamma = 1/2$ for spherical particles; alternately, Johnson and Sen (1981) have found that $\gamma = 3/4$ for randomly-oriented particles with a needle-like geometry. A later section of this thesis will present a sensitivity analysis of the model to variations in γ. Although the Berryman (1980) equation has not been applied in the past to characterize snow as a porous medium, it is used here in the context of this model to provide a

means for calculating the porosity of a porous medium. Although the Berryman (1980) equation may not be completely valid for snow, the equation is still useful in this application. Further work could be done to verify this relationship. Verification of the relationship would entail empirically fitting Eq. 2.11 to a dataset comprised of porosity and tortuosity measurements of snow.

Substituting Eq. 2.11 into Eqs. 2.6 and Eq. 2.10 yields two functions $\Phi\left(\Gamma_1, \phi_1\right) = 0$ and $\Phi\left(\Gamma_k, \phi_k\right) = 0$ that allow for the porosity of a layer L_k of the snowpack to be estimated by an iterative process, given a fixed numerical value for the effective reflection coefficient Γ_k:

$$\Phi\left(\Gamma_1, \phi_1\right) = \left(\frac{\phi_1 - \gamma\phi_1 + \gamma}{\phi_1}\right)^{1/2} - \frac{\phi_1\left(1+\Gamma_1\right)}{1-\Gamma_1} = 0 \tag{2.12}$$

$$\Phi\left(\Gamma_k, \phi_k\right) = \frac{\phi_{k-1}}{\sqrt{\alpha_{k-1}(\omega)}}\left(\frac{\phi_k - \gamma\phi_k + \gamma}{\phi_k}\right)^{1/2} - \frac{\phi_k\left(1+\Gamma_k\right)}{1-\Gamma_k} = 0 \tag{2.13}$$

The acoustic source is assumed to radiate plane waves parallel to the $\hat{\mathbf{y}}$-axis of the physical system with angular frequency $\omega = 2\pi f$. The pressure amplitude of the plane wave radiated from the source is represented in the time domain as a continuous function $s(t)$. In a similar fashion to FMCW radar, the pulse is frequency-swept in a linear fashion between two frequencies f_0 and f_1 (where $f_1 > f_0$) over a time of $\Delta t^* = t_1^* - t_0^*$ (where $t_1^* > t_0^*$). The sound wave changes frequency as $\partial f / \partial t$, radiates toward the snowpack and is reflected at the first interface Ω_1 (Figure 2.1a). The sound wave enters the snowpack and is reflected by the interfaces $\{\Omega_1, \ldots, \Omega_N\}$ that are associated with layers $\{L_1, \ldots, L_N\}$. However, because snow is a dispersive medium, the speed of the pressure wave in the snowpack changes with respect to the frequency of the incident wave. Because the frequency of the source is changing at a rate

of $\partial f / \partial t$, the instantaneous phase velocity c_k of the sound pressure wave in a layer L_k of the snowpack will also change in a corresponding fashion below a certain threshold frequency f_t. Using the Biot theory, Albert (1993a) has shown that the phase velocity of the pressure wave in snow will approach the phase velocity of sound in air ($c_k / c_0 \approx 1$) for $f_i \rightarrow f_c \approx 10^6$ Hz, where f_i is the instantaneous frequency of the wave. For sound at frequencies less than f_c, it is assumed that the effective reflection coefficient for each interface $\{\Omega_1, \ldots, \Omega_N\}$ is a function of the frequency-integrated reflection coefficients:

$$\Gamma_k = \frac{1}{f_1 - f_0} \int_{f_0}^{f_1} \Gamma(f_i)\, df_i \tag{2.14}$$

To determine the average phase velocity of the pulse in the snowpack, it is necessary to consider an analysis by Johnson (1980) and Johnson and Plona (1982) regarding the phase velocity of the slow pressure wave in a porous medium. It is assumed that the compressibility of air in the pore spaces of the snowpack is greater than the compressibility of the skeletal frame of the ice matrix so that the motion of the frame is negligible. Albert (2001) has recognized that this is the case for snow, which is an air-saturated porous material. Thus, as found by Johnson and Plona (1982) and Johnson et al. (1982), the average phase velocity of the Biot slow wave in a porous medium is given by:

$$\overline{c}_k = c_0 / \sqrt{\alpha_k} \tag{2.15}$$

Equation 2.15 also allows for the experimental determination of the shape factor γ used in Equation 2.11. In a similar fashion to Johnson et al. (1982), the phase velocity of the longitudinal pressure wave traveling in the pore spaces of a porous medium is determined either by kinematics or by a relationship involving the electrical conductivity of the medium. Details

regarding the use of the electrical conductivity method is given in Johnson and Sen (1981). After the phase velocity of the sound pressure wave has been determined, it is possible to calculate the shape factor by algebraic re-arrangement of Equation 2.11 after the porosity of the material has been calculated from the measured bulk density. Berryman (1983) further examines the challenges associated with experimentally determining the shape factor.

Because the acoustic pressure wave traveling in the snowpack is a longitudinal wave, it is assumed that the reflection of this wave from the layers $\{L_1,\ldots,L_N\}$ will be evident as a longitudinal pressure wave in the air layer L_0 above the snowpack when the reflected wave from an interface Ω_k passes successively through the rest of the layers across the air-snow boundary. It is assumed that the reflected wave from the snowpack consists primarily of longitudinal waves parallel to the $\hat{\mathbf{y}}$-axis of the physical system. The time of the pulse $\Delta t^* = t_1^* - t_0^* \gg t_k$ where t_k is the time required for a pressure wave to traverse a given layer L_k of the snowpack. Thus, the overall reflection $s'(t)$ from the snowpack (Figure 2.1a) will be complicated due to reflections of the continuously-swept wave $s(t)$ from each of the layers. Treating the snowpack as a digital filter with a given response $r(t)$ that is subjected to an attenuation function $a(t)$, the overall reflection $s'(t)$ is:

$$s'(t) = s(t) * r(t) * a(t) \tag{2.16}$$

where τ is the intrinsic time shift associated with the convolution process.

The measurement system used to send an acoustic pulse into the snowpack is discussed in a later section of this thesis. Eq. 2.16 is now modified to include the effects of this system on the recorded data. The sound source producing the wave is taken to be a loudspeaker, and the overall reflected wave is captured by a microphone. As a notational convention, continuous

functions in the time domain are shown with curved brackets $(\cdots)$ and discrete signals comprised of an ordered set of numbers by square brackets $[\cdots]$. Eq. 2.16 is rewritten as:

$$s'[t] = \left\{ r[t] * \left(s[t] * s_r[t] \right) * a[t] \right\} * m_r[t] + n_s[t] + n_{m\nearrow}[t] + n_e[t] - \left(n_s[t] + n_{m\nearrow}[t] + n_e[t] \right) \tag{2.17}$$

where $s'[t]$ is the digitally sampled overall reflection response from the snowpack, $r[t]$ is the reflection response consisting of the effective (frequency-integrated) pressure reflection coefficients at each of the interfaces $\{\Omega_1, \ldots, \Omega_N\}$, the original numerically-generated frequency sweep is $s[t]$, the response of the loudspeaker is $s_r[t]$, the attenuation function of the snowpack is $a[t]$, the microphone response is $m_r[t]$, the noise in the recording system and ADC is $n_s[t]$, the sound wave of the original sweep from the loudspeaker that travels directly through the air to the microphone is $n_{m\nearrow}[t]$, and $n_e[t]$ is the noise introduced due to environmental phenomena such as wind and blowing snow. If the frequency response of the microphone is flat over the frequency domain of the bandwidth, $m_r[t]$ can be eliminated from Eq. 2.17 since the microphone can be assumed as not playing a significant role in the measurement system. Source code for the computational implementation of this model is given in the Appendix of this thesis (`reflection.m`, `layers.m`, and `correct.m`). The source code was written in Matlab, a proprietary language often used in mathematical modeling and signal processing.

The offline signal processing followed a flowchart (Figure 2.2) that ends with the extraction of depth and density data from each of the layers of the snowpack. The first step in the digital processing flow was accomplished by the program `reflection.m`. To begin the signal processing flow, the signal $s'[t]$ was low-pass filtered to ensure that no frequency

components higher than f_1 were present in the recorded signal. Once $s'[t]$ was filtered, the terms $\{n_s[t], n_{m\nearrow}[t], n_e[t]\}$ were eliminated from the signal by subtraction in the time domain. Each of the signals has the same discrete number of points n_p such that $\text{card}(n_s[t], n_{m\nearrow}[t], n_e[t]) = n_p$.

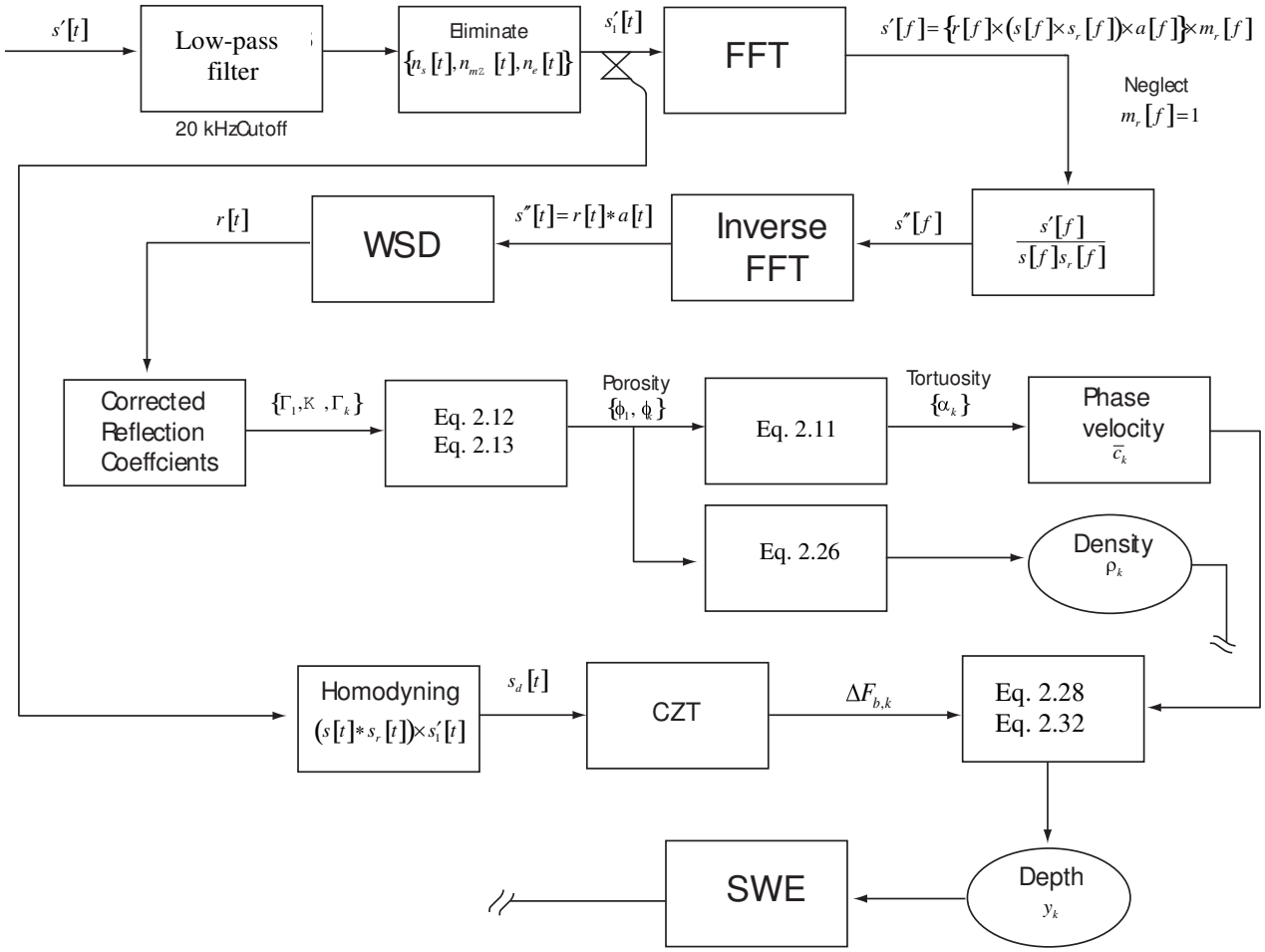

Figure 2.2. Flowchart of digital signal processing. In the diagram above, "WSD" refers to Weiner Spiking Deconvolution, "CZT" refers to the Chirp-Z transform, and "SWE" refers to Snow Water Equivalent.

Thus, the convolution model (Eq. 2.17) now becomes:

$$s'[t] = \left\{ r[t] * \left(s[t] * s_r[t] \right) * a[t] \right\} * m_r[t] + n_s[t] + n_{m\nearrow}[t] + n_e[t] - \left(n_s[t] + n_{m\nearrow}[t] + n_e[t] \right)$$

(2.18)

and

$$s_1'[t] = \left\{ r[t] * \left(s[t] * s_r[t] \right) * a[t] \right\} * m_r[t] \tag{2.19}$$

The time domain signal $s_1'[t]$ was then taken into the frequency domain by the discrete Fast Fourier Transform (FFT). Because convolution in the time domain is equivalent to multiplication in the frequency domain, Eq. 2.19 becomes:

$$s'[f] = \left\{ r[f] \left(s[f] s_r[f] \right) a[f] \right\} m_r[f] \tag{2.20}$$

It is assumed that the microphone response $m_r[f] = 1$ is flat over the frequency range of interest (so that it does not play a significant role in this equation) and that the frequency response of the loudspeaker $s_r[t]$ has already been determined as $FFT\left[s[t] * s_r[t] \right] = s[f] s_r[f]$. Because the frequency response $s[f]$ of the original sweep was known, the reflection response $r[f]$ was expressed as the product:

$$s''[f] = r[f] a[f] = \frac{s'[f]}{s[f] s_r[f]} \tag{2.21}$$

where $s[f] s_r[f] \neq 0$, so there are no zeros in the frequency spectrum. Division in the frequency domain is used here in lieu of cross-correlation to deconvolve the product $r[f] a[f]$ from the rest of the signal. Taking $s''[f]$ back into the time domain by the inverse discrete FFT, it follows that the convolution equation now becomes:

$$s''[t] = r[t] * a[t] \tag{2.22}$$

Eq. 2.22 specifies that the reflection response $r[t]$ is convolved with the attenuation filter of the snowpack $a[t]$. This expresses mathematically the effects of attenuation on the sound wave that passes through the snowpack. The reflection response $r[t]$ is a signal that is comprised of the reflection coefficient at each interface expressed as a function of time. Thus, local maxima in the time-domain representation of $r[t]$ are the reflection coefficients at each interface. However, the attenuation filter $a[t]$ of the snowpack is unknown. To remove $a[t]$ and to estimate the effective frequency-integrated reflection coefficients at each of the interfaces of the snowpack, the Weiner Spiking Deconvolution (WSD) method (Robinson, 1957) was used to find $r[t]$.

Normally, WSD has been applied in the context of impulse seismology to determine the reflection coefficients at the interfaces of layered rocks. However, in this experiment, WSD was used to extract the reflection coefficients from $s''[t]$. Although Mewhort et al. (2002) have argued that spiking deconvolution as applied to a dataset containing a frequency-swept signal (or in this case, a dataset comprised of the overall reflection response) violates the minimum-phase assumption, and according to Gibson and Larner (1984) as well as Brittle and Lines (2001), will therefore cause a phase shift in the data, WSD is only applied here to find the reflection coefficients at the interfaces. Because the reflection signal $r[t]$ is in the time domain, the time at which each of the reflections occurs is usually taken to be the time-of-flight to the interface. Because there might have been a phase shift in the data, the time at which each reflection occurs is not used to calculate the distance to the interface in the snowpack. Rather, signal processing techniques (i.e. Yankielun et al., 2004) derived from FMCW radar technology is implemented to be able to determine the distance to each of the interfaces in the snowpack. Nevertheless, Brittle

et al. (2001) and Brittle and Lines (2001) have noted that the phase shift in the reflection signal $r[t]$ is caused due to cross-correlation with the reference sweep $s[t]$. The embedded Klauder wavelet in the cross-correlated dataset violates the minimum-phase assumption of the deconvolution operation. Thus, Brittle and Lines (2001) suggest division in the frequency domain before deconvolution is applied because unlike cross-correlation, this does not embed the Klauder wavelet in the resulting $r[t]$ signal. Consequently, it is possible to implement a deconvolution operation on the initial dataset using their technique. However, some residual phase shifts might occur by the use of deconvolution on a vibroseis dataset. Although WSD attempts to calculate the minimum-phase wavelet, there may be unpredictable behavior with regard to the phase of the reconstructed reflection response; it is also for this reason that the time to each reflection is not used to calculate the distances to the interface in the snowpack.

WSD was implemented by autocorrelating $s''[t]$ over time. The autocorrelated signal was then pre-whitened. The resulting signal was subjected to the Levinson recursion to determine the reflection response $r[t]$ consisting of the frequency-integrated pressure reflection coefficients $\{\Gamma_1,\ldots,\Gamma_N\}$ associated with the interfaces $\{\Omega_1,\ldots,\Omega_N\}$ of the snowpack. The WSD algorithm used here is based on the algorithm of Sacchi (2003).

If the sound source is too close to the surface of the snowpack, and the surface is not in the far field of the radiated sound source, the extracted reflection coefficients $\{\Gamma_1,\ldots,\Gamma_N\}$ will be spherical, rather than planar. To confirm planar wave reflection coefficients, the extracted set $\{\Gamma_1,\ldots,\Gamma_N\}$ was subjected to a numerical correction process used for sonar by Harrison and Nielsen (2004). This procedure was implemented by the Matlab program `correct.m`. Using a

Hankel transform of the Sommerfeld integral, the corrected plane wave reflection coefficient for a layer L_k was determined by:

$$\Gamma_{\text{k,corrected}} = \left\{ \frac{\exp\left[j \cdot \left[{k_0}^2 - \left(k_0 \cos\theta_g \right)^2 \right] \cdot y_0 \right]}{{k_0}^2 - \left(k_0 \cos\theta_g \right)^2} \right\}^{-1} \times j \int_0^{\infty} \Gamma_{\text{k,uncorrected}} \cdot \frac{\exp\left[j k_0 \left(r^2 + {y_0}^2 \right) \right]}{\left(r^2 + y_0^2 \right)} \times J_0 \left[r \cdot k_0 \cos\theta_g \right] r dr \tag{2.23}$$

where $k_0 = 2\pi f / c_0$ is the angular wavenumber in the air medium, $J_0[\cdots]$ is the Bessel function of the first kind, $\theta_g \to 0$ is the grazing angle of the sound wave source to the surface of the snowpack, $j = \sqrt{-1}$ represents a complex number and the integration is over r on the interval $[0, \infty)$. Harrison and Nielsen (2004) have shown that this transform is the same even when dealing with a multilayered medium, and does not depend on physical properties of the medium. This eliminates the need to use another model to calculate the reflection coefficients at the interfaces of the snowpack. Letting $\theta_g \to 0$ since the loudspeaker was normal to the snow surface, Eq. 2.23 was numerically integrated over $[f_0, f_1]$ so that the reflection coefficients were corrected over the entire frequency range.

Once the corrected reflection coefficients were determined, the porosity of each layer of the snowpack was calculated using Eq. 2.12 and Eq. 2.13. The iterative calculation process was implemented by the program `layers.m`. These equations were evaluated using a Newton-Raphson iteration (i.e. Mathews, 1992). The density ρ_1 of the first layer of the snowpack was found by:

$$\rho_1 = \rho_{\text{ice}} \cdot (1 - \phi_1) \tag{2.24}$$

and this relationship was extended for multiple layers:

$$\rho_k = \rho_{\text{ice}} \cdot (1 - \phi_k) \tag{2.25}$$

Where ρ_{ice} is the nominal density of ice at the freezing point, approximated as $\rho_{\text{ice}} = 917$ kg m^{-3}.

The tortuosity α_1 was estimated using Berryman's (1980) relationship (Eq. 2.11). Both the porosity ϕ_1 and the density ρ_1 were used recursively along with the reflection coefficients of the successive layers $\{\Gamma_2, \ldots, \Gamma_N\}$ and Eqs. 2.12, 2.13 and 2.25 to calculate the density of each snowpack layer. The tortuosity was used to estimate the phase velocity of the Biot slow wave in each of the layers by the use of Eq. 2.15.

The distance between each of the layers was determined by subjecting signal $s[t]$ and $s''[t]$ to a signal processing flow that borrows mathematics from FMCW radar techniques (Figure 2.2). First, both $s[t] * s_r[t]$ and $s_1'[t]$, after being low-pass filtered, were mixed together in the time domain by homodyning (point-by-point multiplication, i.e. $(s[t] * s_r[t])\, s_1[t]$). The resulting signal $s_d[t]$ was then taken into the frequency domain by the Chirp-Z transform (Bluestein, 1968; Rabiner et al., 1969), thereby yielding $s_d[f]$. This particular type of transform is also known as the zoom-FFT because it enables the frequency spectrum to be calculated at a higher resolution for a narrow band of frequencies less than $f_s / 2$. The lower frequencies of $s_d[f]$ correspond to the frequency difference between $s[t] * s_r[t]$ and $s''[t]$. Considering each of the interfaces $\{\Omega_1, \ldots, \Omega_N\}$ between the layers of the snowpack to be a reflector, the homodyned wave will contain peaks in the frequency spectrum which correspond to each of the reflectors. The N peaks in $s_d[f]$ are produced due to time delays between each of the reflections at the interfaces between the layers. Figure 2.3 is a conceptual diagram of the

transmitted signal $s(t;f)$ and the reflected time-shifted signals $r_1(t;f),\ldots,r_N(t;f)$ from each of the layers in the snowpack.

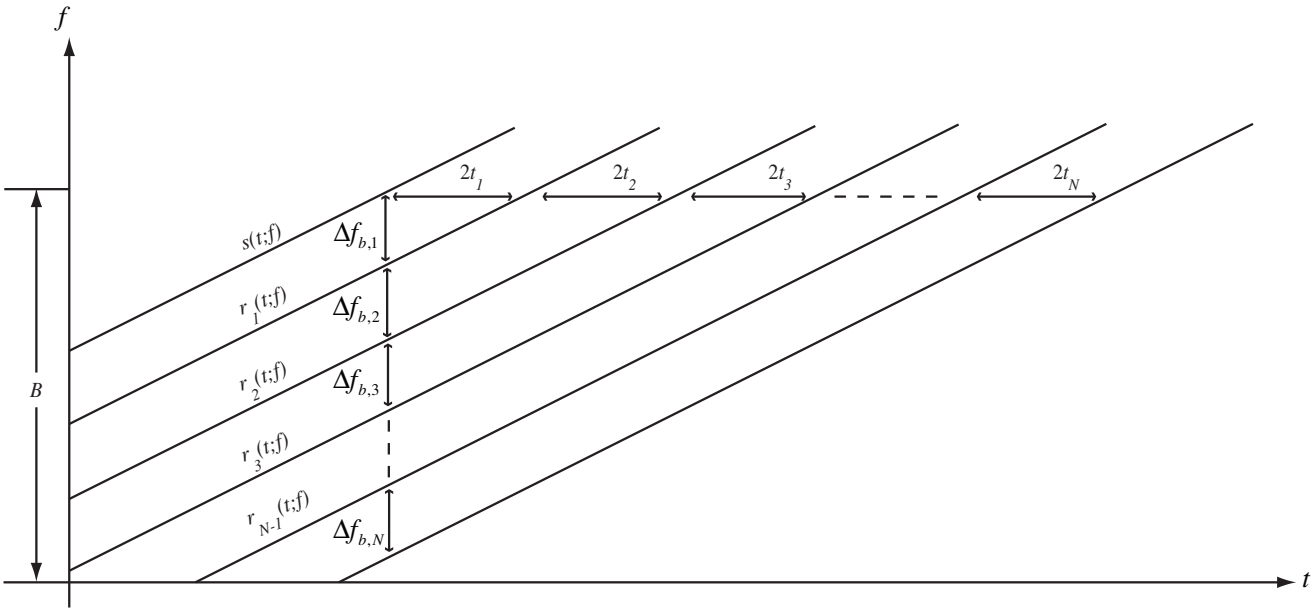

Figure 2.3. Conceptual diagram of the snowpack response. The signal that is transmitted from the speaker is $s[t,f]$. The reflected signals $r_1[t,f],\ldots,r_N[t,f]$ from each of the layers in the snowpack are shifted in frequency by $\Delta f_{b,k}$ for the k^{th} layer of the snowpack system.

The variables $\{B,\Delta t,\Delta f_1,t_1\}$ were related by the proportionality utilized by Yankielun et al. (2004) for FMCW radar:

$$\frac{B}{\Delta t^*}=\frac{\Delta F_{b,1}}{2t_1} \tag{2.26}$$

For reflection from the top of the snowpack, $\Delta F_{b,1}=\Delta f_{b,1}$. By introducing $t_0 = y_0 / c_0$, where t_0 is the time taken to travel the distance y_0 from the transducer to the snowpack, and c_0 is the phase velocity of sound in the air layer $k=0$ above the snowpack, it follows that:

$$y_1=\frac{\Delta F_{b,1}\Delta t^*\overline{c}_1}{2B} \tag{2.27}$$

where the average phase velocity, $\overline{c}_1$, of the sound wave in the air layer, L_0, is calculated following Raichel (2000), $\overline{c}_1 = \sqrt{1.4RT^*}$, where T^* is the ambient environmental temperature (in Kelvin), and R is the thermodynamic gas constant of air ($R = 287\ \mathrm{N}\cdot\ \mathrm{m}\cdot\ \mathrm{kg}^{-1}\cdot\ \mathrm{K}^{-1}$).

Alternately, for reflections from a layer L_k of the air-snowpack system with $k > 1$, Eq. 2.26 can be presented as:

$$\frac{B}{\Delta t^*} = \frac{\left(\Delta F_{b,k} = \sum_{i=1}^{N} \Delta f_{b,i}\right)}{2t_1 + \cdots 2t_k} \tag{2.28}$$

$$2B\left(\frac{y_1}{\overline{c}_1} + \cdots + \frac{y_k}{\overline{c}_k}\right) = \Delta F_{b,k}\Delta t^* \tag{2.29}$$

$$\frac{2By_k}{\overline{c}_k} + 2B\left(\frac{y_1}{\overline{c}_1} + \cdots + \frac{y_{k-1}}{\overline{c}_{k-1}}\right) = \Delta F_{b,k}\Delta t^* \tag{2.30}$$

$$y_k = \frac{\overline{c}_k}{2B}\left(\Delta F_{b,k}\Delta t^* - 2B\sum_{i=1}^{k-1}\frac{y_i}{\overline{c}_i}\right) \tag{2.31}$$

Eq. 2.31 was used to determine the vertical dimension of each layer $\{L_2, \ldots, L_N\}$. Since the density of each layer was found by Eq. 2.25 and the depth by Eq. 2.31, the SWE of the entire snowpack is therefore:

$$S_E = \varphi\sum_{i=1}^{N} y_k\rho_k \tag{2.32}$$

where $\varphi = 1\ \mathrm{m}^2\cdot\mathrm{kg}^{-2}\cdot\mathrm{mm}$ is a continuity constant, and the implicit assumption is that 1 kg of water may be approximated as a uniform depth of 1 mm over an area of 1 m^2 (i.e. Pomeroy and Gray, 1995).

3. APPARATUS

3.1. Introduction

To send an acoustic pulse into the snowpack and to receive the overall reflection of this pulse, two prototype units of an acoustic snow gauge were constructed, one very portable, one less so. The following sections discuss some of the theory associated with the selection of physical parameters for this measurement system, and the design and the specifications of the two prototypes.

3.2. Basic Sampling System Design

The measurement system consists of a speaker and a microphone situated at a height of y_0 above the surface of the snowpack. Both the speaker and the microphone are situated perpendicular to the snow surface in a similar fashion to the setup described by Lee and Rogers (1985). Unlike Moore et al. (1991), only one microphone is placed above the snowpack; no microphones are placed beneath the snow surface. The speaker excited a pressure disturbance in the air layer L_0 above the snowpack. The frequency was swept between frequencies, f_1 and f_2, where $f_2 > f_1$. The duration Δt^* of the pulse was greater than the time taken for the pulse to traverse all of the layers of the snowpack (and subsequently undergo reflections at each of the interfaces). The overall reflection $s'(t)$ from the snowpack was detected by a microphone at the same time that the pressure wave $s(t)$ is being radiated from the speaker.

Five basic aspects of this measurement system must be considered:

(1) The bandwidth, B, of the pulse;

(2) The height y_0 of the microphone and the speaker above the first layer of the snowpack;

(3) The radius r_f of the area of the snowpack insonified by the speaker (also referred to as the "source footprint");

(4) The horizontal distance, x_0, between the microphone and the speaker; and

(5) The sampling frequency f_s of the Analog-to-Digital converter.

3.2.1. Pulse Bandwidth

Pulse bandwidths are defined by (a) the desired accuracy δy of depth measurement; (b) the frequency response of the speaker; and (c) the frequency response of the microphone.

Because the frequency sweep being used in this method is similar in principle to the electromagnetic wave produced by an FMCW radar antenna (i.e. in both methods, the wave being produced has a linear increase of frequency with respect to time), the interfaces $\{\Omega_1,\ldots,\Omega_{N-1}\}$ of the snowpack are treated as targets capable of reflecting back pressure waves from the source. It then follows that δy (i.e. range resolution) is given by (Wehner, 1987):

$$\delta y = \frac{\overline{c}_k}{2B} \tag{3.1}$$

The closed interval $\overline{c}_k \in [100, 331]$ m·s^{-1} is selected as the approximate range of phase velocities of the slow wave calculated for snow. This range is based on the predictions of Albert (1993a). The upper bound of the speed (331 m s^{-1}) is the approximate speed of sound in air at $T^* = 0°\text{C}$. The bandwidth is taken as $B = 20000$ Hz - 20 Hz = 19980 Hz. Thus, the calculated accuracy of the depth measurement ranges over 3×10^{-3} m to 8×10^{-3} m. This implies that the thinnest layer that can be resolved is approximately 1 cm deep. As noted by Yankielun (1992), the approximate resolution of an FMCW radar system is 1 cm. This may suggest that the resolution of the acoustic approach might coincide with that of the resolution of FMCW radar.

The frequency response of a dynamic loudspeaker is dependent upon the ability of its coil to induce a magnetic field in the vicinity of a permanent magnet. Both the cone and the chassis (basket) of the speaker contribute to the range of frequencies that can be produced by the device. Furthermore, the speaker can be electrically considered being comprised of inductive, resistive, and capacitive elements, the frequency response of the speaker will differ from the frequency of the signal present at the output of the amplifier. It is not possible to produce a sweep with the same spectral power density at all frequencies using a commercial speaker; however, these devices can still produce even power density over a subset of the audible (20 Hz to 20 kHz) range. In some high-end speaker systems (i.e. studio monitors), added linearity of frequency response is achieved by using two or more transducers which cover extreme low or high audible frequencies. Often loudspeakers are driven by crossover circuits which shunt higher frequency components to specific drivers. The reason for selecting a commercial speaker is primarily due to portability issues. Smaller commercial speakers operating in the audible sound range can easily be transported to a field site, and the power requirements of such devices are low. Moreover, such speakers are able to produce sound in the range of frequencies required for this experiment, and although the frequency response may not be flat across the entire spectrum, the selection of such a speaker is a reasonable choice. Thus, although a conventional loudspeaker may not have a constant output intensity over its entire frequency range it is conceivable that some frequencies may pass through the snow medium.

Equally important to the functioning of the system is the proper selection of a microphone. Because the pulse is a frequency sweep over 20 Hz to 20 kHz, the microphone must have a frequency response that accommodates this bandwidth. Moreover, to ensure that the frequency of the overall reflection is adequately recorded, it is important to select a microphone

that has a linear response over the frequency range. Unlike dynamic speakers, it is possible to obtain studio recording microphones with a nearly-linear frequency response, although some tapering of this response does occur at high and low frequencies of the operating range.

3.2.2. Microphone and Loudspeaker Height

The height y_0 of the microphone and loudspeaker above the snow surface is selected with recourse to the geometry of the sound wave radiated by the speaker. In the previous section, a model of sound propagation through a layered snowpack was presented. As a means of simplifying the mathematics of this model, it was assumed that the sound source produces a planar wave. However, sound waves produced in air by a conventional source (such as a speaker) have spherical or paraboloidal geometry close to the source, which radiates over an angle of π rad. Thus, if the sound pressure wave contacts a planar surface close to the speaker, the reflection coefficient at the interface will be the reflection coefficient of a spherical wave. However, at much larger distances from the source, the wave can be approximated as planar along a small sector ϑ of the two-dimensional radiated field. To calculate this distance, it is assumed that the speaker has a characteristic dimension L_c. Following Lurton (2002), the far field (planar response) of a transducer with a characteristic length L_c is at a distance y_f from the source:

$$y_f = \frac{L_c}{\lambda_0} \tag{3.2}$$

where λ_0 is the wavelength of the sound pressure wave in air. If the bandwidth has endpoint frequencies of $f_0 = 20$ Hz and $f_1 = 20$ kHz, and the characteristic length of the transducer is selected to be $L_c = 9$ cm (found by physical measurement of the speaker used in the experiments

associated with this thesis), the far field of the transducer is situated at approximately $y_{f,0} = 1.7$ cm from the source for a frequency of $f_0 = 20$ Hz, and $y_{f,1} = 5.4$ m from the source for a frequency of $f_1 = 20$ kHz. For reflectors situated closer to the microphone and speaker than these distances, the reflection coefficient will be a spherical wave reflection coefficient and will need to be corrected by Eq. 2.23.

Moreover, the height of the speaker and the microphone above the snowpack can be no more than a certain height due to the possible presence of temperature gradients which exist above a snowpack. A sound wave traveling through the air would undergo changes in speed, and may even undergo refraction due to temperature gradients near the snow surface (Johnson, 1985). This should not pose a difficulty in the context of this method because what is being considered is the average phase velocity of the pulse in the air medium above the snowpack. However, Johnson (1985) mentions that warmer layers of air are increasingly apparent at higher distances above the snowpack and it is conceivable that these temperature gradients will have a refractive effect on the overall reflected sound wave. Because refraction causes bending of the sound wave path, thereby not allowing the beam to be detected by the microphone, it is conceivable that the speaker and microphone setup can be placed no more than 50 cm above the snow surface.

3.2.3. Source Footprint

As the sound wave from the speaker radiates toward the surface of the snowpack, it continues to spread in a spherical fashion until reaching the first interface. The "source footprint" is the approximate diameter of the surface area that is insonified by the sound source.

This parameter influences the area over which SWE of the snowpack is estimated. From Yankielun (1992):

$$r_f = y_0 \tan\left(\frac{1}{2}\theta_{\text{bw}}\right) \tag{3.3}$$

where r_f is the radius of the projected footprint, and θ_{bw} is the angular beamwidth of the source. It is assumed that the speaker used has an angular beamwidth of approximately 85º (estimated by the curvature of the speaker), and that the speaker and the microphone are to be positioned at distances between 15 cm to 40 cm from the surface of the snowpack. Thus, the diameter of the projected footprint ranges between approximately $d_1 = 18$ cm for a height of $y_0 = 10$ cm and $d_2 = 73$ cm for a height of $y_0 = 40$ cm above the surface of the snowpack. This calculation indicates that the overall area over which the acoustic pulse propagates can be approximated by the diameter of a large gravimetric snow sampler (for a distance above the snowpack of $y_0 = 10$ cm), and by the approximate dimension of a snow shovel (for a distance above the snowpack of $y_0 = 40$ cm).

3.2.4. Horizontal Distance between the Microphone and Loudspeaker

The distance x_0 between the microphone and the speaker must be small enough to permit the microphone to adequately sample the spatial sound field of the overall reflection $s'(t)$ from the snowpack. If the microphone is situated beyond a maximum distance x_{max} from the speaker, the reflected wave will be detected perpendicularly, thereby leading to parallax error. In FMCW radar, the disadvantage of having two separate antennas can be overcome by utilizing only one antenna to send and receive the continuous-wave pulse at the same time. In an acoustic system,

the sensitivity of the speaker when it is used as a microphone is often very low. Due to the significant challenges associated with the design of a transducer that can send and receive at the same time, a speaker and a microphone are used as two separate components. Taking the point directly below the speaker as being the approximate center of the footprint, $\theta_{x,\max}$ is defined as the maximum angle of displacement that is permitted before the reflected sound pressure field becomes too diffuse for accurate detection due to specular reflection from the snow surface at grazing angles of incidence. Moreover, it is also assumed that the angle $\theta_{x,\max}$ is small enough such that the assumption of only pressure waves being detected at the microphone still holds. This angle is taken to be no more than $\theta_{x,\max} \approx 30^{\circ}$. This is because approximately 95% of the energy from the wave is within 30° from the normal (Claerbout, 1984). Thus, the maximum separation distance, x, between the speaker and the microphone as measured from a point on the outside of the footprint on the surface of the snowpack is such that:

$$x \leq \left(x_{\max} = y_0 \tan \theta_{x.\max} \right) \tag{3.4}$$

Thus, the distance between the outer edge of the footprint and the centre of the microphone must be ≤ 5.8 cm $\leq$ 23 cm. Since the footprint has a diameter of approximately $d_1 = 18$ cm and a radius of approximately $r_1 = 9.2$ cm for a minimum distance of $y_0 = 10$ cm above the snowpack, the appropriate maximum distance between the speaker and the microphone is $x_{\max} \leq (9.2 \text{ cm} + 5.8 \text{ cm}) = 15$ cm so that the microphone can adequately capture the overall reflected wave from any point on the circumference of the insonified snow surface.

3.2.5. Sampling Frequency of the ADC

To be able to convert the overall reflection $s'(t)$ into a signal that can be processed by a computer, the analog signal from the microphone must be converted to a digital signal by an Analog-to-Digital Converter (ADC). From the Nyquist theorem, the ADC must sample the continuous analog signal at a rate $f_s > 2f_1$, where f_1 is the highest frequency of the signal that will be produced by the speaker. If frequency components exist in the sampled signal that are greater than f_1, the higher frequency components will be apparent in the sampled signal as artifacts that are indistinguishable from the actual lower frequency components of the signal $s'(t)$. It is therefore beneficial to select a sampling frequency such that $f_s \gg 2f_1$, so that frequency components greater than f_1 can be digitally filtered. Because $f_1 = 20$ kHz, the sampling frequency of the ADC was selected to be such that $f_s \gg 2f_1$.

3.3. Prototype Devices

Two measuring devices were built as prototypes to generate and capture the reflected wave from the snowpack. These devices were used during the development of the theory, and provided a means by which the results of signal processing could be tested in a field setting.

The first prototype consisted of a pair of speakers and a microphone that was mounted on a metal frame (Figure 3.1). The frame was attached to the end of a 1 m arm that extended over the surface of the snowpack. The arm length was such that the body of the stand would not interfere with the projected area of the source on the snowpack. The arm could be raised and lowered above the snow surface, but during experiments, the distance of the loudspeaker and microphone above the snow surface ranged between 15 cm and 40 cm.

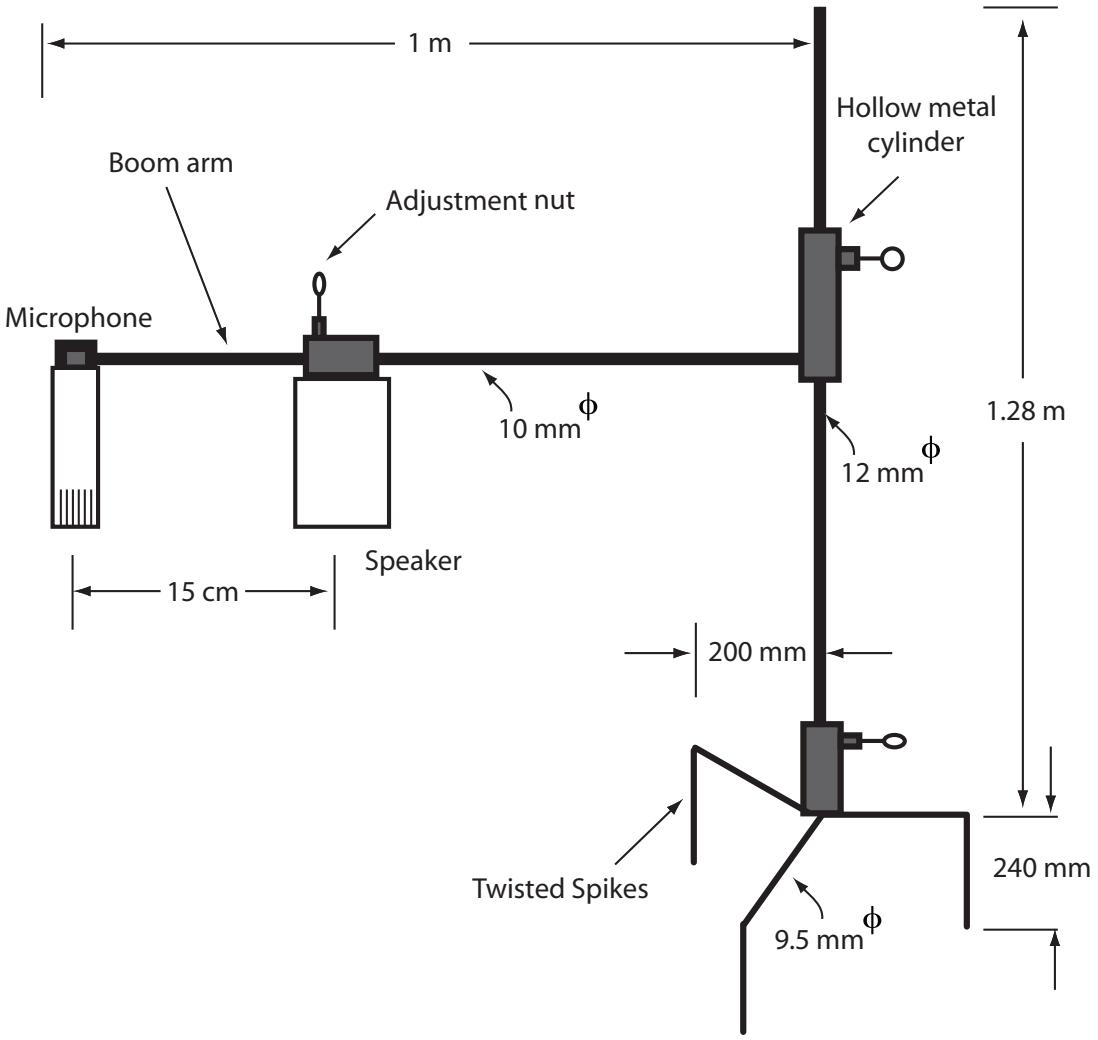

Figure 3.1. Diagram of metal frame used to hold the loudspeaker and microphone in place over the snowpack for the Saskatchewan sites. The arm length is 1 m, and the distance between the microphone and the speaker could be adjusted, but for all experiments was approximately 15 cm. During deployment, both the speaker and the microphone were situated at distances ranging between 15 cm and 40 cm above the snow surface. A series of twisted spikes enabled the stand to be pushed into the ground to ensure that the measurement system would be stable.

The separation distance between the speaker and the microphone was approximately 15 cm. The mounting stand of the apparatus was equipped with a set of twisted spikes that enabled the device to be pushed into the snowpack so that the metal frame holding the loudspeaker and the microphone could be placed perpendicular to the snow surface.

A more portable version was also constructed for carrying the device to a remote field location (Figure 3.2). This consisted of a smaller metal structure with a shaft and a handle. The same metal frame used on the end of the boom arm was placed on the end of the structure, and the same loudspeaker and microphone were used in all of the trials conducted using both of the stands. The speaker and the microphone were separated by 15 cm. The speaker and the microphone were situated no more than 40 cm above the snow surface, with a minimum distance of approximately 15 cm.

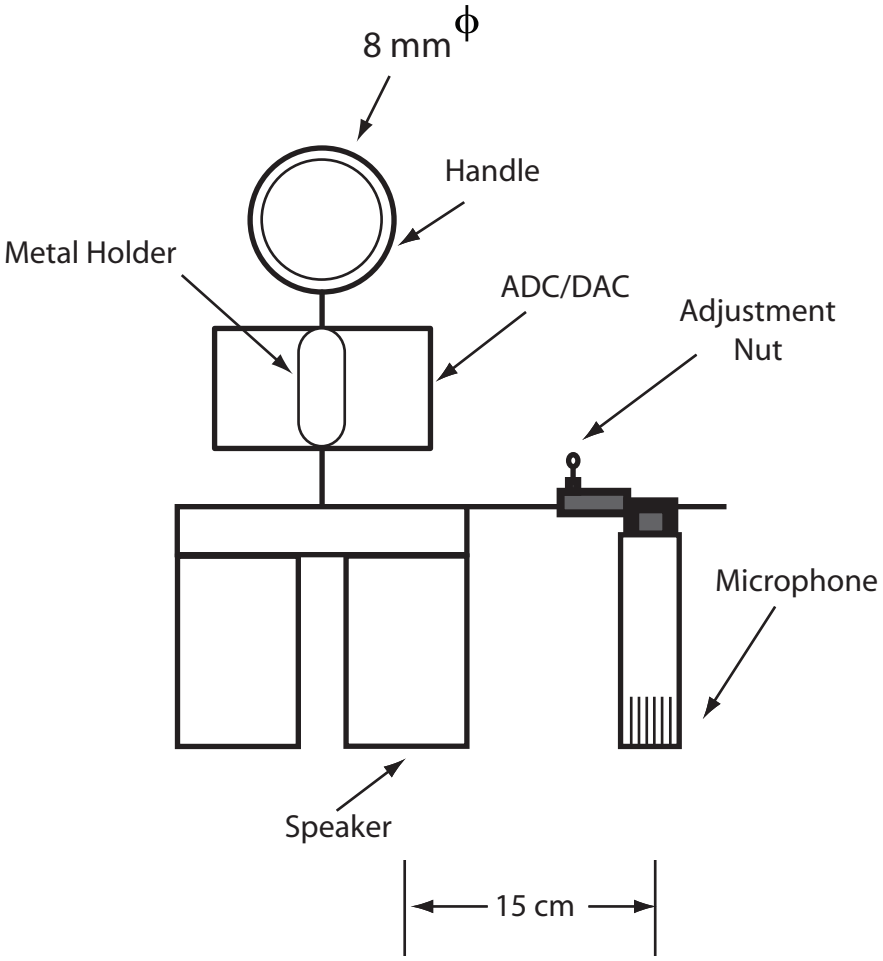

Figure 3.2. Diagram of the metal frame used to hold the loudspeaker and the microphone in place over the snowpack for the Lake O'Hara sites. The separation distance between the speaker and the microphone was 15 cm. During deployment, both the speaker and the microphone were situated between 15 cm and 40 cm above the snow surface.

Due to its high sensitivity, low noise and wide frequency response (~20 Hz to ~20 kHz), the microphone selected for the purpose of these two prototypes was a Behringer B-5 gold-sputtered diaphragm condenser microphone. The frequency response of this microphone is generally flat over the frequency range of interest if the low-frequency roll-off switch is not set. The B-5 microphone is available with a series of caps that enabled conversion of the microphone's pickup pattern so that sound would be picked up from the surface of the snowpack (and not from other directions). The sound wave from the loudspeaker that was picked up

directly by the microphone was removed by digital signal processing. Current was supplied to the microphone via an XLR cable connected to a low-noise Rolls +48V phantom power supply. A 12V battery pack was used to power this phantom supply via an adapter. Output from the microphone was fed directly into a Behringer FCA202 24-bit Analog-to-Digital/Digital-to-Analog Converter (ADC/DAC) operating at a sampling rate of $f_c = 96$ kHz, which was above the Nyquist threshold. The data was later subjected to offline digital signal processing on a laptop computer using the signal processing flow shown in Figure 2.2. The loudspeaker pair used in this experiment was a battery-powered Koss SXM/7 portable loudspeaker pair with an incorporated amplifier. This was attached to the DAC section of the FCA202 interface. Each loudspeaker consisted of a single driver and did not contain crossovers allowing for the use of two transducers (i.e. a middle-range loudspeaker and a tweeter). Because both loudspeakers were permanently attached together with a cable, it was impossible to separate them. Consequently, the pulse was produced by only one loudspeaker, and the other loudspeaker was placed next to the first loudspeaker. Both loudspeakers were not driven at the same time to ensure that spatial interference did not occur between the two separate sources.

4. DATA COLLECTION

4.1. Experimental Locations

The two experimental setups described in this paper were deployed at field sites situated near Saskatoon, Saskatchewan and near Lake O'Hara in Yoho National Park, British Columbia, Canada. These two sites were chosen because they were representative of locations where snow with a wide range of SWE could be observed. Other sites could be selected, but due to the location of the University of Saskatchewan and the close proximity of this academic institution to sites representative of Prairie and sub-alpine environments, these were two locations that were readily accessible.

These sites are indicative of two different snow environments—(1) the Saskatchewan sites were typical of Prairie windblown snowpacks; and (2) the Lake O'Hara sites were indicative of Rocky mountain sub-alpine forest snowpacks. Although these two sites are not inclusive of all possible environments under which such a device could be deployed and tested, a range of deep and shallow, cold and isothermal, dense and light, and dry and wet snowpacks were sampled.

The Saskatchewan sites were assigned identifiers which are listed in Table 4.1 and are indicative of various Rural Municipalities surrounding Saskatoon (420-540 m above sea level, 52°7'N 106°39'W). The Saskatchewan sites are typical of the agricultural mixed grass prairie region, with gently sloping large fields of grass or grain stubble dotted with aspen stands and shelterbelts along the sides of fields.

Rural Municipality and number	Dominant Sub-nival Vegetation	Average Vegetation Height (cm)	Forest Cover	Slope (°)	Fetch (m)
Dundurn 1	Mixed Grass	10.2	Open	2	<200
Dundurn 2	Mixed Grass	8.7	Open	2	<200
Dundurn 3	Mixed Grass	9.2	Open	2	<600
Bradwell	Stubble	3.9	Open	3	<700
Aberdeen	Fallow	9.9	Open	3	>1000
Corman Park	Mixed Grass	11.5	Open	2	<300
Vanscoy	Fallow	10.6	Open	4	<200

Table 4.1. Overview of the Saskatchewan sites. Fetch refers to unobstructed upwind distance for blowing snow transport.

The British Columbia sites are demarcated by a number in Table 4.2. These sites are typical of the sub-alpine forest zone, with evergreen (fir and spruce) stands on slopes up to 15°, interspersed with small grassy or mossy clearings. Figure 4.1 is a photograph indicative of field locations where the method was attempted in Saskatchewan, whereas Figure 4.2 shows an example photograph of the Lake O'Hara research sites.

Site	Dominant Sub-nival vegetation	Average Vegetation Height (cm)	Forest Cover	Slope (°)	Fetch (m)
1	Short grass	10	Fir & Spruce	10	100
2	Short grass	14	Fir & Spruce	15	100
3	Short grass	12	Mixed	15	100
4	Short grass	10	Open	2	300
5	Short grass	10	Mixed	14	100
6	Mosses	0.10	Mixed	2	300
7	Lichen	0.10	Mixed	15	100

Table 4.2. Overview of the Lake O'Hara sites. Fetch refers to unobstructed upwind distance for blowing snow transport.

Figure 4.1. Photograph of observation site Dundurn 1 in Blackstrap Provincial Park, Saskatchewan Canada.

Figure 4.2. Photograph showing an example of the Lake O'Hara research sites, British Columbia. The topography of the snow-covered area in the foreground of the photograph is gently undulating, and the forested slopes (with a slope angle of approximately 15°) was also used to collect data.

Most of the trials of the acoustic sounding method were conducted at the Saskatchewan sites in January and March 2006 and at the Lake O'Hara sites in April 2006. The average temperature at the Saskatchewan sites during the January observations was approximately -8°C, while in March it was above freezing. The January snowpack was observed to be cold and dry. However, by March active melt was occurring and so the snowpack was very wet because of rapid melt and poor drainage due to impeding ice layers. The maximum snow depth observed at Saskatchewan sites was 0.5 m. At the Lake O'Hara site, the average air temperature was approximately -3°C during observations. The snowpack at the Lake O'Hara sites was considerably wetter than the snowpack observed in Saskatchewan during January (but not as wet as that observed in March) because the melt period was beginning and insolation was high. However, the wetness of the snowpack observed at the Lake O'Hara sites was considerably less than the wetness of the snowpack in March 2006 at the Saskatchewan research sites. The maximum depth of snow observed at the Lake O'Hara site was 1.5 m. Blowing snow was not observed at either site during observation periods.

4.2. Procedure

Mounting stands were taken to each of the sites. The loudspeaker and the microphone were attached, and current was applied to the microphone before it was plugged into the FCA202 interface to ensure that the microphone was stabilized prior to taking measurements. With the first apparatus, a level was used to ensure that the loudspeaker and the microphone were situated perpendicular to the surface of the snowpack. This could not be done for the second, more portable, apparatus due to the lack of a stand. For the second apparatus, the loudspeaker and microphone were held at a position that was believed to be perpendicular to the surface of the

snowpack. Then, a frequency-swept sound pulse was sent from the loudspeaker. The duration of the pulse was selected to be $\Delta t^* = 1$ s, but different times of the sweep were also attempted ($\Delta t^* = 0.1$ s to 5.0 s). The frequency sweep was created by a computer program, and was therefore repeatable. It was found that the $\Delta t^* = 1.0$ s sweep gave the best results, and it is these results that are presented in this paper. The bandwidth of the pulse was chosen to be $B = 20000 \text{ Hz} - 20 \text{ Hz} = 19980 \text{ Hz}$. Although this might have not been the effective bandwidth of the method that was used to characterize the snowpack, these were the frequencies of the reference sweep $s[t]$ that were sent to the loudspeaker. Because a crossover circuit was not used with two separate transducers, the loudspeaker did not reproduce all frequencies equally, but reproduced a subset of the frequencies that were produced. The (Sound Pressure Level) SPL of the pulse sent into the snowpack was measured with a sound-level meter at the source and was determined to be close to 100 dB at all sites. The ambient environmental temperature T^*, used to determine the phase velocity of the pulse in the first layer L_0 above the surface of the snowpack, was determined by the use of a thermocouple.

After the acoustic measurement had been taken, the depth and density of the snow was determined by a ruler and gravimetric sampling. The sampling point for this measurement was situated directly underneath of the loudspeaker. At locations where the layers of the snowpack were visible, gravimetric samples were taken from each of the layers, and weighted average density was used to determine SWE. Gravimetric sampling was the primary means of determining physical measurements at each of the Saskatchewan sites. Gravimetric snow sampling using an MSC snow tube and calibrated weight scale were used to establish SWE, depth and density at the Lake O'Hara site.

The three signals $\{n_s[t], n_{m\nearrow}[t], n_e[t]\}$ were determined immediately prior to experimentation and field work. The noise in the system $n_s[t]$ was determined by the use of a loopback test, where a cable was used to connect the input of the Analog-to-Digital converter to the output of the Digital-to-Analog converter. Then, a 1 s sample was taken with the cables attached. This was thought to be representative of the noise in the system. The sound wave of the original sweep from the loudspeaker that travels directly through the air to the microphone $n_{m\nearrow}[t]$ was determined by taking a 1 s sample with the microphone situated under the loudspeaker, but at a 90º angle to the driver so that the sound would arrive directly on the side of the microphone. Because the loudspeaker and the microphone were situated parallel to each other, this measurement of $n_{m\nearrow}[t]$ was believed to be indicative of the oblique wave from the loudspeaker that traveled through the air and was consequently received from the microphone. The noise $n_e[t]$ caused by environmental phenomena such as wind was found by taking successive 1 s samples for 5 minutes at each of the field locations. One sample was taken every 10 seconds. This procedure was followed to ensure that an adequate representation of the environmental noise at the field site could be determined. This included additional noise caused by wind gusts. The samples were then averaged together to find the overall average environmental noise $n_e[t]$.

The signal sent out from the loudspeaker $s[t] * s_r[t]$ was determined by placing the microphone close to the loudspeaker and recording the frequency-swept wave at a 0º (direct-on) angle of incidence for a time of $\Delta t = 1$ s. Although the presence of the microphone might have affected the spatial sound field of the loudspeaker, this provided a crude estimate of the sound wave $s(t)$ that was sent into the snowpack. Further attempts in deploying this apparatus might

rely on the use of mathematical modeling to reconstruct the sound wave $s[t] * s_r[t]$ sent from the loudspeaker, given that the precise frequency response $s_r[t]$ of the loudspeaker can be numerically determined.

5. RESULTS

5.1. Introduction

The results of this method are considered in the two following sub-sections. In the first section, the application of this method to determine the SWE of two layered snowpacks is demonstrated. In the second section, the application to estimate SWE is considered.

5.2. Demonstrations of Procedure

5.2.1. Snowpack with $N = 1$ Layers

The signal processing flow (Figure 2.2) was applied to a one-layered snowpack that was observed at the Dundurn1 site. Representation of the signals being used in this analysis is given in Figure 5.1. The original wave sent from the speaker into the snowpack is given as Figure 5.1a, whereas Figure 5.1b is the raw (unprocessed) signal received at the microphone. By spectral division in the frequency domain, the signal $s'[t] * a[t]$ was determined. The spectral division was observed to be stable, so there were no zeros in the frequency domain. After subjecting the signal to Weiner deconvolution, the reflection coefficients at each of the interfaces were represented in the time domain (Figure 5.1c).

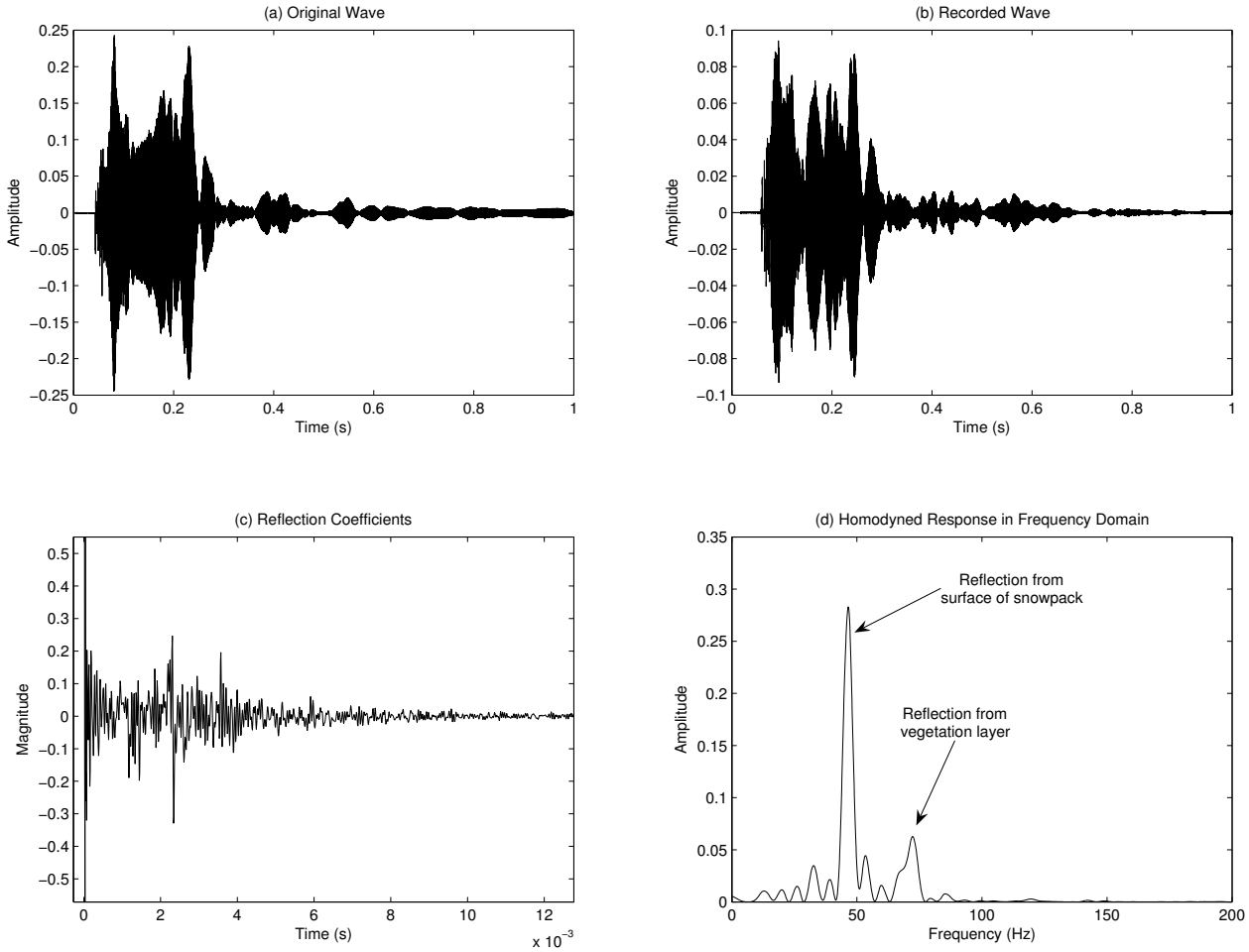

Figure 5.1. Signals in the time and frequency domains for the $N = 1$ layered snowpack in Dundrun1 site. a) original wave, b) recorded wave, c) reflection coefficients, d) homodyned response in frequency domain. The amplitudes of Figures 5.1a, 5.1b, and 5.1c are normalized. The beat frequency $\Delta F_{b,k}$ is given in Figure 5.1d.

The large spike at the beginning of the signal was assumed to be caused by the starting circuitry associated with the ADC. Because there is only one major reflection (as marked on Figure 5.1d), it is apparent that this is from the surface of the snowpack. By inspection of Figure 5.1c, it appears that the reflection coefficient $\Gamma_1 = 0.22$. The corrected reflection coefficient, calculated using Eq. 2.23, was $\Gamma_1 = 0.20$. This is taken to be the frequency-integrated plane wave reflection coefficient at the interface Ω_1 of the snowpack. By Newton-Raphson iteration

of Eq. 2.12, the porosity of the first layer of the snowpack was found to be $\phi_1 = 0.75$. Applying Eq. 2.24, the density of the snow was determined from this porosity as 229 kg m^{-3}. Because only one layer of snow was clearly visible, gravimetric sampling using a scoop could be performed. For comparison, the density determined by gravimetric sampling was 233 kg m^{-3}. The percentage difference between the density determined by the acoustic method and the density determined by gravimetric sampling was found to be approximately 2%.

Assuming that at the Saskatchewan sites, snow can be considered to have a geometry such that $\gamma = 0.80$, the tortuosity of the first layer of the snowpack was found to be $\alpha_1 = 1.25$. The reason for this choice of γ is discussed in the sensitivity analysis section of this thesis. Although there are no widely-published values for the tortuosity of snow, Jones et al. (1999) mention that this quantity has been assumed to be approximately equal to unity ($\alpha \approx 1$), and that using this value provided for suitable gas diffusion calculations. The value found for the tortuosity of the snow ($\alpha_1 = 1.25$) seems to be in general agreement with this observation. However, further research is necessary to verify this claim.

By use of Eq. 2.15, the average phase velocity of the Biot slow wave was calculated as $\overline{c}_1 = 296$ m s^{-1}. This is in the range of Albert's (1993a) calculated values for the Biot slow pressure wave in snow, and it is much less than the speed of sound in the air layer above the snowpack. This helps to support the notion that the Biot slow wave is being detected. To determine the depth of snow, the signal $s''[t]$ was homodyned with the original signal that has been sent out from the speaker. After taking the Chirp-Z transform of the homodyned signal, the frequency spectrum indicated that there were two peaks indicative of reflections; these are thought to be from the top of the snowpack and from the vegetation at the bottom of the deposited snow layer (Figure 5.1d). The first peak is found at a beat frequency

of $\Delta F_{b,1} = 46.6$ Hz. The phase velocity of the sound wave in the air layer above the snowpack was calculated to be 330 m s^{-1} at a temperature of -2.2ºC. By the use of Eq. 2.27, the distance to the top of the snowpack from the speaker and microphone was determined to be 0.38 m. Alternately, the distance from the speaker to the top of the snowpack was measured to be 0.35 m. The percentage difference between the two measurements is approximately 9%. Then, recursively applying Eq. 2.31 for the second frequency peak at $\Delta F_{b,2} = 72.3$ Hz, the depth of the one-layered snowpack was found as $y_1 = 0.19$ m. This initially appeared to differ from the measured depth of snow, which was determined to be 0.28 m, and it was thought to represent an approximate 36% error between the measurement of snow depth by the use of the acoustic method and the measurement of snow depth by the use of a rod. However, this discrepancy between actual and measured depths may be explained by considering that the measured snow depth is the depth to the un-vegetated ground surface. Because the depth of vegetation was measured to be 0.08 m (which is less than the average height of vegetation listed in Table 1), subtraction of this depth from the measured depth to the ground surface yields 0.20 m. This revised estimate of the snow depth represents a 5% difference between the measured and acoustically-determined depth of snow on the ground surface. There are considered to be no other peaks in the beat frequency spectrum, with the smallest visible peak at the highest beat frequency being indicative of the ground or vegetation layer. Peaks are defined as having amplitudes greater than the mean amplitude of the beat frequency spectrum.

This simple test case may suggest that scattering and attenuation of the sound wave by vegetation will only permit physical parameters of the snowpack to be determined to the top of the vegetation layer. However, further research is required to assess the effects of vegetation on

this method. This includes considering whether the vegetation density structure or objects (such as buried twigs or leaves) contained in the snowpack will affect this method.

Finally, calculating the SWE of the snow layer using the depth and density of snow determined by the acoustic data, it was found by the use of Eq. 2.32 that the SWE was $S_{E,\mathrm{a}} = 43.5$ mm. Alternately, using gravimetric data, the SWE was calculated as $S_{E,\mathrm{m}} = 46.6$ mm. This represents a difference of calculated SWE of approximately 7% between both of the methods. By repeating this calculation without using the correction of Eq. 2.24 and taking the reflection coefficient to be $\Gamma_1 = 0.22$, the acoustically-determined SWE was determined to be $S_{E,\mathrm{a}} = 53.2$ mm. This represents a difference of approximately 14% between both of the methods. By correcting the reflection coefficient for potential spherical spreading, it is apparent that the percentage difference between the estimation of SWE by both methods is reduced by 7%.

5.2.2. Snowpack with Multiple Layers

The same procedure for the single layer case was repeated for a snowpack containing multiple layers. As shown by this example, these layers do not necessarily correspond with the physical layers of a snowpit. The numerical results of this calculation are summarized in the following Table 5.1.

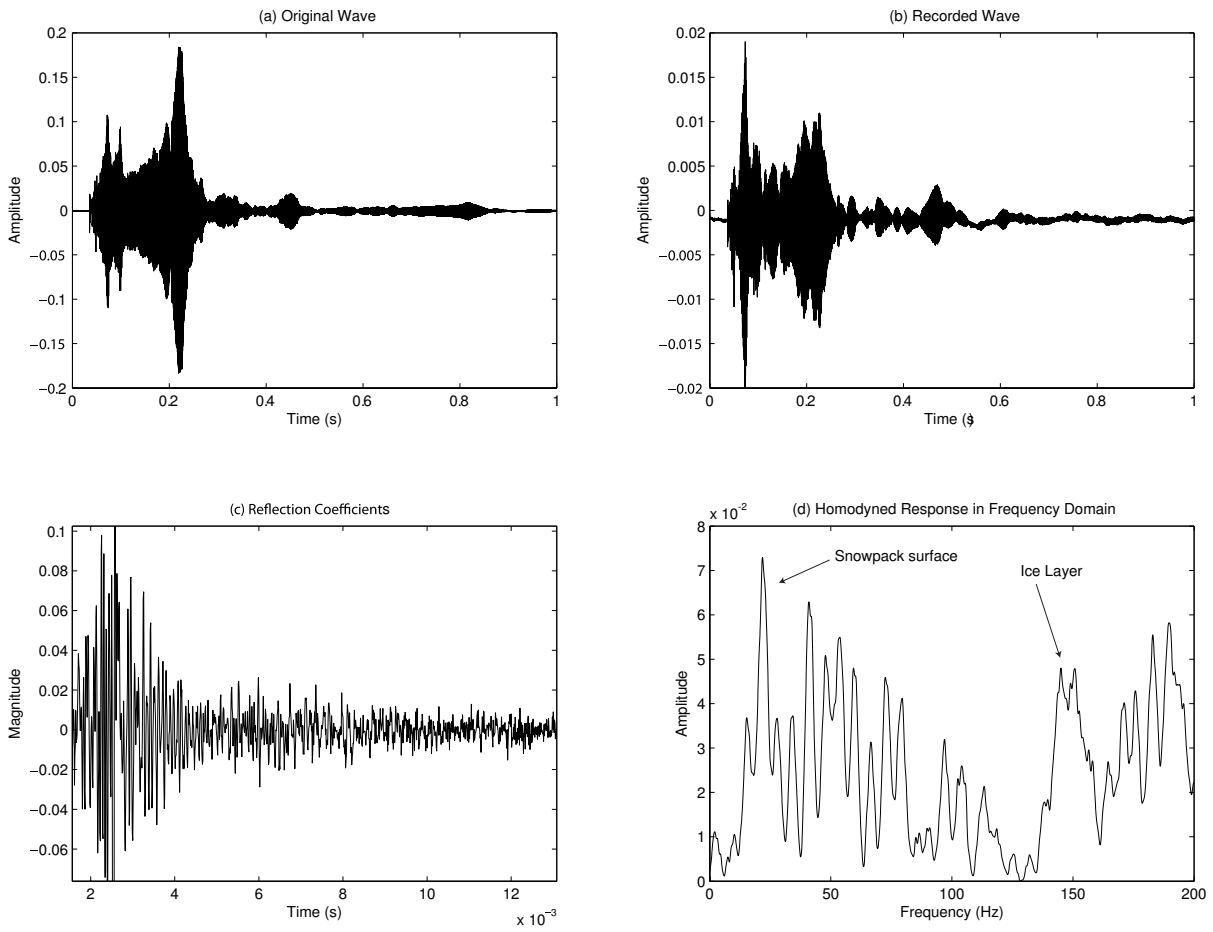

Figure 5.2. Example for the snowpack with many layers that are not easily distinguishable (Lake O'Hara). a) original wave, b) recorded wave, c) reflection coefficients, d) homodyned response in frequency domain. It is believed that the reflections after the beat frequency of 150 Hz are from a frozen layer of ice near the ground. The amplitudes of Figures 5.2a, 5.2b, and 5.2d are normalized. The beat frequency $\Delta F_{b,k}$ is given in Figure 5.2d.

Figure 5.2 graphically depicts the results of the calculations. The shape factor $\gamma \simeq 0.70$ was utilized for the calculation of this example. The snowpack was observed at the Lake O'Hara site, and the phase velocity of the sound wave in the snowpack gradually decreased with depth. The acoustically-determined SWE was determined to be $S_{E,\mathrm{a}} = 288$ mm. The SWE determined by gravimetric sampling was determined to be $S_{E,m} = 297$ mm. This represented an approximate 3% difference between the SWE values determined by the two techniques. When the same

method was attempted without using the correction of Eq. 2.23, the SWE was calculated to be $S_{E,\mathrm{a}} = 320$ mm. This represents a difference of approximately 8% between both of the methods. This case may demonstrate that the method also works for snowpacks in which discrete layers cannot be readily observed.

Interface Number (k)	$\Delta F_{b,k}$ (Hz)	Γ_k	ϕ	ρ_k (kg m-^{1})	α_k	$\overline{c}_k$ (m s^{-1})	y_{k-1} (m)
1	22	0.16	0.79	211	1.19	304	0.18
2	35	0.01	0.78	222	1.20	302	0.099
3	41	0.017	0.76	241	1.22	299	0.045
4	48	0.011	0.75	253	1.24	298	0.052
5	53.5	0.015	0.73	269	1.26	295	0.041
6	59.5	0.021	0.71	291	1.29	292	0.044
7	66.5	0.01	0.70	301	1.30	290	0.051
8	72.5	0.011	0.69	312	1.32	288	0.044
9	79.4	0.013	0.67	325	1.34	286	0.050
10	87	0.013	0.66	338	1.36	284	0.054
11	91	0.011	0.65	348	1.37	282	0.028
12	97	0.011	0.64	358	1.39	281	0.042
13	104	0.012	0.63	369	1.41	279	0.049
14	150	N/A	N/A	N/A	N/A	N/A	0.32

Table 5.1. Calculations for a layered snowpack. The distance from the loudspeaker and the microphone to the first interface of the snowpack is $y_0 = 0.18$ m. The surface of the snowpack is coincident with a beat frequency of $\Delta F_{b,1} = 22$ Hz. The depth y_{k-1} is the calculated depth of the layer L_{k-1}. Thus, y_{k-1} is the distance between interfaces Ω_{k-1} and Ω_k. The last interface Ω_{14} has been neglected because this is presumed to be the frozen ground and is not of interest in calculating SWE. The distance $y_{13} = 0.32$ m is the vertical dimension of layer L_{13}. Values in this table represent rounded estimates.

5.3. Overview of SWE Data

For the Saskatchewan observations, the correlation between the measured and the modeled SWE (Figure 5.3) for dry snow (January) was r^2 = 0.86 (slope = 1.12; Root Mean-

Squared Error = 9.7 mm) from 84 samples. These samples were collected from sites that all had vegetation (grass and shrub) heights <30 cm, no visible ice layers, and smooth interfaces between the snow layers. For wet snowpacks (March), the calculated results from 35 samples showed a very weak correlation of $r^2 = 0.30$ (slope = 0.51, Root Mean-Squared Error = 92.7 mm) between the measured and the modeled values of SWE. This was interpreted as being caused by excessive attenuation of the acoustic pressure wave due to the liquid water filling the pore spaces of the snow-ice matrix.

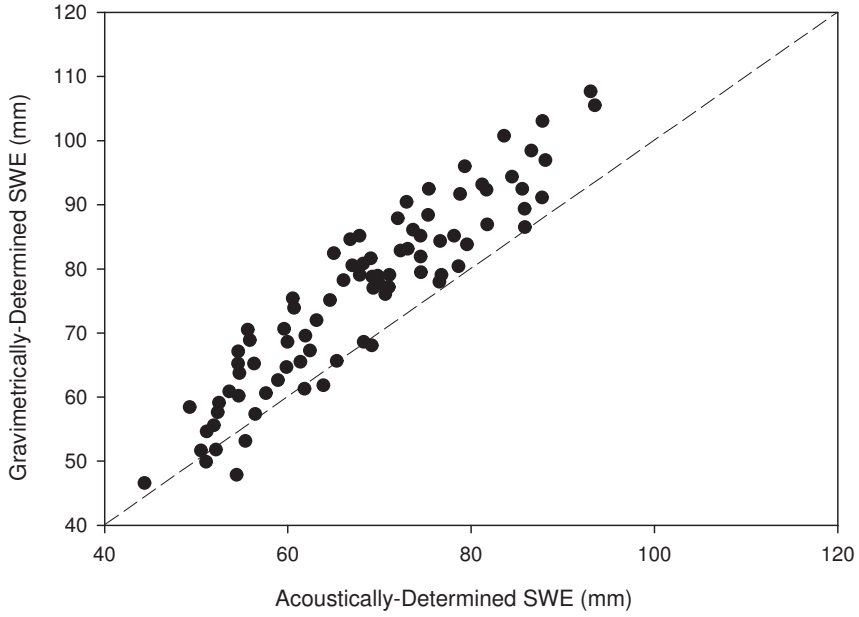

Figure 5.3. Saskatchewan site results for the relationship between gravimetrically measured and acoustically-determined SWE for January, dry snow conditions. The dashed pattern ---------- represents the 1:1 line.

At Lake O'Hara, the majority of physical density samples were collected by the use of an older MSC snow sampling tube. Snow was melting slowly and so a mixture of dry snow and moderately wet, well drained snow was sampled. For all of these sites, the correlation between

the values of measured and modeled values of SWE (Figure 5.4) was found to be $r^2 = 0.78$ (slope = 1.02; Root Mean-Squared Error = 7.0 mm) from 84 samples.

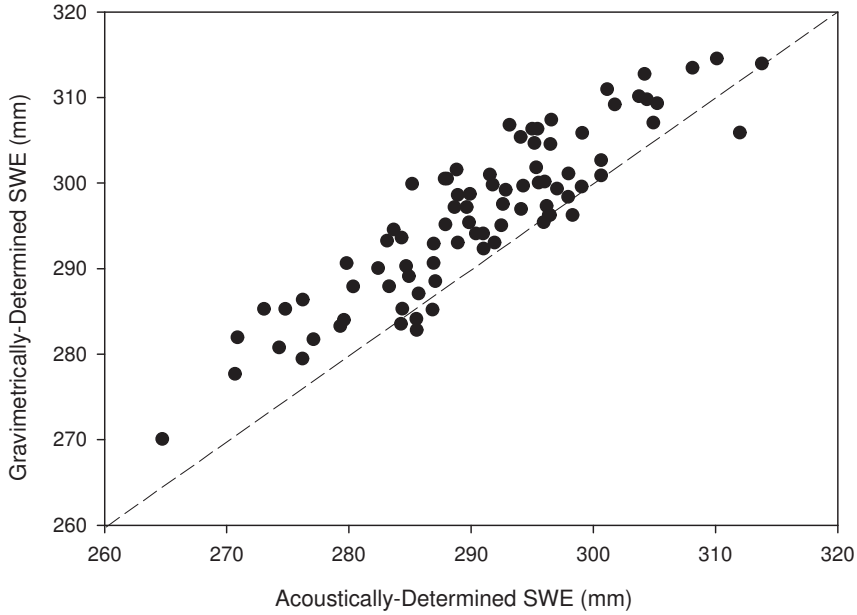

Figure 5.4. Lake O'Hara site results for the relationship between gravimetrically-measured and acoustically-determined SWE. The dashed pattern ---------- represents the 1:1 line.

It was suspected that the correlation for the Lake O'Hara sites showed a weaker relationship as compared to the correlations found from the Saskatchewan sites due to (a) higher snow liquid water content than the dry prairie snow sites in January, and (b) deeper snow. The maximum depth of snow tested at the Lake O'Hara sites was 1.5 m, thereby indicating the method's utility for deep mountain snowpacks as well as shallow prairie snowpacks. A lower r^2 value at the Lake O'Hara site could also have been caused due to the portable device, which was not mounted at a fixed height above the snow surface. Small angular deviation from normal incidence at the surface of the snowpack could have violated the assumptions of the acoustic

model, which assumes that the loudspeaker and the microphone are situated along an axis parallel to the snow surface.

Both Figure 5.3 and Figure 5.4 indicate that there is a systematic error in the acoustic data of approximately 10 mm SWE, with the gravimetrically-determined SWE being higher than the acoustically-determined SWE estimates. It is conceivable that this shift might have occurred due to depth measurements made from the reflections from each of the interfaces in the snowpack. Because the phase velocity of the sound wave in the snowpack varies with frequency, the acoustically-determined depth of snow is less than the depth of snow determined by physical measurement. This is because the sound wave will travel at different phase velocities in the snowpack at different frequencies. Thus, because the depth of snow is underestimated by the acoustic measurement, the gravimetrically-determined SWE is greater then the acoustically-determined SWE for both the Saskatchewan and Lake O'Hara sites. However, further research is required to verify this claim.

5.4. Sensitivity Analysis

A sensitivity analysis was performed to determine the effect of the most uncertain parameter on the calculations. The most uncertain parameter is the γ shape factor, which is used in Eqs. 2.12 and 2.13 to determine the porosity and the tortuosity of each layer. Because the porosity is used to calculate both the density and the average phase velocity in each layer, the sensitivity of the γ shape factor is crucial to calculated SWE. Two cases are considered: (1) the sensitivity of γ at the air-snow interface; and (2) the sensitivity of γ at snow-snow interfaces.

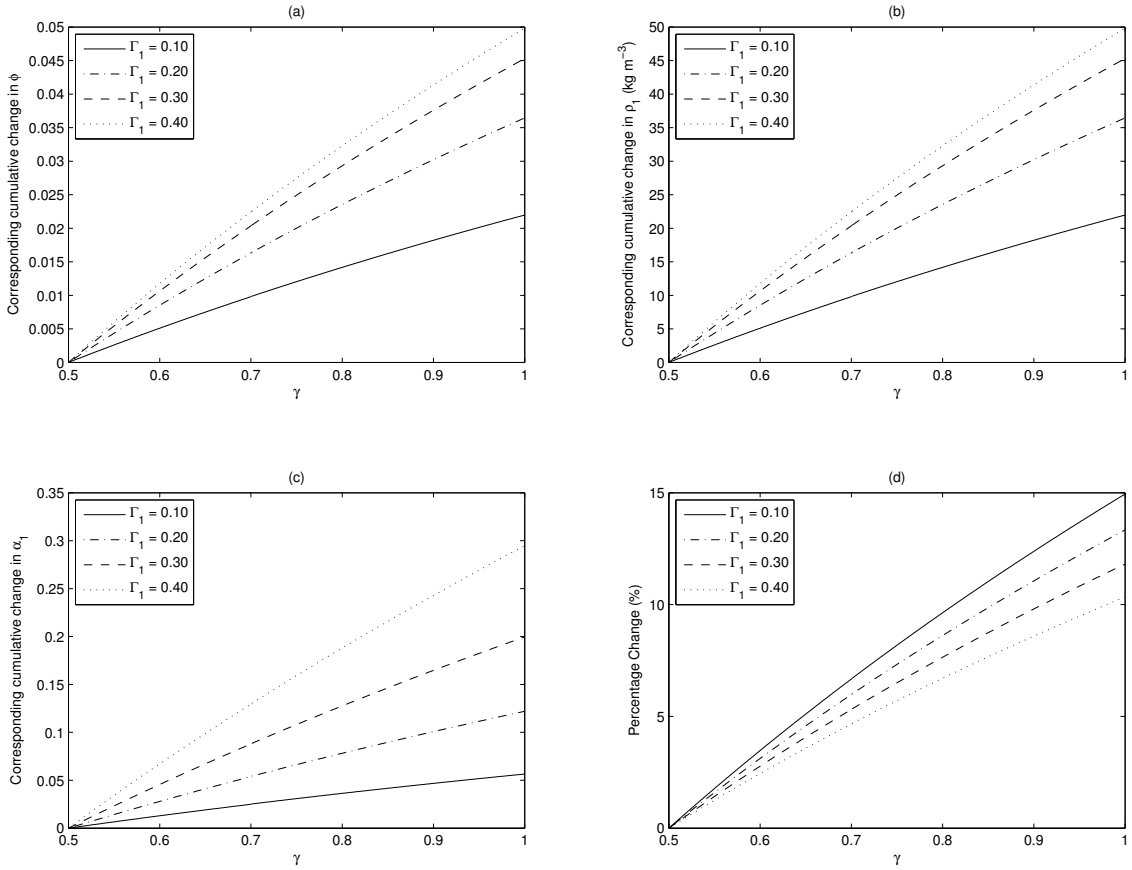

Figure 5.5. Sensitivity analysis for the air-snow interface. a) Examining sensitivity of ϕ to change in shape factor γ; b) Examining sensitivity of ρ_1 to change in shape factor γ; c) Examining sensitivity of α_1 to change in shape factor γ; d) Percentage difference of ρ_1 due to change in shape factor γ.

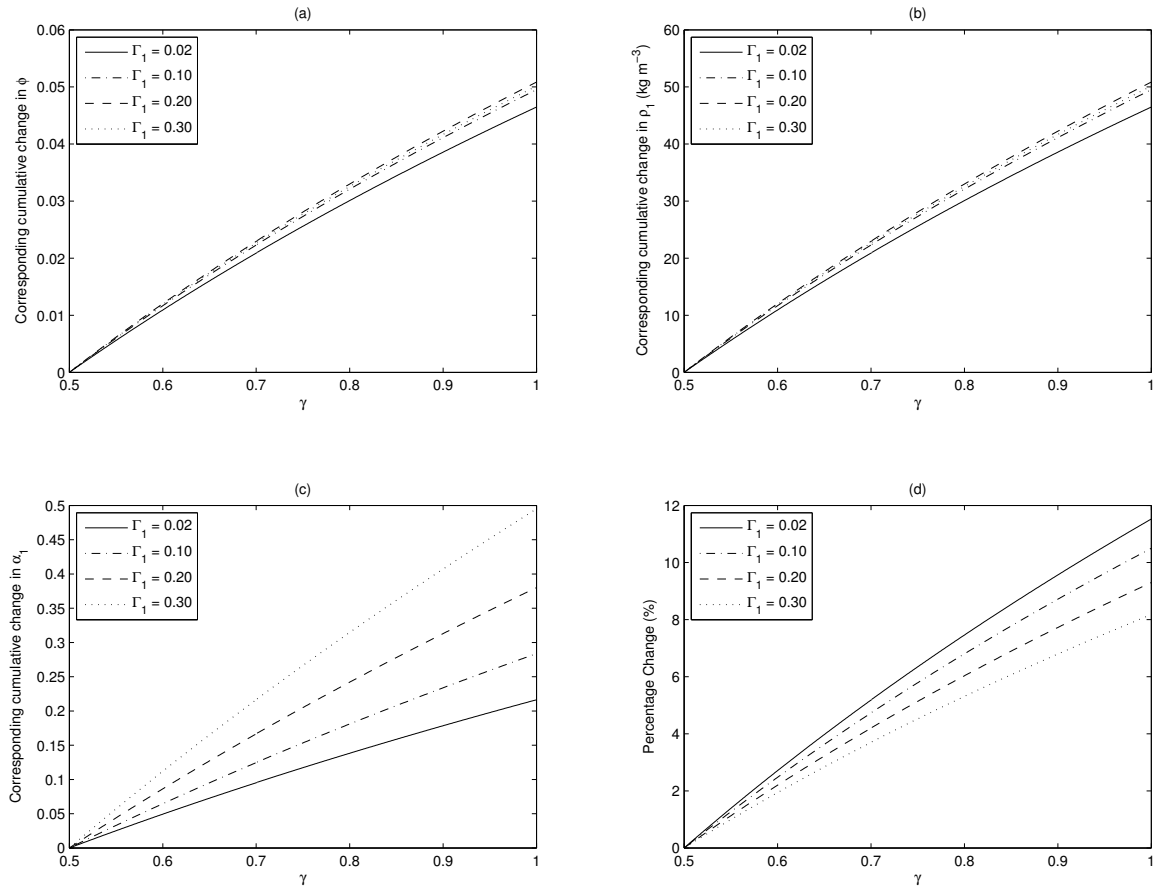

Figure 5.6. Sensitivity analysis of the snow-snow interface. a) Examining sensitivity of ϕ to change in shape factor γ; b) Examining sensitivity of ρ_1 to change in shape factor γ; c) Examining sensitivity of α_1 to change in shape factor γ; d) Percentage difference of ρ_1 due to change in shape factor γ.

Figure 5.5 shows the results of a sensitivity analysis where γ was varied on the interval [0.5 1.0], which represents the range of the particle shape factor γ and a range of reflection coefficients, Γ_1. The results indicate that for larger reflection coefficients at the air-snow interface, the cumulative changes in the calculated porosity ϕ_1, density of the first layer ρ_1, and tortuosity α_1 are greater than for the changes observed with reflection coefficients of a lower magnitude. Moreover, for reflection coefficients of a greater magnitude, the cumulative change in the calculated density will be of a corresponding greater magnitude. The numerical

experiments show that if the shape factor is selected from the interval [0.5 1.0], the error in the determined density ρ_1 will be no greater than approximately 15%. This indicates that the calculated density ρ_1 is relatively insensitive to variations in γ.

Figure 5.6 indicates a similar trend for the snow-snow interfaces in the snowpack; however, the corresponding change in the calculated porosity ϕ_k and density ρ_k are even less sensitive to variations of the reflection coefficient. However, the calculated tortuosity α_k exhibits approximately the same sensitivity as shown in Figure 5.5. The percentage change in the calculated density due to variations in the γ shape factor at the snow-snow interfaces is approximately the same as the change in the variation in the γ shape factor at the air-snow interface. Using the aggregated data for this experiment, it was found that $\gamma \simeq 0.80 > 3/4$ for the Saskatchewan sites best fitted the acoustic estimation of SWE to gravimetric samples, whereas for the Lake O'Hara sites, $\gamma \simeq 0.70 > 1/2$ resulted in the best fit. Due to melt metamorphism, it is conceivable that the snow crystals at the Lake O'Hara site would have more of a rounded shape than the snow crystals at the Saskatchewan site due to cold temperature gradient metamorphism. However, because observations were not made of the snow crystal geometry at both of the sites, it is not possible to make quantitative comparisons and the differences in γ could be due to other factors.

Another uncertainty was introduced by the use of Eq. 2.23, which corrects for spherical spreading of the sound wave. The data presented in Figure 5.3 and Figure 5.4 has been processed using this correction. Eq. 2.23 reduces the percentage error between the acoustically-determined and gravimetrically measured calculations by approximately 5% for all of the sites. Applying Eq. 2.23 to the data for the Lake O'Hara sites, the percentage error is reduced by

approximately 8%. This indicates that the Eq. 2.23 can be used in the data processing flow to improve the accuracy of acoustically-determined SWE estimates.

To investigate the effects of air temperature on the acoustic model, a sensitivity analysis of temperature was also examined with respect to changes in the calculated SWE. Assuming that the temperature is such that $-30°\text{C} \leq T^* \leq 0°\text{C}$, Figure 5.7 shows that the calculated SWE will change by only 0.003% when the acoustic model is evaluated over this range. This indicates that the acoustic model is not very sensitive to changes in temperature and that errors in determining this quantity will have a negligible effect on the calculated SWE.

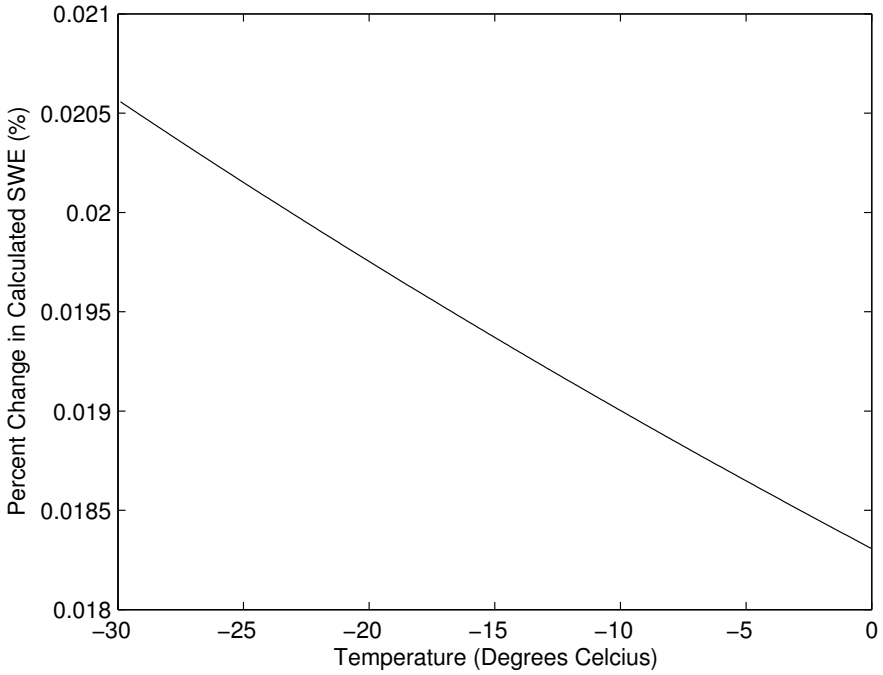

Figure 5.7. Examining the change in temperature with respect to the change in calculated SWE

6. DISCUSSION

The experiment and theoretical development suggest that sound can be used to determine the physical properties of snow and SWE can be estimated by the use of an acoustic wave. This helps to support the notion that a simplified version of the Biot theory can be used to determine the physical properties of seasonal snowcovers. Although the Berryman (1980) formulation has been used as Eq 2.11 to be able to solve for the porosity of snow, this equation has never been tested for snow as a porous medium. Given the results of this experiment, it is possible to suggest that the Berryman (1980) equation is useful in the application presented in this thesis. Although snow is a porous medium that strongly attenuates sound, it is suggested that it is possible to determine the physical properties of an undisturbed snowpack at depths up to at least 1.5 m. This represents the greatest depth of snow that has been observed in the context of this study.

The Biot slow wave that propagates in the air spaces of the snowpack was used to determine SWE. This method relies on the reflection of sound from the "layers" in a snowpack that have been created by metamorphism, melt, sublimation, blowing snow and depositional processes. The method does not take into consideration changes in physical properties that increase with depth within a layer because it depends on reflections that are caused by changes in acoustic impedance. Moreover, because this method deals with physical acoustic properties, it is likely not possible to distinguish between snow and organic layers of similar density which are situated under the snowpack. Further testing with organic layers is required to fully understand the limitations of the acoustic method when it is used to determine the physical properties of snow in such environments.

Another aspect of acoustic measurement of snow that would benefit from further research is a study of the effects of irregular snow-surface topography and vegetation on the reflection response of the signal. It is possible that in the same manner as any other diffuse reflector, vegetation can cause scattering of the reflected sound wave, thereby decreasing the effectiveness of the method. It is also conceivable that a similar effect could occur when the snow surface is irregular, such as in the vicinity of a tree well or in close proximity to other depositional features caused by vegetation. In a similar fashion, one of the tests presented by Albert (2001) showed that the acoustic waveform inversion may occasionally determine only the depth to a particular interface in the snowpack. Other effects of scattering may be caused by ice layers in the snowpack. However, these effects were not observed in the field trials.

Noting these concerns, the overall error in the gravimetrically measured SWE and the SWE determined by the acoustic technique at all of the sites for dry to moderately wet snow conditions was approximately 10%. An analysis given by Goodison et al. (1981) indicated that the mean maximum error between SWE determined by a tube snow sampler and SWE determined by carefully weighing bagged samples was approximately 10%. This suggests that the acoustic technique has an average error similar to that between two gravimetric techniques. The estimates of SWE presented here are therefore likely adequate for use in snow surveying for hydrological and climatological purposes and are certainly as good as two gravimetric methods compared to each other. Further physical refinement of the device and calibration of its output would reduce these errors.

Further experimentation is planned to both verify the results reported in this paper and extend the method so that it is sufficiently reliable and robust for operational use. One task of additional research would be to determine the effective frequency range over which the sweep

can be used to characterize snow. Additional research would help to verify the relationships identified in this paper and further investigate the limitations of the method in the context of other environmental situations.

7. CONCLUSIONS

This thesis has presented and tested a theory that allows for the calculation of SWE by the use of an acoustic wave. Although the physics of sound propagation in a snowpack (Johnson, 1982) can be explained by the Biot (1956a, 1956b) theory, this thesis helps to support the notion that a simplified version of the Biot theory used along with the Berryman (1980) equation can be used to determine the physical properties of seasonal snowcovers. It is also possible to make a few conclusions regarding the nature of this method. From the research that has been conducted, a number of conclusions can be identified:

1. Despite the high variability of snow distribution over natural landscapes, it has been shown possible to use a frequency-swept acoustic pulse to determine SWE. This pulse was produced by a system with the following characteristics:

- The pulse has a frequency in the range of 20 Hz to 20 kHz;
- The pulse has a duration of no more than 1s;
- The pulse is produced by a loudspeaker that has a non-linear frequency response;
- The loudspeaker is mounted at a minimum distance of 15 cm and no more than 40 cm above the surface of the snowpack; and
- The separation distance between the speaker and the microphone is no more than 15 cm.

2. Unlike most prior work in snow acoustics, the technique presented in this thesis does not rely on invasive measurements to determine SWE. This technique can be placed into the same category of techniques as Lee and Rogers (1985) and Albert (1998, 2001), where acoustic observations are taken above the snowpack. However, the technique presented in this thesis extends the work of Lee and Rogers (1985) and Albert (1998, 2001) because it does not rely on

iterating the parameters of a porous acoustics model to generate a waveform which is then matched with the recorded waveform. Rather, the technique presented in this thesis is used to analyze an acoustic wave, and from this analysis, SWE is estimated. This eliminates the step of generating and comparing a separate acoustic waveform.

3. Although Lee and Rogers (1985) were able to determine the porosity of snow deposited on a metal roof of a building and Albert (1998, 2001) was able to determine snow depth in a natural environment, this thesis presents the results of what is believed to be the first observations of SWE estimated by the use of a sonic impulse. This is also the first time that acoustics has been used to determine SWE in both prairie and alpine environments.

4. Further research is required to:

- Validate the maximum depth to which a frequency-swept wave can estimate SWE;
- Establish the range of effective frequencies over which SWE can be estimated and determine whether the entire 20 Hz to 20 kHz bandwidth used in this thesis is applicable; and
- Ascertain the effects of vegetation and the ground surface on the acoustically-determined SWE.

To quickly deploy instrumentation capable of sending out an acoustic wave and capturing the overall reflection from the snowpack, further research is planned to construct a SWE gauge that can automatically apply some aspects of the mathematics and signal processing described in this thesis. This gauge will be deployed in portable (hand-held) and met-station mounted (stationary) configurations.

LIST OF REFERENCES

Adams, W.P., and Rogerson, R.J. 1968. Snowfall and snowcover at Knob Lake, Central Labrador-Ungava. *Proceedings of the Eastern Snow Conference* 25: 110-139.

Akinremi, O.O., McGinn, S. M., and Cutforth, H. W. 1999. Precipitation Trends on the Canadian Prairies. *Journal of Climate* 12(10): 2996-3003.

Albert, D.G. 1987. The effect of snow on vehicle-generated seismic signatures. *Journal of the Acoustical Society of America* 81(4): 881-887.

———., and Orcutt, J.A. 1990. Acoustic pulse propagation above grassland and snow: comparison of theoretical and experimental waveforms. *Journal of the Acoustical Society of America* 67(1): 93-100.

———1992. Acoustic surface wave propagating horizontally above a seasonal snow cover. *Journal of the Acoustical Society of America* 91(4): 2455.

———. 1993a. *Attenuation of outdoor sound propagation levels by a snow cover, CRREL Report 93-20*. Hanover, New Hampshire: Cold Regions Research and Engineering Laboratory.

———. 1993b. A comparison between wave propagation in water-saturated and air-saturated porous materials. *Journal of Applied Physics* 73(1): 28-36.

———. 1998a. Snow cover effects on impulsive noise propagation in a forest. *Noise Control Engineering Journal* 46: 208-214.

———. 1998b. Theoretical modeling of seismic noise propagation in firn at the South Pole, Antarctica. *Geophysical Research Letters* 25(23): 4257-4260.

———. 2001. Acoustic waveform inversion with application to seasonal snow covers. *Journal of the Acoustical Society of America* 109(1): 91-101.

Arcone, S.A. 1997. Reflection profiling of Arctic lake ice using microwave FMCW radar. *IEEE Transactions on Geoscience and Remote Sensing* 35(2): 436-443.

Ashmore P., and Church, M. 2001. *The impact of climate change in rivers and river processes in Canada*, *Geological Survey of Canada Bulletin 555, GSC Miscellaneous Report No. 70.* Ottawa: Minister of Supply and Services.

Attenborough, K. 1985. Acoustical impedance models for outdoor ground surfaces. *Journal of Sound and Vibration* 99(4): 521-544.

———., and Buser, O. 1998. On the application of rigid-porous models to impedance data for snow. *Journal of Sound and Vibration* 124(2): 315-327.

Berryman, J.G. 1980. Confirmation of Biot's Theory. *Applied Physics Letters* 37 (4):382-384.

———. 1983. Effective conductivity by fluid analogy for a porous insulator filled with a conductor. *Physical Review B* 27(12): 7789-7792.

Bilello, M.A. 1957. A survey of Arctic snow-cover properties as related to climate conditions. In *SIPRE Research Report 39, 1-9*.

Biot, M.A. 1956a. Theory of propagation of elastic waves in a fluid-saturated porous solid. I. Low Frequency Range. *Journal of the Acoustical Society of America* 28(2): 168-178.

———. 1956b. Theory of propagation of elastic waves in a fluid-saturated porous solid. II. Higher frequency range. *Journal of the Acoustical Society of America* 28(2): 179-191.

Blackstock, D.T. 2000. *Fundamentals of Physical Acoustics*. New York: John Wiley and Sons.

Bluestein, L.I. 1968. A linear filtering approach to the computation of the discrete Fourier transform. *Northeast Electronics Research and Engineering Meeting Record* 10 (218-219).

Bogorodskii, V.V., and Dobrotin, D.D. 1963. Results of an investigation of the physicomechanical properties of the snow cove on ice floes. *Soviet Physics Acoustics* 9: 89-90.

———. Gavrillo, V.P., and Niktin, V.A. 1974. Characteristics of sound propagation in snow. *Soviet Physics Acoustics* 20: 121-122.

Bowling, L.C., Pomeroy, J.W., and Lettenmaier, D.P. 2004. Parameterization of blowing-snow sublimation in a macroscale hydrology model. *Journal of Hydrometeorology* 5: 745-762.

Brittle, K., and Lines, L. 2001. Vibroseis deconvolution: an example from Pikes Peak, Saskatchewan. *CSEG Recorder* May 2001:28-35.

———., Lines, L.R., and Dey, A.K. 2001. Vibroseis deconvolution: a comparison of cross-correlation and frequency-domain sweep deconvolution. *Geophysical Prospecting* 49(6): 675-686.

Budd, W.F., Dingle, W.R.J., and Radok, U. 1966. The Byrd snow drift project: outline and basic results. In *Studies in Antarctic Meteorology, American Geophysical Union Antarctic Research Series 9*.

Bunnell, F.L., McNay, R.S., Shank, C.C. 1985. *Trees and Snow: the deposition of snow on the ground--a review and quantitative synthesis*. Victoria, British Columbia: Research Branch, Ministries of Environment and Forests.

Burkard, M.B., Whiteley, H.R., Schroeter, H.O., and Donald, J.R. 1991. Snow depth/area relationships for various landscape units in southwestern Ontario. *Proceedings of the Eastern Snow Conference* 48:51-65.

Buser, O. 1986. A rigid frame model of porous media for the acoustic impedance of snow. *Journal of Sound and Vibration* 111(1): 71-92.

Byrd, G.P., Weinbeck, R.S., and Ansett, R.A. 1988. Probing lake-effect snowbands using a portable radiosonde unit. *Proceedings of the Eastern Snow Conference* 45: 7-26.

Canyan, D.R. 1996. Interannual climate variability and snowpack in the western United States. *Journal of Climate* 9: 928-948.

Carr, D.A. 1983. Northern Ontario precipitation estimates. *Proceedings of the Eastern Snow Conference* 40: 207-211.

Carroll, T.R. 1987. Operational airborne measurements of snow water equivalent and soil moisture using terrestrial gamma radiation. *Proceedings of the Large Scale Effects of Seasonal Snow Cover, International Association of Scientific Hydrologists* 166: 213-223.

Champoux, Y., and Allard, J.F. 1991. Dynamic tortuosity and bulk modulus in air-saturated porous media. *Journal of Applied Physics* 70(4): 1975-1979.

Chung, Y.S., Hage, K.D., and Reinelt, E.R. 1976. On lee cyclogenesis and air-flow in the Canadian Rocky Mountains and East Asian Mountains. *Mon. Weather Rev.*104: 879-891.

Church, J.E. 1912. The conservation of snow--its dependence on forests and mountains. *Scientific American Supplement* 74(1914): 152-155.

———. 1933. Snow surveying: its principles and possibilities. *Geographical Review* 23(4): 529-563.

Claerbout, J. 1984. *Imaging the Earth's Interior*. Paulo Alto, California: Blackwell Science.

Colliander, S.W. 1954. Russian ski patrols in action. *Befael* 37(1): 22-25.

Collier, C.G. 1998. Snow. In *Encyclopedia of Earth Sciences, Hydrology and Lakes*, edited by R. W. Fairbridge, and Michael R. Rampino. Berlin: Springer-Verlag.

Cork, H.F., and Loijens, H.S. 1980. The effect of snow drifting on gamma snow survey results. *Journal of Hydrology* 48: 41-51.

Davis, R.T. 1973. Operational Snow Sensors. *Proceedings of the Eastern Snow Conference* 13: 57-70.

Derksen, C., Brown, R., Walker, A., and Brasnett, B. 2002. Comparison of model, snow course, and passive microwave derived Snow Water Equivalent Data for western North America. *Proceedings of the Eastern Snow Conference* 59:203-213.

———., Ledrew, W., Walker, A., and Goodison, B. 2000. Winter season variability in North American prairie SWE distribution and atmospheric circulation. *Proceedings of the Eastern Snow Conference* 57: n.p.

Déry, S.J., and Yau, M.K. 2001. Simulation of an Arctic ground blizzard using a coupled blowing snow-atmosphere model. *Journal of Hydrometeorology* 2:579-598.

Dingman, S.L. 2002. *Physical Hydrology, Second Edition*. Upper Saddle River, New Jersey: Prentice-Hall.

Donald, J.R., Soulis, E.D., Seglenieks, F., and Kouwen, N. 1991. Snow depth estimates for shallow snowpacks from GOES visible imagery. *Proceedings of the Eastern Snow Conference* 48: 149-161.

Elder, K., Dozier, J., and Michaelsen, J. 1991. Snow accumulation and distribution in an alpine watershed. *Water Resources Research* 27(7): 1541-1552.

———., Davis, R.W., Bales, R.C. 1991. Terrain classification of snow-covered watersheds. *Proceedings of the Eastern Snow Conference* 48: 39-49.

Ellerbruch, D.A., and Boyne, H.S. 1979. Snow stratigraphy and water-equivalence measured with an active microwave system. *Journal of Glaciology* 26: 225-234.

Engman, E.T. 1966. Review of snow measuring instrumentation and evaluation of a pressure pillow snow-measuring device. *Proceedings of the Eastern Snow Conference* 23: 1-17.

Environment Canada. 1992. Great Lakes Surface Water Temperature Climatology, Climatological Studies 43. Downsview, Ontario: Atmospheric Environment Service.

Essery, R., Li, L., and Pomeroy, J. 1999. A distributed model of blowing snow over complex terrain. *Hydrological Processes* 13: 2423-2438.

———. 2001. Spatial statistics of windflow and blowing snow over complex topography. *Boundary-layer meteorology* 100: 131-147.

———., and Pomeroy, J. 2004. Vegetation and topographic control of wind-blown snow distributions in distributed and aggregated simulations for an arctic tundra basin. *Journal of Hydrometeorology* 5: 735-744.

———., Granger, R., and Pomeroy, J. 2006. Boundary-layer growth and advection of heat over snow and soil patches: modeling and parameterization. *Hydrological Processes* 20: 953-967.

Faria, D.A., Pomeroy, J.W., and Essery, R.L.H. 2000. Effect of covariance between ablation and snow water equivalent on depletion of snow-covered area in a forest. *Hydrological Processes* 14: 2683-2695.

Fassnacht, S.R., Yusuf, F., and Kouwen, N. 2002. January 1999 storms dumped snow on southern Ontario, yet limited streamflow resulted. *Proceedings of the Eastern Snow Conference* 59: 223-233.

Föhn, P.M.B., and Meister, R. 1983. Distribution of snow drifts on ridge slopes: measurements and theoretical approximations. *Annals of Glaciology* 4: 52-57.

Gibson, B., and Larner, K. 1984. Predictive deconvolution and the zero-phase source. *Geophysics* 49(4): 329-397.

Goita, K., Walker, A., and Goodison, B. 2003. Algorithm development for the estimation of Snow Water Equivalent in the boreal forest using passive microwave data. *International Journal of Remote Sensing* 24(5): 1097-1102.

Golding, D.L., and Swanson, R.H. 1978. Snow accumulation and melt in small forest openings in Alberta. *Canadian Journal of Forestry Research* 8 (4):380-388.

Goodison, B.E., Ferguson, H.L., and McKay, G.A. 1981. Measurement and Data Analysis. In *Handbook of Snow*, edited by D. M. Gray and D. H. Male. Toronto: Pergamon Press Canada.

———., Wilson, B., Wu, K., and Metcalfe, J.R. 1984. An inexpensive remote snow-depth gauge: an assessment. *Proceedings of the Western Snow Conference* 52: 188-191.

———., Metcalfe, J.R.., Wilson, R.A., and Jones, K. 1988. The Canadian automatic snow depth sensor: a performance upgrade. *Proceedings of the Western Snow Conference* 56: 178-181.

———., and Walker, A. 1995. Canadian development and use of snow cover information from passive microwave satellite data. In *Passive Microwave Remote Sensing of Land-Atmosphere Interactions*, edited by B. Choudhury, Kerr, Y., Njoku, E., and Pampaloni, P. Utrecht, Netherlands: Brill Academic Publishers.

Gorodetskaya, I.V., Cane, M., Tremblay, L.-B., and Kaplan, A. 2006. The effects of sea-ice and land-snow concentrations on planetary albedo from the Earth Radiation Budget Experiment. *Atmosphere-Ocean* 44(2): 195-205.

Granburg, H.B., and Kingsbury, C.M. 1984. Tests of new snow density samplers. *Proceedings of the Eastern Snow Conference 41*:224-240.

Granger, R.J., Pomeroy, J.W., and Parviainen, J. 2002. Boundary-layer integration approach to advection of sensible heat to a patchy snow cover. *Hydrological Processes* 16: 3559-3569.

———., Essery, R., and Pomeroy, J.W. 2006. Boundary-layer growth over snow and soil patches: field observations. *Hydrological Processes* 20: 943-951.

Gray, D.M. 1970. Snow Hydrology of the Prairie Environment. In *Snow Hydrology : proceedings of the workshop seminar / [sponsored by the Canadian National Committee [for the] International Hydrological Decade [and the University of New Brunswick, 1968]*, edited by Canadian National Committee for the International Hydrological Decade. Toronto: Queen's Printer for Canada.

———. 1979. Snow accumulation and distribution. In *Proceedings, Modeling Snow Cover Runoff*, edited by S. C. Colbeck, and M. Ray. Hanover, New Hampshire: Cold Regions Research and Engineering Laboratory.

Groisman, P.Ya., and Davies, T.D. 2001. Snow Cover and the Climate System. In *Snow Ecology: An Interdisciplinary Examination of Snow-Covered Ecosystems*, edited by H. G. Jones, Pomeroy, J.W., Walker, D.A., and Hoham, R.W. Cambridge, UK: Cambridge Unversity Press.

Gubler, H. 1981. An inexpensive snow depth gauge based on ultrasonic wave reflection from the snow surface. *Journal of Glaciology* 27(95): 157-163.

———., and Hiller, M. 1984. The use of microwave FMCW radar in snow and ice research. *Cold Regions Science and Technology* 9: 109-119.

Gustafsson, D., Waldner, P.A., and Stähli, M. 2004. Factors governing the formation and persistance of layers in a subalpine snowpack. *Hydrological Processes* 18:1165-1183.

Hall, D.K., Benson, C.S., and Chien, J.Y.L. 1993. Analysis of visible and microwave satellite data for snow mapping in Alaska. *Joint Proceedings of the 50th and 61st Eastern and Western Snow Conferences*: 129-137.

Harazono Y., Mano M., Kitauchi H., Miyata A., and Oechel W.C. 2002. Winter fluxes of CO_2 and energy at tundra in the Arctic. *AGU poster*, GC72B-0235.

Hardy, J.P., Melloh, R., Jordan, R. 2000. Incorporating effects of forest litter in a snow process model. *Proceedings of the Eastern Snow Conference* 57: n.p.

Harrison, C., and Nielsen, P.L. 2004. Plane wave reflection coefficient from near field measurements. *Journal of the Acoustical Society of America* 116(3): 1355-1361.

Hartley, S. 1997. Atlantic ocean-atmosphere interactions and snowfall in Southern New England. *Proceedings of the Eastern Snow Conference* 54: 69-79.

———., and Keables, M. J. 1998. Synoptic associations of winter climate and snowfall variability in New England, USA, 1950-1992. *International Journal of Climatology* 18(3): 281-298.

Hedstrom, N.R., and Pomeroy, J.W. 1998. Measurements and modeling of snow interception in the boreal forest. *Hydrological Processes* 12: 1611-1625.

———., Granger, R.J., Pomeroy, J.W., Gray, D.M., Brown, T., and Little, J.L. 2001. Enhanced indicators of land use change and climate variability impacts on prairie hydrology using the Cold Regions Hydrological Model. *Proceedings of the Eastern Snow Conference* 58: n.p.

Huges, M.G., and Robinson, D.A. 1993. Snow cover variability in the Great Plains of the United States: 1910-1988. *Proceedings of the Eastern Snow Conference* 50: 35-42.

Iacozza, J. and D.G. Barber. 2001. Ablation patterns of snow cover over smooth first year sea ice in the Canadian Arctic. *Hydrological Processes* 15: 3359-3569.

Isard, S.A., and Schaetzl, R.J. 1993. Southern Michigan's Snow Belt: Modeled Impacts on Soil Temperatures and Freezing. *Joint Proceedings of the 50th and 61st Eastern and Western Snow Conferences*: 247-253.

Ishida, T. 1965. Acoustic properties of snow. *Contributions of the Institute of Low Temperature Science (Series A)* 20: 23-63.

Jin, J., Miller, N.L., Sorooshian, S., and Gao, X. 2006. Relationship between atmospheric circulation and snowpack in the western USA. *Hydrological Processes* 20:753-767.

Jiusto, J.F., and Kaplan, M.L. 1971. Snowfall properties of Lake Erie and Ontario storms. *Proceedings of the Eastern Snow Conference* 28:17-24.

Johnson, D.L. 1980. Equivalence between fourth sound in Liquid He II at low temperatures and the Biot slow wave in consolidated porous media. *Applied Physics Letters* 37: 1065-1067.

———., and Sen, P.N. 1981. Multiple scattering of acoustic waves with application to index of refraction of fourth sound. *Physical Review B* 24(5): 2486-2496.

———., and Plona, T.J. 1982. Acoustic slow waves and the consolidation transition. *Journal of the Acoustical Society of America* 72(2): 556-565.

———., Plona, T.J., Scala, C., Pasierb, F., Kojima, H. 1982. Tortuosity and acoustic slow waves. *Physical Review Letters* 49(25): 1840-1844.

———., Koplik, J., Dashen, R. 1987. Theory of dynamic permeability and tortuosity in fluid-saturated porous media. *Journal of Fluid Mechanics* 176: 379-402.

Johnson, J.B. 1982. On the application of Biot's theory to acoustic wave propagation in snow. *Cold Regions Science and Technology* 6: 49-60.

———. 1985. Audibility within and outside of deposited snow. *Journal of Glaciology* 31(108): 136-142.

———., and Marks, D. 2004. The detection and correction of snow water equivalent pressure sensor errors. *Hydrological Processes* 18: 3513-3525.

Jones, H.G., Pomeroy, J.W., Davies, T.D., Tranter, M., and Marsh, P. 1999. CO_2 in Arctic snow cover: landscape form, in-pack gas concentration gradients, and the implications for the estimation of gaseous fluxes. *Hydrological Processes* 13:2977-2989.

Karl, T.R., Groisman, P.Ya. Knight, R.W., and Heim, R.R., Jr. 1993. Recent variations of snow cover and snowfall in North America and their relation to precipitation and temperature variations. *Journal of Climate* 6: 1327-1344.

Kaye, G.W.C., and Evans, E.J. 1939. Sound absorption of snow. *Nature (London)* 143:80.

Kennett, B.L.N. 2001. *The Seismic Wavefield. Volume I: Introduction and Theoretical Development*. Cambridge, UK: Cambridge University Press.

Kind, R.J. 1981. Snow drifting. In *Handbook of Snow: Principles, Processes, Management, and Use*, edited by D. M. Gray, and D.H. Male. Toronto: Pergamon Press Canada.

Kobayashi, D. 1987. Snow accumulation on a narrow board. *Cold Regions Science and Technology* 13(3): 239-245.

Koh, G. 1993. FMCW radar investigation of snow pack evolution. *Proceedings of the Eastern Snow Conference* 50: 123-127.

———., Mulherin, N.D., Hardy, J.P., Davis, R.E., and Twombly, A. 2002. Microwave interaction with snowpack observed at the Cold Land Processes Experiment. *Proceedings of the Eastern Snow Conference* 59: 251-254.

Krasser, L.M.A. 1967. Sound phenomena of deposited snow. In *Physics of Snow and Ice: International Conference on Low Temperature Science, Vol. 1, Part 2*. Japan: Institute of Low Temperature Science, Hokkaido University.

Lafarge, D., Lemariner, P., Allard, J.F., and Tarnow, V. 1997. Dynamic compressibility of air at audible frequencies. *Journal of the Acoustical Society of America* 102: 1995-2006.

Langham, E.J. 1981. Physics and Principles of Snowcover. In *Handbook of Snow: Principles, Processes, Management, and Use*, edited by D. M. Gray, and D.H. Male. Toronto: Pergamon Press Canada.

Lansing, L. 1964. Lake effect snow east and southeast of Lake Ontario as observed by radar. *Proceedings of the Eastern Snow Conference* 21: 63-77.

Leathers, D.J., and Ellis, A.W. 1993. Relationships between synoptic scale weather type frequencies and snowfall trends in the lee of Lake Erie and Ontario. *Joint Proceedings of the 50th and 61st Eastern and Western Snow Conferences*: 325-320.

Lee, S., Klein, A., and Over, T. 2004. Effects of the El Niño-southern oscillation on temperature, precipitation, snow water equivalent, and resulting streamflow in the Upper Rio Grande river basin. *Hydrological Processes* 18: 1053-1071.

Lee, S.M., and Rogers, J.C. 1985. Characterization of snow by acoustic sounding: a feasibility study. *Journal of Sound and Vibration* 99(2): 247-266.

Li, L., and Pomeroy, J.W. 1997a. Estimates of threshold wind speeds for snow transport using meteorological data. *Journal of Applied Meteorology* 36: 205-213.

———. 1997b. Probability of blowing snow occurrence by wind. *Journal of Geophysical Research* 102: 21,955-21,964.

Luck, D.G.C. 1949. *Frequency Modulated Radar*. New York: McGraw-Hill.

Lundberg, A., and Koivusalso, H. 2003. Estimating winter evaporation in boreal forests with operational snow depth data. *Hydrological Processes* 17: 1479-1493.

Lurton, X. 2002. An Introduction to Underwater Acoustics: Principles and Applications. New York: Springer; Chichester, UK: Praxis Publishing.

Maas, S.A. 1986. *Microwave Mixers*. Norwood, MA: Artech House.

Male, D.M. Gray and D.H. 1975. Problems in a Physically Based Snowmelt Model. *Canadian Journal of Civil Engineering* 2: 474-488.

Marks, D., Cooley, K.R., Robertson, D.C., Winstral, A. 2001. Long-term snow database, Reynolds Creek Experimental Watershed, Idado, USA. *Water Resouces Research* 37: 2835-2838.

———., Winstral, A., and Seyfried, M. 2002. Simulation of terrain and forest shelter effects on patterns of snow deposition, snowmelt, and runoff over a semi-arid mountain catchment. *Proceedings of the Eastern Snow Conference* 59: 181-202.

Marsh, P., and Pomeroy, J.W. 1996. Meltwater fluxes at an arctic forest tundra site. *Hydrological Processes* 10: 1383-1400.

Marshall, H.P., Koh, G., Forster, R.R. 2004. Ground-based frequency-modulated continuous wave radar measurements in wet and dry snowpacks, Colorado, USA: an analysis and summary of the 2002-03 NASA CLPX data. *Hydrological Processes* 18:3609-3622.

Marshall, S., Oglesby, R.J., and Nolin, A.W. 2003. The predictability of winter snow cover over the western United States. *Journal of Climate* 16:1062-1073.

Matthews, J.H. 1992. *Numerical Methods for Mathematics, Science and Engineering*. New Jersey: Prentice-Hall.

McKay, G.A. 1970. Problems of measuring and evaluating snowcover. In *Snow Hydrology : proceedings of the workshop seminar / [sponsored by the Canadian National Committee [for the] International Hydrological Decade [and the University of New Brunswick, 1968]*, edited by Canadian International Committee for the International Hydrological Decade.

———., and Gray, D.M. 1981. The distribution of snowcover. In *Handbook of Snow: Principles, Processes, Management and Use*, edited by D. M. Gray, and Male, D.H. Toronto: Pergamon Press.

Meiman, J.R. 1970. Snow accumulation related to elevation, aspect, and forest canopy. In *Snow hydrology : proceedings of the workshop seminar / [sponsored by the Canadian National Committee [for the] International Hydrological Decade [and the University of New Brunswick, 1968]*, edited by Canadian International Committee for the International Hydrological Decade. Ottawa: Queen's Printer.

Melloh, R.A., Hardy, J.P., Bailey, R.N., and Hall, T.J. 2002. An efficient snow albedo model for the open and sub-canopy. *Proceedings of the Eastern Snow Conference* 59: 119-132.

Metsämäkia, S., Vepsäläinena, J., Pulliainenb, J., and Sucksdorffa, Y. 2002. Improved linear interpolation method for the estimation of snow-covered area from optical data. *Remote Sensing of the Environment* 82(1): 64-78.

Mewhort, L., Bezdan, S., and Jones, M. 2002. Does it matter what kind of vibroseis deconvolution is used? *CSEG Geophysics 2002*: 1-4.

Miller, D.H. 1966. Transport of intercepted snow from trees during snow storms. *Forestry Service Research Paper PSW-33*: United States Department of Agriculture.

Moore, H.M., Attenborough, K., Rogers, J., and Lee, S. 1991. In situ acoustical investigations of deep snow. *Applied Acoustics* 33 (4):281-301.

Neumann, N., and Marsh, P. 1998. Local advection of sensible heat in the snowmelt landscape of Arctic tundra. *Hydrological Processes* 12:1547-1560.

Niziol, T., Reinkling, R.F., Kropfli, R.A., Byrd, G., Ballentine, R., Stamm, A., Penc, R., Caiazza, R., and Bedford, C. 1990. The Lake Ontario Winter Storms (LOWS) project. *Proceedings of the Eastern Snow Conference* 47: 175-187.

Nkemdirim, L.C. 1991a. Chinooks and winter evaporation. *Theoretical and Applied Climatology* 43 (3): 129-136.

———. 1991b. An empirical relationship between temperature, vapour pressure deficit and wind speed and evaporation during a winter Chinook. *Theoretical and Applied Climatology* 43: 123-128.

Orfanidis, S.J. 1988. *Optimum Signal Processing: An Introduction*. New York: McGraw-Hill.

Otake, K. 1980. Snow survey by aerial photographs. *GeoJournal* 4(4): 367-369.

Oura, A. 1952a. Reflection of sound at snow surface and mechanisms of sound propagation in snow. *Low Temperature Science Series A, Physical Sciences* 9: 179-186.

———. 1952b. Sound velocity in the snow cover. *Low Temperature Science Series A, Physical Sciences* 9: 171-178.

Paine, D.A., and Kaplan, M.L. 1971. The parameterization and prediction of synoptic-scale influences on Great Lakes snowstorms. *Proceedings of the Eastern Snow Conference* (28):81-94.

Parry, T. 1955. *A history of Welsh literature*. Translated by H. I. Bell. Oxford: Clarendon Press.

Perry, B., and Konrad, C.E. 2005. The Influence of the Great Lakes on Snowfall Patterns in the Southern Appalachians. *Proceedings of the Eastern Snow Conference* 62:269-279.

Plona, T.J. 1992. Attenuation of sound in porous materials. *Journal of the Acoustical Society of America* 91 (4):2378-2379.

Pohl, S., and Marsh, P. 2006. Modeling the spatial-temporal variability of spring snowmelt in an arctic catchment. *Hydrological Processes* 20: 1773-1792.

Pomeroy, J.W., and Gray, D.M. 1990. Saltation of snow. *Water Resources Research* 26(7): 1583-1594.

———. 1991. Transport and sublimation of snow in wind-scoured alpine terrain. In *Snow Hydrology and Forests in High Alpine Areas, IAHS Publication No. 205*, edited by H. L. H. Bergmann, W. Frey, D. Issler, and B. Salm. Wallingford: IAHS.

———., Gray, D.M., and Landine, P.G. 1991. Modeling the transport and sublimation of blowing snow on the prairies. *Proceedings of the Eastern Snow Conference* 48:175-188.

———., and Male, D.H. 1992. Steady-state suspension of snow. *Journal of Hydrology* 136:275-301.

———., Gray, D.M., and Landine, P.G. 1993. The Prairie Blowing Snow Model: characteristics, validation, operation. *Journal of Hydrology* 144:165-192.

———., and Gray, D.M. 1994. Sensitivity of snow relocation and sublimation to climate and surface vegetation. In *Snow and Ice Covers: Interactions with Atmosphere and Ecosystems, IAHS Publication No. 223*, edited by H. G. Jones, T.D. Davies, A. Ohmura, and E.M. Morris. Wallingford, U.K.: IAHS Press.

———., and Gray, D.M. 1995. *Snowcover Accumulation, Relocation, and Management, National Hydrology Research Institute Science Report No. 7*, Saskatoon: National Water Research Institute.

———., and Dion, K. 1996. Winter radiation extinction and reflection in a boreal pine canopy: measurements and modeling. *Hydrological Processes* 10:1591-1608.

———., and Goodison, B.E. 1997. Winter and Snow. In *The Surface Climates of Canada*, edited by W. G. Bailey, Oke, T.R., and Rouse, W.R. Montreal; Kingston, London, Buffalo, NY: McGill-Queen's University Press.

———., and Granger, R.J. 1997. Sustainability of the western Canadian boreal forest under changing hydrological conditions. I. Snow accumulation and ablation. In Sustainability of Water Resources under Increasing Uncertainty. *IAHS Publication 24*. D. Rosbjerg et al. (Eds.) IAHS Press, pp. 237-242.

———., Granger, R.J., Pietroniro, A., Elliot, J., Toth, B., and Hedstrom, N.R. 1997a. Hydrological pathways in the Prince Albert Model Forest. In *NHRI Contribution Series No. CS-97004*. Saskatoon: National Hydrology Research Institute.

———., Marsh, P., and Gray, D.M. 1997b. Application of a distributed blowing snow model to the Arctic. *Hydrological Processes* 11:1451-1464.

———., and Marsh, P. 1997. The application of remote sensing and a blowing snow model to determine snow water equivalent over northern basins. In *Applications of Remote Sensing in Hydrology, NHRI Symposium No. 17*, edited by A. P. G.W. Kite, and T.J. Pultz. Saskatoon, Saskatchewan: National Hydrology Research Institute.

———., Parviainen, J., Hedstrom, N., and Gray, D.M. 1998. Coupled modeling of forest snow interception and sublimation. *Hydrological Processes* 12:2317-2337.

———., and Essery, R. 1999. Turbulent fluxes during blowing snow: field tests of model simulation predictions. *Hydrological Processes* 13: 2963-2975.

———., Hedstrom, N., Parviainen, J. 1999. The snow mass balance of Wolf Creek, Yukon: Effects of snow sublimation and redistribution. In *Wolf Creek Research Basin: Hydrology, Ecology, Environment, Proceedings of a Workshop held in Whitehorse, Yukon, 5-7 March 1998, Cat. No. En 37-121/1999E*, edited by J. W. Pomeroy, and Granger, R.J. Saskatoon: National Water Research Institute.

———., and Li, L. 2000. Prairie and arctic areal snow cover mass balance using a blowing snow model. *Journal of Geophysical Research* 105(D21): 26 629-26 634.

———., and Brun, E. 2001. Physical Properties of Snow. In *Snow Ecology: An Interdisciplinary Examination of Snow-Covered Ecosystems*, edited by H. G. Jones, Pomeroy, J.W., Walker, D.A., and Hoham, R.W. Cambridge, UK: Cambridge University Press.

———. Gray, D.M., Hedstrom, N.R., and Janowicz, J.R. 2002. Prediction of seasonal snow accumulation in cold climate forests. *Hydrological Processes* 16:3543-3558.

———., Toth, B., Granger, R.J., Hedstrom, N.R., and Essery, R.L.H. 2003. Variation in surface energetics during snowmelt in a subarctic mountain catchment. *Journal of Hydrometeorology* 4:702-719.

———., Bewley, D.S., Essery, R.L.H., Hedstrom, N.R., Link, T., Granger, R.J., Sicart, J.E., Ellis, C.R., and Janowicz, J.R. 2005. Shrub tundra snowmelt. *Proceedings of the Eastern Snow Conference* 62: 237-251.

Price, A.G. 1988. Prediction of snowmelt rates in a deciduous forest. *Journal of Hydrology* 101:145-157.

Prowse, T.D. 1990. Northern Hydrology: An Overview. In *Northern Hydrology: Canadian Perspectives, NWRI Science Report No. 1*, edited by T. D. Prowse, and C.S.L. Ommanney. Saskatoon: Environment Canada.

Rabiner, L.R., Schafer, R.W., and Rader, C.M. 1969. The chirp-z transform algorithm and its application. *IEEE Transactions on Audio Electroacoustics* 17(2): 86-92.

Raichel, D.R. 2000. *The Science and Applications of Acoustics*. New York: Springer-Verlag.

Rhea, J.O., and Grant, L.O. 1974. Topographic influences on snowfall patterns in mountainous terrain. In *Advanced Concepts and Techniques in the Study of Snow and Ice Resources*. Washington, DC: National Academy of Sciences Press.

Robinson, E.A. 1957. Predictive decomposition of seismic traces. *Geophysics* 22(4): 767-778.

Ryerson, C.C., and Bates, R.E. 1990. Regional snowfall intensity and the Great Lakes Anomaly. *Proceedings of the Eastern Snow Conference* 47: 189-199.

Sacchi, M.D. 2003. SeismicLab Software, http://www. geo.phys.ualberta.ca/saig/SeismicLab/SeismicLab/DECON/.

Savelyev, S.A., Gordon, M., Hanesiak, J., Papakyriakou, T., and Taylor, P.A. 2006. Blowing snow studies in the Canadian Arctic Shelf Exchange Study, 2003-04. *Hydrological Processes* 20: 817-827.

Schemenauer, R.S., Berry, M.O., and Maxwell, J.B. 1981. Snowfall Formation. In *Handbook of Snow: Principles, Processes, Management, and Use*, edited by D. M. Gray, and D.H. Male. Toronto: Pergamon Press Canada.

Schmidt, R.A. 1982. Vertical profiles of wind speed, snow concentration, and humidity in blowing snow. *Boundary-Layer Meteorology* 23: 223-246.

———., and Pomeroy, J.W. 1990. Bending of a conifer branch at subfreezing temperatures: implications for snow interception. *Canadian Journal of Forestry Research* 20(8): 1250-1253.

———., and Gluns, D.R. 1991. Snowfall interception on branches of three conifer species. *Canadian Journal of Forestry Research* 21:1262-1269.

Seligman, G. 1939. Sound absorption of snow. *Nature (London)* 143:1071.

Shiotani, M., and Arai, H. 1953. A short note on the snow storm. *Proceedings of the Japanese National Congress of Applied Mechanics* 2:217-218.

Sicart, J.E., Pomeroy, J.W., Essery, R.L.H., Hardy, J., Link, T., and Marks, D. 2004. A sensitivity study of daytime net radiation during snowmelt to forest canopy and atmospheric conditions. *Journal of Hydrometeorology* 5: 774-784.

———., Pomeroy, J.W., Essery, R.L.H., and Bewley, D. 2006. Incoming longwave radiation to melting snow: observations, sensitivity and estimate on in Northern environments. *Hydrological Processes* 20: 3697-3708.

Skene, W.F. 1868. *The Four Ancient Books of Wales*. Edinburgh, UK: Edmonston & Douglas.

Skolnik, M.I. 1990. *Radar Handbook*. New York: McGraw-Hill.

Smith, J.L. 1965. *The elastic constants, strength and density of Greenland snow as determined from measurements of sonic wave velocity, CRREL Technical Report 167*. Hanover, New Hampshire: Cold Regions Research and Engineering Laboratory.

Smith, N. 1969. *Determining the Dynamic Properties of Snow and Ice by Forced Vibration, CRREL Technical Report 216*. Hanover, New Hampshire: Cold Regions Research and Engineering Laboratory.

Sommerfeld, R.A. 1982. A review of snow acoustics. *Reviews of Geophysics and Space Physics* 20(1): 62-66.

Stepphun, H. 1976. Areal water equivalents for prairie snowcovers by centralized sampling. *Proceedings of the Western Snow Conference* 44:63-68.

———., and Gray, D. 1978. Modification of a conceptual model to estimate the sublimation potential for wind transported snow, Internal Report, Division of Hydrology. In *Internal Report, Division of Hydrology, University of Saskatchewan*. Saskatoon: University of Saskatchewan.

———. 1981. Snow and Agriculture. In *Handbook of Snow: Principles, Processes, Management, and Use*, edited by D. M. Gray, and D.H. Male. Toronto: Pergamon Press Canada.

Stove, A.G. 1992. Linear FMCW radar techniques. *IEE Proceedings-F. Radar and Signal Processing* 139(5): 343-350.

Sturm, M., Holmgren, J., and Liston, G.E. 1995. A seasonal snow classification system for local to global applications. *Journal of Climate* 8: 1261-1283.

———. 1999. *Self-recording snow depth probe, U.S. Army Corps of Engineers Cold Regions Research and Engineering Laboratory Fact Sheet*. Hanover, New Hampshire: CRREL.

———., and Holgren, J. 1999. *Self-recording snow depth probe. Patent issued to the U.S. Army Corps of Engineers by the U.S. patent office*.

———., McFadden, J.P., Liston, G.E., Chapin III, F.C., Racine, C.H., and Holmgrem, J. 2001. Snow-shrub interactions in the arctic tundra: a hypothesis with climatic implications. *Journal of Climate* 14: 336-344.

Swanson, R.H., and Golding, D.L. 1982. Snowpack management on Marmot watershed to increase late season streamflow. *Proceedings of the Eastern Snow Conference* 39:215-218.

Takada, M., Ohkhochi, S., and Nasu, N. 1954. On the absorption coefficient of snow and the propagation of sound along snow surface. *Journal of the Acoustical Society of Japan* 10: 23-27.

Trivett, N.B.A., and Waterman, S.E. 1980. Evaluation of the spatial and temporal distribution of snowpack parameters in the Saint John River Basin. *Proceedings of the Eastern Snow Conference* 37: 19-35.

Umnova, O., Attenborough, K., Shin, H.C., and Cummings, A. 2005. Deduction of tortuosity and porosity from acoustic reflection and transmission measurements on thick samples of rigid-porous materials. *Applied Acoustics* 66:607-624.

Van der Kamp, G., Hayashi, M., Gallen, D. 2003. Comparing the hydrology of grassed and cultivated catchments in the semi-arid prairies. *Hydrological Processes* 17: 559-575.

Wang, L., Sharp, M., Brown, R., Derksen, C., Rivard, B. 2005. Spring snow covered area depletion in the Canadian Arctic from NOAA snow charts. *Remote Sensing of the Environment* 95: 453-463.

Wehner, D.R. 1987. *High-resolution radar*. Norwood, Massachusetts: Artech House.

Weickmann, H.K., Jiusto, J., McVehil, G., Pilie, R., and Warbuton, JK. 1970. The Great Lakes Project. *Proceedings of the Eastern Snow Conference* 27: 18-31.

Woo, M.K., and Marsh, P. 1977. Determination of snow storage for small eastern high arctic basins. *Proceedings of the 1988 Western Snow Conference* 34:147-162.

———. 1982. Snow hydrology of the High Arctic. *Eastern Snow Conference* 39:63-74.

———., and Steer, P. 1986. Monte Carlo simulation of snow depth in a forest. Water Resources Research 22(6): 864-868.

———., and Giesbrecht, M.A. 2000. Simulation of snowmelt in a subarctic spruce woodland: scale considerations. *Nordic Hydrology* 31: 301-316.

Woodhouse, C. 2003. A 431-year reconstruction of western Colorado snowpack from tree rings. *Journal of Climate* 16: 1551-1561.

Yankielun, N. 1992. An airborne millimeter-wave FM-CW radar for ice thickness profiling of freshwater ice. *CRREL Report 92-20*. Hanover, New Hampshire: Cold Regions Research and Engineering Laboratory.

———., Rosenthal, W., Davis, R.E. 2004. Alpine snow depth measurements from aerial FMCW radar. *Cold Regions Science and Technology* 40: 123-134.

Zarek, J.H.B. 1978. Sound absorption in flexible porous materials. *Journal of Sound and Vibration* 61: 205-234.

APPENDIX

COMPUTER CODES

```
%%%%%%%%%%%%%%%%%%%%%%%%%%%%%%%%%%%%%%%%%%%%%%%%%%%%%%%%%%%%%%%%%%%%%%%
%Program:       reflection.m
%Description:   Matlab program to determine the reflection
%               response and the homodyned wave
%Dependencies:  Signal Processing Toolbox, Matlab v7.1 R14
%%%%%%%%%%%%%%%%%%%%%%%%%%%%%%%%%%%%%%%%%%%%%%%%%%%%%%%%%%%%%%%%%%%%%%%

%The original wave sent out from the loudspeaker
original = wavread('original.wav');
%The reflection from the snowpack
recorded = wavread('recorded.wav');
n = length(recorded);

%The air-coupled wave arriving on the side
%of the microphone
side = wavread('side.wav');

%The averaged environmental noise
en = waveread('noise.wav');

%Noise in the recordings system found by
%the loopback test
nrc = wavread('nrc.wav');

%The sampling rate of the ADC (96000 Hz)
fs = 96000;
period = 1/fs;
t = period*(1:n);

%filter all of the waves to prevent
%higher frequency components from being
%in the signal

%the highest frequency cutoff is 25 kHz,
%which is situated greater than 20 kHz to ensure that
%frequencies below 20 kHz are unaffected by
%filter roll-off

%the filter being used here is a low-pass
%Chybyshev filter, the numerator coefficients
%of which are created using 'fdatool'

%load the numerator coefficients of the filter
load('filter.mat')

%filter the sweeps
original = filter(G,1,original);
recorded = filter(G,1,recorded);
side = filter(Num,1,side);
en = filter(Num,1,en);
nrc = filter(Num,1,nrc);

%Calculate sPrime
%Note that the vectors have to be all
%the same size
sPrime = recorded-side-en-nrc;
```

```
%Take sPrime into the frequency domain by
%use of the discrete Fast Fourier Transform
sPrimeF = fft(sPrime);

%Take the original sweep into the frequency domain
originalF = fft(original);

%Perform the division in the frequency domain
%No zeros are present in the spectrum
%so that division by zero is not an issue
sDoublePrimeF = originalF(:,1)./sPrimeF(:,1);

%Take the reflection response back into the time
%domain by use of the inverse FFT
sDoublePrimeT = ifft(sDoublePrimeF);

%Apply Weiner Spiking Deconvolution (WSD) to the reflection response
%to remove the snowpack attenuation

%set the length of the spiking operator
%this is set by trial and error
spikingop = 29;
%set the length of the pre-whitening
%this is also set by trial and error
prewhit = 0.1;
%size of the vector
n = size(sDoublePrimeT);

%compute the autocorrelation of the signals
ar = xcorr(sDoublePrimeT(:,1), sDoublePrimeT(:,1), spikingop);
%set up for the levinson recursion
s = ar(:,1).*hamming(spikingop*2+1);
ref = s(spikingop+1:2*spikingop,1);
p = ref(1,1)*(1+0.1/100.);  %pre-whitening procedure
ref(1,1) = p;

%find the levinson coefficients
c = levinson(ref,spikingop);
c = c';

%convolution of the data with the filter
cdfilter = conv2(sDoublePrimeT,c);
dfg = cdfilter(1:n,:);
maxi = max(max(dfg));
mult = dfg * maxi/(max(max(sDoublePrimeT)));

%mult now contains the reflection response from the snowpack

%FMCW section of the code
%multiply both of the waves together (homodyning)
%note that what we do here is multiply the original wave
%the multiplication is repeated in the time domain
mm = sPrime(:,1).*original(:,1);

%set up the parameters for the chirp-z transform
fs = 96000; f1 = 0.00001; f2 = 100;  % in hertz
%fs = 96000; f1 = 20; f2 = 50;
```

```
m = 2048;
w = exp(-j*2*pi*(f2-f1)/(m*fs));
a = exp(j*2*pi*f1/fs);

%calculate the chirp-z transform
z = czt(mm,m,w,a);
N = length(z);
Pyy = z.* conj(z)/N;
Pyy = Pyy./1500000;

%The next step is to plot all of the data


%Plot the original wave sent out from the loudspeaker
subplot(2,2,1); plot(t, original);
title(' (a) Original Wave');
xlabel('Time (s)');
ylabel('Amplitude');
set(findobj(gca,'Type','line'),...
                'Color','black');


%Plot the recorded wave
subplot(2,2,2); plot(t, recorded);
title(' (b) Recorded Wave');
xlabel('Time (s)');
ylabel('Amplitude');
set(findobj(gca,'Type','line'),...
                'Color','black');


%Plot the reflection response in the time domain
subplot(2,2,3); plot(t,mult);
title(' (c) Reflection Coefficients');
xlabel('Time (s)');
ylabel('Magnitude');
set(findobj(gca,'Type','line'),...
                'Color','black');


%Plot the homodyned wave
fz = ((0:length(z)-1)'*(f2-f1)/length(z)) + f1;
subplot(2,2,4); plot(fz,Pyy);
title(' (d) Homodyned Response in Frequency Domain');
xlabel('Frequency (Hz)');
ylabel('Amplitude');
set(findobj(gca,'Type','line'),...
                'Color','black');
```

```
%%%%%%%%%%%%%%%%%%%%%%%%%%%%%%%%%%%%%%%%%%%%%%%%%%%%%%%%%%%%%%%%%%%%%%%
%Program: layers.m
%Description: Matlab program to calculate the SWE of
%             the snowpack using reflection coefficients
%             and frequency shifts
%Dependencies: Matlab v7.1 R14
%%%%%%%%%%%%%%%%%%%%%%%%%%%%%%%%%%%%%%%%%%%%%%%%%%%%%%%%%%%%%%%%%%%%%%%

%The inputs to this program are the frequencies (frequency.txt) at which
%each of the peaks occur in the homodyned response, and the
%reflection coefficients (reflection_coefficients.txt)

f = load('frequency.txt');
reflectioncoeff = load('reflection_coefficients.txt');
N = length(reflectioncoeff);

%allocate memory for the arrays
porosity = zeros(N);
tortuosity = zeros(N);
density = zeros(N);
speed = zeros(N);

%define gamma constant
%gamma = 0.80 for the Saskatchewan sites
%gamma = 0.70 for the Lake O'Hara
gamma = 0.70;
%define the speed in the air layer above the
%surface of the snowpack
c0 = 331;

for i = 1:N-1

        R = reflectioncoeff(i);

        %---Do this only for the first interface air-snow)---
        if (i == 1)
            %define the variables for Newton iteration
            k = 0;      %the interator
            x0 = 1;     %the starting approximation
            max = 10;   %the maximum number of iterations
            %set the starting variables
            p0 = x0;
            p1 = p0;
            while (k < max)
                p0 = p1;
                p1 = p0- (sqrt((gamma + p0 - gamma*p0)/p0) - ...
                (p0*(1 + R))/(1 - R))/(((1 - gamma)/p0 - ...
                (gamma + p0 - gamma*p0)/p0*p0)/(2*sqrt((gamma + ...
                p0 - gamma*p0)/p0)) - (1 + R)/(1 - R));
                k = k+1;
            end
        end

        %---Do this for all of the other interfaces (snow-snow)---
        if (i > 1)
            %define the variables for Newton iteration
            k = 0;      %the interator
```

```
            x0 = 1;     %the starting approximation
            max = 10;   %the maximum number of iterations
            p0 = x0;
            p1 = p0;
            phik1 = porosity(i-1);
            alphak1 = tortuosity(i-1);
            while (k < max)
                p0 = p1;
                p1 = p0- ((sqrt((gamma + p0 - gamma*p0)/p0)*phik1)/ ...
                sqrt(alphak1) - (p0*(1 + R))/(1 - R))/...
                ((((1 - gamma)/p0 - (gamma + p0 - gamma*p0)/ ...
                p0*p0)*phik1)/ ...
               (2*sqrt(alphak1)*sqrt((gamma + p0 - gamma*p0)/p0)) ...
                - (1 + R)/(1 - R));
                k = k+1;
            end
        end

        %stuff the values in the vectors
        porosity(i) = p1;
        density(i) = 1000*(1-p1);
        tortuosity(i) = 1-gamma*(1-(1/p1));
        speed(i) = c0/sqrt(tortuosity(i));
end


%---now that you have the speed, calculate the distance---
y = zeros(N);
deltat = 1;             %sweep time
B = 19980;              %bandwidth (20Hz - 20 kHz)
cumulativetime = 0;     %set the variable for the cumulative time

for i = 1:N

    freqshift = f(i);

    %---do this only for the first time---
    %for y0 (the distance from the source to the snowpack)
    if (i==1)
        y(i) = (freqshift*deltat*c0)/(2*B);
        cumulativetime = cumulativetime + (y(i)/c0);
    end

    %--do this all of the other times---
    %for y1,...,y_n
    if (i > 1)
        y(i) = (speed(i-1)/(2*B))*((freqshift*deltat)-2*B*cumulativetime);
        cumulativetime = cumulativetime + y(i)/speed(i-1);
    end
end
%determine the SWE
SWE = 0;
for i = 1:N
    %we ignore y0 since this is the air layer
    SWE = SWE + y(i+1)*density(i);
end
```

```
%%%%%%%%%%%%%%%%%%%%%%%%%%%%%%%%%%%%%%%%%%%%%%%%
%Program: correct.m
%Description: Matlab program to correct for the reflection coefficients
%Dependencies: Matlab v.7.1.R14
%%%%%%%%%%%%%%%%%%%%%%%%%%%%%%%%%%%%%%%%%%%%%%%%

k = 379.65;             %the angular wavenumber in the medium
y0 = 0.30;              %the distance to the reflector (snow surface)
reflection = 0.22;      %the measured reflection coefficient
thetaG = 0.001;         %this is a small angle to the normal

r = 0:600000;   %take the evaluation of the integral as far as you can go
integrand =
@(r)((exp(j.*k.*sqrt((r.^2)+y0)).*r.*besselj(0,k.*cos(thetaG).*r))./...
sqrt(r.^2+y0.^2));
part1 = real(trapz(integrand(r)));

part2 = (exp(j.*(k.^2-(k.*cos(thetaG).^2).*y0))./((k.^2)-...
    (k.*cos(thetaG)).^2);
answer = real(-j*part1*(part2.^(-1))*reflection);
```